University of Huddersfield Repository

Li, Guoxing

Investigation into the dynamic responses and tribological characteristics of cylinder liners in a IC engine with alternative fuels

Original Citation

Li, Guoxing (2016) Investigation into the dynamic responses and tribological characteristics of cylinder liners in a IC engine with alternative fuels. Doctoral thesis, University of Huddersfield.

This version is available at http://eprints.hud.ac.uk/id/eprint/30287/

The University Repository is a digital collection of the research output of the University, available on Open Access. Copyright and Moral Rights for the items on this site are retained by the individual author and/or other copyright owners. Users may access full items free of charge; copies of full text items generally can be reproduced, displayed or performed and given to third parties in any format or medium for personal research or study, educational or not-for-profit purposes without prior permission or charge, provided:

- The authors, title and full bibliographic details is credited in any copy;
- A hyperlink and/or URL is included for the original metadata page; and
- The content is not changed in any way.

For more information, including our policy and submission procedure, please contact the Repository Team at: E.mailbox@hud.ac.uk.

http://eprints.hud.ac.uk/

INVESTIGATION INTO THE DYNAMIC RESPONSES AND TRIBOLOGICAL CHARACTERISTICS OF CYLINDER LINERS IN A CI ENGINE WITH ALTERNATIVE FUELS

GUOXING LI

A thesis submitted to the University of Huddersfield in partial fulfilment of the requirements for the degree of Doctor of Philosophy

School of Computing and Engineering

The University of Huddersfield

July 2016

Abstract

Promoted by the realisation of dwindling fossil fuel supplies and their adverse environmental impacts, there more and more types of alternative fuels to fossil diesel have been used and investigated in compression ignition engines. However, the majority of researches on alternative fuels mainly focus on their power performance, efficiency and emission performance, without fully investigating the potential effects on the vibro-acoustic emissions and tribological characteristics of engines caused by their significant differences in physical and chemical properties. Consequently, the impacts of long-term use of alternative fuels on structural failure, lubrication degradation, friction aggravation, overall service life spans and associated maintenance activities of internal combustion (IC) engines have not yet been fully understood.

To reduce this gap this thesis focuses on the investigation into the vibration responses of cylinder liners in a diesel engine to accurately characterises the tribological behaviour between the piston rings and cylinders which is one of the most decisive sub-processes that determine engine performance and yet is correlated with the combustion of different fuels. In particular, the investigation was carried out by coupling the hydrodynamic lubrication model with structural vibration effects through a series of extensive numerical simulations and systematic experimental evaluations in order to establish a vibration based technique to monitoring tribological behaviour and thereby accurately assess the influence.

Based on the dynamic coupling mechanisms between the combustion characteristics of alternative fuels and the tribological behaviours of cylinder liners, the most significant influences from the fuel burning on tribological behaviour of cylinder liners concerned in this study is a direct and physical approach such as the effect of liner vibrations on cylinder friction process, even though an indirect and chemical but very slow approach such as the deterioration of oil properties by combustion products can happen.

To characterise the direct influence a finite element dynamic model was developed and validated for predicting the dynamic responses of cylinder liners to respective excitation sources including the highly nonlinear combustion pressure shocks and subsequent piston slap impacts. The realistic consideration of both the characteristics of structural modes up to 15kHz and nonlinearities of elastic assembly constraints allows obtaining accurate prediction that the combustion shocks cause vibrations in a frequency range around 10kHz with an amplitude order of 0.01μm, whereas the piston slaps in frequency range from 1k to 5kHz with an amplitude order 0.2μm, which gives a clear and quantitative indication of the nonlinear phenomena of liner vibration due to combusting alternative fuels and varying lubrication conditions. In addition, a decomposition analysis of piston side-thrust forces provides more insight of the localized response characteristics corresponding to coupling interactions of combustion force with inertia force of piston assembly.

To further investigate the potential influences of structural deformations to tribological behaviours of cylinder assemblies, a new dynamic deformation based lubrication model was developed based on an employment of improved shearing factors in which the effect of inevitable liner vibrations is included to obtain a more realistic lubricating film formation, distribution and tribological behaviours. The simulation studies show that this advancement in modelling oil films predicts that the biodiesel with more intense vibration emissions is able to reduce the friction loss between pistons and liners, whereas the methanol-diesel blend with weakened liner dynamic response may exacerbate the friction loss of IC engines. This finding confirms further that the vibration responses allow a straightforward and in-depth indication of the effect generated by using different fuels.

In addition, a further experimental investigation was carried out based on a motoring engine test, in which high frequency sinusoidal vibrations at 25 kHz, 30 kHz and 40 kHz are added to the external surface of the linear. The observable changes in motoring torque verify that proper external vibrations can affect the tribological behaviours between the pistons and liners, including both asperity friction and viscous friction, and resulting in

the friction reduction of IC engines. Particularly the 40 kHz vibration at the maximal driving power of the test device can achieve a reduction of 1.79% in the motoring torque. This has demonstrated more on the effectiveness of this vibration based diagnostic method in assessing the influences of alternative fuels upon tribological behaviours of piston ring and cylinder liners.

Finally, further researches on the subjects is also proposed in order to complete the vibration based diagnostics in achieving more accurate assessment of engine lubrication conditions and effective friction reduction.

Acknowledgements

This work has been carried out in the school of Computing and Engineering, Centre for Efficiency and Performance Engineering (CEPE) and Automotive and Marine Engineering Group (AMEG) at the University of Huddersfield, U. K. This work was financially supported by the Fee-waiver Scholarship scheme from the University of Huddersfield. I would like to offer my grateful acknowledgements to the University of Huddersfield, CEPE and AMEG group for their support during my research.

I would like first to express a sincere gratitude to my main supervisor, Professor Andrew Ball, for his guidance and continuous support during the course of my research. It is his inspiration which encourages me to cope with all the faced challenges and gain the rewarding research skills.

I am especially like to thank my co-supervisor, Dr. Fengshou Gu, Principle Research Fellow at the University of Huddersfield, for his sincere and warm-hearted help both academically and personally. His guidance helped me in all the time of research and writing of this thesis. I could not have imagined having a better mentor for my Ph.D study.

My thanks are also extended to my co-supervisor, Professor Tie Wang, at the University of Huddersfield and Taiyuan University of Technology for his continual guidance and support.

I also appreciate the help from all my friends I have met in Huddersfield, especially Xiang'e Tian, Guojin Feng, Ruichen Wang, Nasha Wei and Ibrahim Rehab, who have over the years made my time such a great experience on a professional and personal level. Grateful thanks to my research mates and friends in China, especially Xia Yuan, Zhi Chen, Jing Peng, TianTian Yang, Xiuquan Sun, Yuandong Xu, Longjie Yang, Wei Feng, Qiang Shi, Jie Zhao, Huanhuan Wang, Miaoshuo Li, Haoyu Lu, Xingchen Lu, Xuan Dang and Hu Zhang.

Special and grateful thanks to my parents and my brother for their unstinting support, encouragement, high expectations and love.

Sincerely thanks to my wife, Dan Song, for her continual encouragement and amazing support over the years.

Statement of Originality

I hereby certify that all of the work described within this thesis is the original work of the author. Any published (or unpublished) ideas and/or techniques from the work of others are fully acknowledged in accordance with the standard referencing practices.

(Guoxing Li)

Publications

1. Li, G., Gu, F., Wang, T., Wei, N., Xu, Y. and Ball, A. (2016) 'A validated finite element model for predicting dynamic responses of cylinder liners in an IC engine' In: the 22nd International Conference on Automation and Computing (ICAC2016), 7th-8th September 2016, Essex, UK.

2. Li, G., Wang, T., Zhang, R., Gu, F. and Shen, J. (2015) 'An Improved Optimal Slip Ratio Prediction considering Tyre Inflation Pressure Changes' Journal of Control Science and Engineering, 2015, pp. 1-8. ISSN 1687-5249.

3. Li, G., Gu, F., Wang, T. and Ball, A. (2013) 'The Potential Effects of Alternative Fuels on the Lubricating Condition of Compression-ignition Engines'. In: Proceedings of Computing and Engineering Annual Researchers' Conference 2013: CEARC'13. Huddersfield: University of Huddersfield. p. 233. ISBN 9781862181212.

4. Li, G., Wang, T. (2014). 'Influence of long-waved road roughness on fatigue life of dump truck frame'. Journal of Vibroengineering, 2014, *16*(8).

5. Wei, N., Gu, F., Wang, T., Li, G., Xu, Y., Yang, L. and Ball, A. (2015) 'Characterisation of Acoustic Emissions for the Frictional Effect in Engines using Wavelets based Multi-resolution Analysis'. In: Proceedings of the 21st International Conference on Automation and Computing (ICAC). : IEEE. . ISBN 978-0-9926801-0-7.

6. Wei, N., Gu, F., Li, G., Wang, T. and Ball, A. (2014) 'Characterising the friction and wear between the piston ring and cylinder liner based on acoustic emission analysis'. In: 21st International Congress on Sound and Vibration, 13th - 17th July, 2014, Beijing, China.

7. Hamed, M., Tesfa, B., Aliwan, M., Li, G., Gu, F. and Ball, A. (2013) 'The Influence of Vehicle Tyres Pressure on the Suspension System Response by Applying the Time-Frequency Approach'. In: Proceedings of the 19th International Conference on Automation and Computing (ICAC) 2013: Future Energy and Automation. London, UK: Brunel University. . ISBN 978-1908549082.

Table of Contents

List of Figures

List of Tables

List of Abbreviations

ATS	Anti-Thrust Side
BD	Biodiesel
BSFC	Brake Specific Fuel Consumption
BTB	Back-To-Back
CFD	Computational Fluid Dynamics
CWT	Continuous Wavelet Transform
DAQ	Data Acquisition system
DOF	Degree Of Freedom
EHL	Elasto–Hydrodynamic Lubrication
FEA	Finite Element Analysis
FFT	Fast Fourier Transform
FMEP	Friction Mean Effective Pressure
FTIR	Fourier Transform Infra-Red
HRR	Heat Release Rate
IC	Internal Combustion
LHV	Lower Heating Value
M15	15% Methanol-diesel blended fuel
MOFT	Minimum Oil Film Thickness
NVH	Noise, Vibration and Harshness
PRR	Pressure Rise Rate
PPI	Performance Parameter Index
RMS	Root Mean Square
SDOF	Single Degree Of Freedom
STFT	Short-Time Fourier Transform

SMD	Surface Mount Device
TDC	Top Dead Centre
TFR	Time Frequency Representation
TPI	Time Performance Index
TS	Thrust Side
UI	User Interface
Ⓒo	Combustion Oscillation (induced event)
Ⓒs	Combustion Shock (induced event)
Ⓐ …Ⓘ	Piston slap induced events

List of Notation

A_a	Apparent contact area	[m^2]
B	The axial height of piston ring	[m]
E	Composite material modulus	[Pa]
E_1	Young's modulus of ring	[Pa]
E_2	Young's modulus of liner	[Pa]
F_c	Lateral combustion force	[N]
F_i	Lateral inertia force of piston assembly	[N]
F_h	Hydrodynamic component of average friction force	[N]
F_a	Asperity component of average friction force	[N]
F_f	Total friction force	[N]
$F_n(t)$	Dynamic normal force	[N]
$F_f(t)$	Dynamic friction force	[N]
$f(\delta)$	Restoring force	[N]
f	Probability density function of roughness	[-]
H_m	Minimum film thickness-roughness ratio	[-]
$h(x,z,t)$	Distribution of oil film thickness	[m]
$h_T(x)$	Local film thickness	[m]
l	Length of the connecting rod	[m]
P_c	Longitudinally acting combustion force	[N]
P_i	Axial inertia force of piston assembly	[N]
P	Normal load	[N]

P_a	Average contact pressure	[Pa]
$p(x,z,t)$	Oil film hydrodynamic pressure field	[Pa]
$\bar{p}$	Mean pressure	[Pa]
$R(\phi)$	Radial co-ordinate	[m]
U	Sliding speed	[m/s]
V_s	Instantaneous velocity	[m/s]
W_a	Total asperity contact load	[N]
ω	Rotating speed of crankshaft	[rad]
x_p	Piston lateral displacement	[m]
r_c	Crank radius	[m]
ϕ	Angular co-ordinate	[rad]
η	Lubricant viscosity	[Pa s]
Δ_1	Surface roughness amplitude of piston ring	[μm]
Δ_2	Surface roughness amplitude of cylinder liner	[μm]
Δ	Combined roughness of the ring and liner	[μm]
Δ_x	Axial deformation of liner surface	[μm]
Δ_y	Circumferential deformation of liner surface	[μm]
σ	Composite RMS roughness of ring and liner	[μm]
ϕ_c	Contact factor	[-]
μ	Density of asperities	[-]
v_1	Poisson's ratio of ring	[-]
v_2	Poisson's ratio of liner	[-]

τ	Local shear stress	[Pa]
ϕ_f	Correction factor for the effect of varying film thickness	[-]
ϕ_{fp}	Correction factor for the mean pressure flow	[-]
ϕ_{fs}	Correction factor for the sliding roughness	[-]
γ	Directional properties of roughness	[-]
μ_f	Friction coefficient under lubricated contact	[-]
r	Crank radius	[m]
e_1	Piston ring surface height	[m]
ρ	Oil density	[kg/m^3]
$\mu(t)$	Instantaneous friction coefficient	[-]
μ_{av}	Average friction coefficient	[-]
δ	Contact compression	[m]

Chapter 1

Introduction

This chapter presents a general introduction to the potential influences of burning alternative fuels in diesel engines on the dynamic responses and the tribological behaviours of engine components. It then flows by the description of the backgrounds, motivations, objectives and organisations for this research establishment.

1.1 Introduction

To improve the mechanical efficiency and operational performance, lubrication optimization, friction reduction, and limitation of vibration emissions are the chief objectives of the automotive industry. In recent years, promoted by the realisation of dwindling fossil fuel supplies and their adverse environmental impacts, there more and more types of alternative fuels to fossil diesel have been used and investigated in diesel engines. However, due to the differences in physicochemical properties, the usage of alternative fuels can result in potential negative effects on engines, which include not only the influences on power output performance, emission levels but also the changes in dynamic behaviours of critical components and degradation process of lubricating oil, which will eventually affect the friction losses, overall service life spans and associated maintenance activities of internal combustion (IC) engines.

Due to the differences in physicochemical properties, the combustion behaviours of alternative fuels exhibit many different characteristics from the fossil diesel. In addition to combustion force itself, as the driving source of piston lateral movement, variations in combustion characteristics can cause evident changes in piston side-thrust forces, thus lead to variations in cylinder vibrations and tribological behaviours. However, it is difficult to characterise these differences caused by combusting of alternative fuels experimentally due to multiple sources, strong background noise, and nonlinear transfer paths in IC engines.

Previous studies[1]–[3] indicated that approximately 40%-50% of the total mechanical friction in IC engines is attributed to the reciprocating motions of piston-cylinder assemblies. The piston assembly is one of engine's key subsystems that determine the performances of friction, lubrication, noise, vibration and hence service lifespan of engines. In modelling of oil film formation and distribution on the cylinder liners, the cylinder wall is often taken as a perfect cylindrical surface by majority of researches[4]–[7], neglecting the potential influences of liner distortions to the friction behaviour. However, according to numerical studies performed in this research, the amplitude of liner deformations

induced by piston slaps is at the order of 0.1 microns, being about 20% of roughness amplitude, this may affect the distribution of oil film on cylinder wall. Therefore, it is essential to investigate the tribological characteristics of piston-cylinder assemblies with consideration of dynamic deformations of cylinder liners fuelled with alternative fuels.

Based on the study about the impacts of vibrations to friction process, a more realistic question could be subsequently raised: If the influence of structural vibration on tribological behaviour can be positive, is it possible to improve the lubrication state and to reduce the friction and wear of engines, by optimizing the parameters of additional vibration? To understand the mechanism of vibration induced friction reduction, many research works have been carried out. However, the vast majority of studies on vibration induced friction reduction are just conducted based on limited prototype or mechanical test benches, rather than on machines in actual operations, especially on an actual IC engine.

Therefore, to achieve safe and efficient use of alternative fuels, it is essential to investigate the influence mechanism of alternative fuels on the dynamic responses and subsequently to explore their corresponding tribological characteristics, which will be the basis for minimising the frictional losses and increasing service lifetime for engines running with alternative fuels.

1.2 Background

Numerous techniques have been reported and examined for evaluating the impacts of alternative fuels to vibration and noise performance of IC engines. It has been confirmed that the dynamic responses of engines can be significantly affected by the different physicochemical properties of alternative fuels, but so far there has been no linear correlation between them observed or extracted.

Combustion characteristics of alternative fuels is one of the most important factors that affect the dynamic behaviours, but its effect is implemented by coupling with inertia force of piston assembly rather than directly acts on the liner structure, thereby resulting in much

complex nonlinear tendencies in dynamic responses. Furthermore, due to the overlapping excitation sources, strong background noise, time-varying transfer properties, severe reverberation and dispersion, both the occurrence time and frequency range of combustion shock-induced and piston slap-induced dynamic events, which are closely associated with combustion properties of fuel types, can hardly be precisely identified and located from measured vibration signals.

Due to the absence of in-depth understanding on generating mechanism of dynamic responses, especially the dynamic deformations, of cylinder liners motivated by combustion of alternative fuels, their consequent influences on the friction and lubrication behaviours between the pistons and liners have not been yet fully studied. While, according to numerical studies performed in this research, the amplitude of liner deformations induced by piston slaps has been proved to be close to the 20% of surface roughness amplitude, which would certainly affect the friction status of cylinder assemblies. In other words, the variations in combustion behaviours of alternative fuels will certainly cause changes in the friction behaviours between pistons and liners. As a result, researchers began studying the influence of liner deformations to friction and lubrication behaviours of IC engines.

To study the effects of cylinder distortions to friction process, many studies have turned to take the static and quasi-static deformations of cylinder liners into consideration in the modelling of film formation and distribution between piston rings-liners. However, under the excitations of combustion shocks and piston slaps, in addition to these elastic deformations, there exist more dynamic deformations associated with structural modes of cylinder liner on the liner surface. The potential influence of these dynamic deformations to cylinder friction is not completely understood.

Furthermore, about whether it is possible to reach friction reduction through superimposing appropriate external vibrations, many theoretical and experimental works have been done in the last decade. However, vast majority of studies on vibration-induced friction reduction were conducted based on limited prototype or mechanical test benches.

There is no experimental study about the influence of additional vibrations to friction reduction has been performed and reported based on an IC engine in actual operations.

Therefore, in this research a validated finite element (FE) model of cylinder assembly considering both the characteristics of structural modes and nonlinearities of assembly constraints is developed for investigating dynamic responses to combustion shocks and piston slaps in a IC engine with alternative fuels. Then the predictions gained from the established model are evaluated against experimental results under different engine operating conditions fuelled with alternative fuels. Based on the validated FE dynamic model, dynamic deformations of liner surface are extracted and introduced into the mathematical model of oil film thickness for predicting the dynamic friction behaviours between the piston rings and liners. Finally, to explore the potential possibility of friction reduction achieved by superimposing external vibrations, a motoring test bench is designed and constructed based on a single-cylinder engine in this research.

1.3 Research Motivation

The motivations for the present study come from a desire to understand the influences of alternative fuels onto the dynamic responses and tribological characteristics of cylinder liners in IC engines. In parallel, it is also driven by the continuous demand of improving engine efficiency. The impacts of alternative fuel usage on the in-cylinder combustion and oil degradation processes have not yet been fully understood. It is essential to investigate the influence mechanisms of alternative fuels upon the dynamic process and tribological behaviour of cylinder liners in order to build a more realistic lubrication model for piston rings and cylinder liners, which can subsequently establish a comprehensive assessment of the influences of alternative fuels on engine dynamic responses and tribological behaviours and possible ways of reduce frictional losses.

As surveyed and outlined in the overviews (see in Chapter 2), clear gaps between previous research works and the practical engineering applications exist in following aspects:

- Limited work on the modelling of cylinder dynamic behaviours considering the characteristics of structural modes and nonlinearities of assembly constraints.

- Limited work on the extraction of feature information from vibration signals related to the structural mode characteristic of cylinder liners.
- Limited work on the influences of cylinder dynamic deformations on the friction and lubrication process of piston-liner pairs.
- No work on the modelling of cylinder lubrication behaviours was carried out by coupling the hydrodynamic lubrication models with structural vibration effects.
- No work is studying the effects of alternative fuels on the lubrication process between the piston rings and cylinder liners.
- No work has been found in investigating the influence of additional vibrations on the friction behaviours of cylinder assembly based on an IC engine in actual operations.

1.4 Research Aim and Objective

1.4.1 Research Aim

The overall aim of this research is to study the influences of alternative fuels' burning on the dynamic responses and tribological characteristics of cylinder liners in internal combustion engines. It further seeks to disentangle the effects of dynamic responses on the friction and lubrication processes between piston rings and liners, by introducing dynamic deformations of liners into a two-dimensional mathematical model of film formation and distribution. Obviously, any achievements in understanding of the correspondence between the friction behaviours of cylinder assemblies with the vibration excitations will possess significance, both in the engine's performance evaluation and dynamic responses analysis, as well as the friction and lubrication monitoring. Even further, a vibration and noise-based non-intrusive monitoring and diagnostic technique for in-cylinder combustion conditions can be achieved, resulting in benefits for design and optimization of multi-component alternative fuels.

1.4.2 Research Objectives

The principal goal of this research is to investigate the potential impacts of alternative fuels usage on the dynamic responses and tribological characteristics of cylinder liners. It

further seeks to study the potential influence of structural vibrations on friction behaviours between piston rings and liners, to pave the way for achieving friction reduction by applying optimized vibration excitations.

To achieve the aim of this research, a number of objectives are identified and prioritised as follows:

- To perform a literature review and identify any gaps in the theory, evidence and knowledge in relation to the influences of alternative fuels on dynamic responses and frictional behaviours of IC engines (see Chapter 2).
- To develop a finite element dynamic model of cylinder assembly for prediction and interpretation of liner responses to two main excitation sources: in-cylinder combustion shocks and piston side-thrust slaps (see Chapter 3).
- To theoretically study the influences of alternative fuels on the excitation sources and their consequent dynamic responses of liners based on the established FE model (see Chapter 4). This includes a diagnostic analysis to explore the localised features of dynamic responses for better understanding of the correspondence between response characteristics and unique combustion properties of alternative fuels.
- To verify and diagnostically analyse the impacts of alternative fuels on the dynamic responses of cylinder liners (see Chapter 6) based on a single-cylinder diesel engine test rig (see Chapter 5).
- To theoretically study the differences in minimum oil film thickness and friction forces of piston-cylinder assembly between the conditions with and without consideration of dynamic deformations (see Chapter 7).
- To explore the influence of additional vibrations on the friction behaviours between pistons and liners, especially the potentials for friction reduction achieved by adjusting frequency and input power of vibration excitations (see Chapter 8).

1.5 Structure of the Thesis

As shown by the flow chart in Figure 1-1, the influences of alternative fuels on the dynamic responses and frictional behaviours of cylinder assemblies, have been studied

based on a FE model, which considering the effects of excitation sources and structural properties. A brief introduction is listed to outline the thesis as follows:

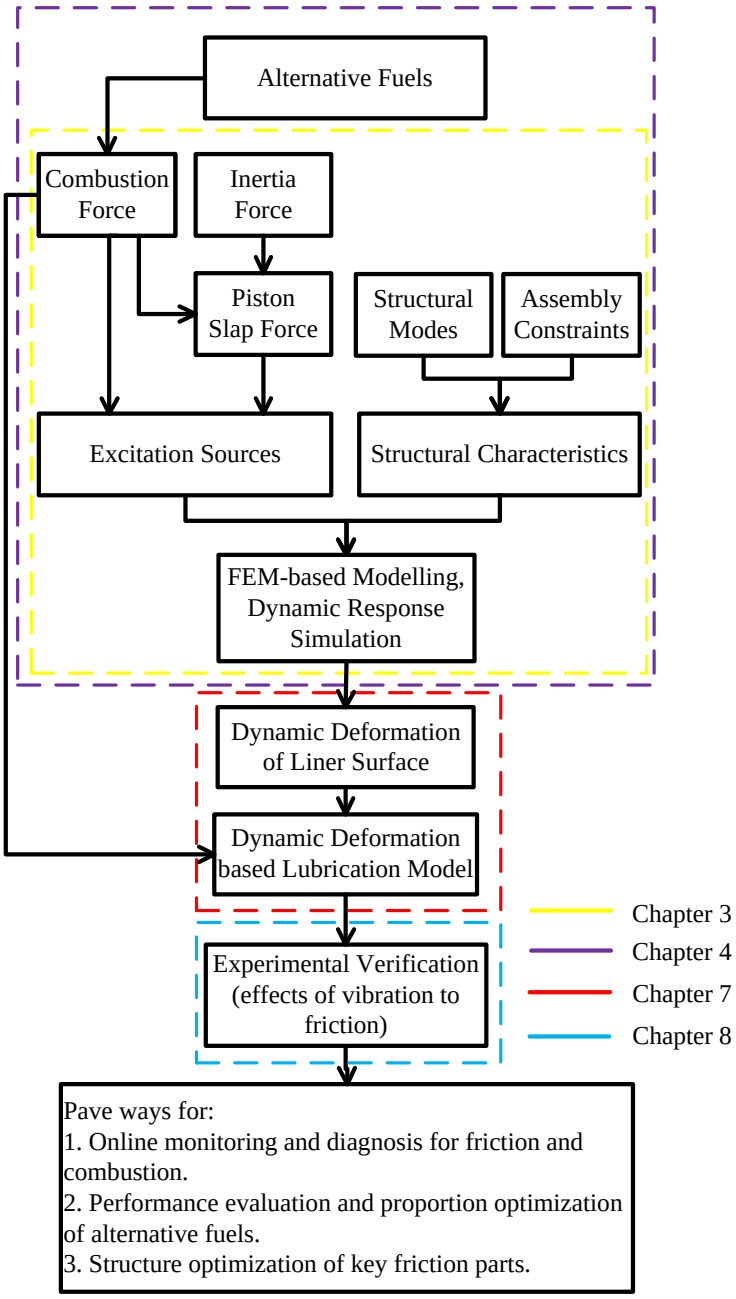

Figure 1- 1 Logical schematics of the research work

Chapter 1 - This chapter presents the motivation and background of this research work and gives a brief introduction to the influences of burning alternative fuels to the

dynamic responses and the tribological behaviours of engines. The aims, objectives and organisation of thesis are also presented.

Chapter 2 - The review of excitation sources of liner vibrations (see Section 2.2), vibration and noise performances of engines (see Section 2.3) and tribological characteristics of cylinder assemblies (see Section 2.4) affected by burning of alternative fuels were presented. Finally, the basic mechanism of vibration-induced friction reduction and its development in mechanical engineering was reviewed in Section 2.5. This assists in avoiding replication of previous work.

Chapter 3 - describes the establishment of a finite element dynamic model of cylinder assembly to predict the dynamic responses of liners under different excitation sources. The model takes into account both the characteristics of structural modes and nonlinearities of assembly constraints when selecting adequate elements for efficient computation of the responses under both the highly nonlinear combustion pressure excitations and subsequent piston slap impacts.

Chapter 4 - According to the physical and chemical characteristics of alternative fuels, the changes in in-cylinder combustion force and piston side-thrust force induced by combustion of alternative fuels are compared and analysed in this chapter. Then the dynamic responses of cylinder liners under respective excitations are calculated and in-depth analysed.

Chapter 5 - details the test facility used for the study and lists the equipment used together with the specifications and operating principles of the rig. Test procedures are also detailed in this chapter.

Chapter 6 - The predictions presented in Chapter 3 and Chapter 4 are evaluated against experimental results. To confirm the generality of the results, the evaluation was carried out under different engine operating conditions, two representative alternative fuels and three lubricating oils.

Chapter 7 - presents the development of a dynamic deformation based lubrication model of film formation with consideration of the liner dynamic deformations. Based on classic hydrodynamic lubrication theory, the dynamic defamation of cylinder liners is

taken into account through a rationally modified shear factors subsequently. The influences of structural deformation on cylinder frictional characteristics are predicted based on the improved model.

Chapter 8 - details the establishment of motoring test bench used for investigating the influence of additional vibrations to friction behaviours between pistons and liners in IC engines. The reduction amplitudes of friction losses corresponding to different excitation conditions (frequency and exciting power) are presented and analysed.

Chapter 9 - summarises the results and conclusions drawn from this research. Furthermore, suggestions are also given for the future work in related research areas.

Chapter 2
Literature Review

To precisely define the research path ways, this chapter presents an in-depth reviews of the literature on the excitation sources of liner vibrations, the vibrational performances of engines and the tribological characteristics of cylinder assemblies affected by the use of alternative fuels. It includes the development of theoretical research, especially the mathematical modelling studying, on the tribo-dynamic behaviours between piston rings and liners. Finally, the basic mechanism of vibration-induced friction reduction and its development in mechanical engineering is reviewed.

2.1 Introduction

Cylinder liners, also known as cylinder sleeves, are the central components of a reciprocating engine. Figure 2-1 shows a typical construction of the cylinder liner. The upper flange of the cylinder liner is connected to the cylinder head and body through bolts, thus limiting its axial degree of freedom. Both the upper and lower external surfaces of the liner are mounted onto the cylinder block within clearance fitting. To prevent the leakage of liquid coolant into the crankcase, the lower end of the wet liner is sealed with the help of a rubber sealing ring rather than be forced constrained with the engine block.

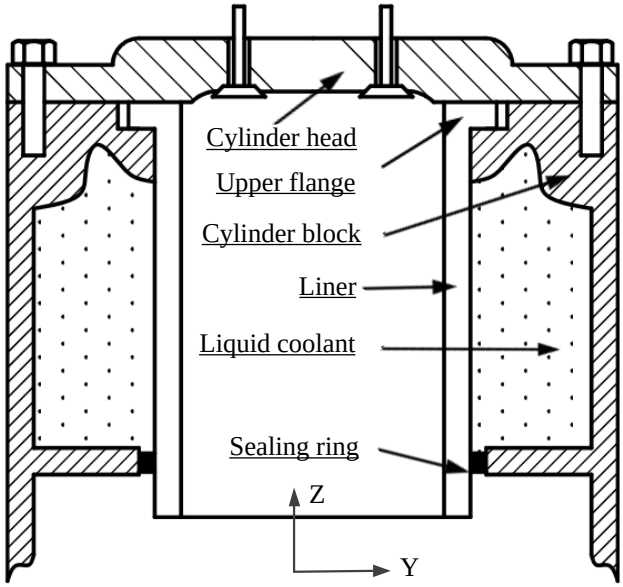

Figure 2- 1 Construction of wet cylinder liner

In addition to forming part of the combustion chamber and swept space in which a piston reciprocates, cylinder liners are also responsible for some additional functionalities associated with operational reliability and mechanical efficiency. These functions of cylinder liners are listed as follows.

1) Heat transfer

The cylinder liner receives combustion heat through the combustion gas, lubricant film, piston and piston rings and transmits the heat into the coolant jacket. Engine designers are always committed to obtaining an optimisation state so that the engine's mechanical

components, especially the piston and cylinder pairs, are not subjected to excessive stresses due to combustion pressure-induced mechanical loading and thermal loading. Meanwhile, to obtain a higher mechanical efficiency, the engine should not lose a significant amount (15% to 35%) of heat in cooling these components [8]. In order to achieve such a condition an optimised structure design of striking a balance between mechanical strength and heat transfer efficiency is essential, and this balance, in turn, determines that the structures of cylinder liners used in different engines, especially diesel engines, substantially follow a uniform geometric shape.

2) Compression gas sealing

The efficiency of the engine depends upon the effective sealing between the piston and liners. Gas leakage will reduce compression pressure and cause serious loss in power output. The cylinder liner prevents the in-cylinder compressed gas and combustion gas from escaping outside. It is essential that a cylinder liner should be built hard enough to resist substantial deformation which may be induced by the high pressure and high temperature in the cylinder chamber.

3) Formation of the sliding surface for piston rings

The cylinder liner, serving as the internal wall of an engine cylinder, forms a sliding surface for the piston rings and piston skirt while retaining the lubricating oil within. The most significant function of liners is their excellent performance as a sliding surface based on four necessary properties described as follows.

- Excellent anti-galling properties
- Less wear on the liner surface
- Less wear on the surface of piston rings
- Less consumption of lubricating oil

Since a longer service life is required of engines for trucks and other heavy-duty machineries, cast iron cylinders with excellent wear-resistant properties have been widely used in heavy-duty diesel engines although, with the recent trend of light-weighting for engines, materials for engine bodies have been shifting from traditional cast iron to

lightweight material aluminium alloys. However, as the sliding surface for the piston assembly, the direct sliding motion of aluminium alloys has weaknesses in deformation during operation and wear-resistance. For this reason, cast iron cylinder liners are still used in most cases.

In addition to increasing the stiffness of the liner material, to enhance the wear-resistant property, another common practice is to optimise the surface texture on the internal surface of the cylinder liner. In other words, high demands are set on the surface finishing of the cylinder liner. In order for the liner to hold a sufficient amount of lubricating oil and to reduce friction between the piston rings and liner wall, the liner surface is typically processed to consist of a mixture of sufficiently deep valleys and smooth plateaus. The scratches in the surface make out a crosshatch pattern and the angle between these scratches is called the crosshatch angle [9]. The distribution of the crosshatch pattern within a cylinder liner can be seen in Figure 2-2.

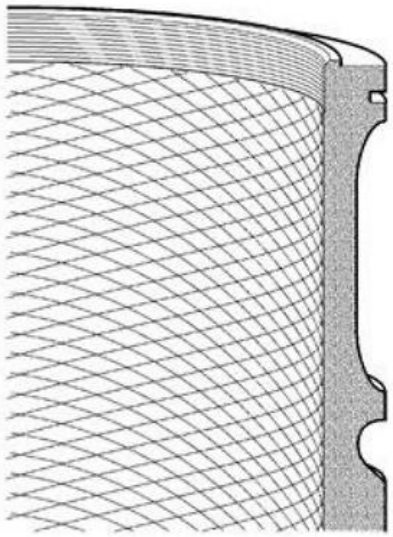

Figure 2- 2 Section view of a cylinder liner with crosshatch pattern[9]

At present, several studies focusing on friction reduction by optimising the surface texture show that the friction and lubrication properties of cylinder can be drastically affected by changes to the geometric morphology of the liner surface. Jeffrey Jocsak's work [10] showed that reducing the honing crosshatch angle from 90 to 30 degrees decreased total

ring-pack FMEP(friction mean effective pressure) by approximately 6%. This shows that the changes of the surface morphology can significantly affect the friction loss of the cylinder assembly. Moreover, in addition to the effect of geometric morphology, the amplitude of liner distortions caused by assembly constraints and mechanical excitations has been proved to be close to the order of surface roughness amplitude[11]–[13], which may also affect the friction behaviour and lubrication characteristics between piston rings and liners. Therefore, it is essential to investigate the generating mechanism and response characteristics of liner vibrations for an in-depth understanding of liner friction characteristics.

Previous studies[14] have shown that over 80% of the total engine vibration and noise emissions can be attributed to the dynamic response of cylinder liners under the excitation of the in-cylinder combustion shocks and its consequent piston slaps, which is higher than the contributions of fuel injection, gear mesh, oil pump, valve impacts and other events. Moreover, this high fraction of vibration implies that dynamic interactions are rather intensive amongst mixture combustions, hydrodynamic lubrication, and liner dynamics. This high fraction of vibration implies that dynamic interactions are rather intensive amongst mixture combustions, hydrodynamic lubrication, and liner dynamics. Therefore, many researches have attempted to understand the generating mechanism of the liner vibrations, specifically about the two main excitations: in-cylinder combustion shocks and piston slaps.

2.2 Excitations of Liner Dynamic Responses

2.2.1 In-cylinder Combustion Shocks

Diesel engines, also known as compression ignition (CI) engines, produce complex vibration and noise emissions whose intensity is strongly dependent on the in-cylinder combustion process. The complex dynamic responses of the cylinder liner near the combustion TDC are essentially due to the harsh and irregular self-ignition of the fuel. In a

diesel engine, the ignition of fuel injected into the combustion chamber is initiated by the high temperature of air-fuel mixture as a result of greatly volume compression (adiabatic compression). This contrasts with spark-ignition engines such as a petrol engine or gas engine (using a gaseous fuel), which use a spark plug to ignite the air-fuel mixture in the combustion chamber.

The essential features of the diesel engine combustion behaviour can be summarised as follows. Fuel is injected by the fuel-injection system into the combustion chamber toward the end of the compression stroke and subsequent power stroke. In the injection process, fuel vaporises and mixes with the high-temperature air in the cylinder. Because the air temperature is higher than the ignition point of fuel under high pressure conditions, the spontaneous ignition of portions of the already-mixed fuel and air occurs after a delay period, which is called the ignition delay period. The in-cylinder pressure increases with the occurrence of the fuel-air mixture combustion. The consequent flame spreading and propagation process shortens the delay period before ignition for the fuel and air, which has mixed to within combustible limits, and which then burns rapidly. Fuel injection continues until the desired amount of fuel has entered the combustion chamber. Atomisation, vaporisation, fuel-air mixing, and combustion continue until essentially all of the fuel has passed through each process. [15].

To obtain quantitative information on the progress of combustion, in-cylinder pressure versus crank angle signal over the compression and power strokes of the engine operating cycle has always been the most direct observations. In-cylinder pressure changes with the crank angle as a result of cylinder volume change, combustion, heat transfer to the cylinder walls, flow into and out of the gap and leakage. The four combustion stages of the overall compression ignition combustion process can be defined and identified based on the heat release rate (HRR) shown in Figure 2-3. The heat release rate can be used to judge the start of combustion, indicating the ignition delay period of the combustion process, the fraction of fuel burned in the premixed mode, and differences in the combustion properties of fuels [16].

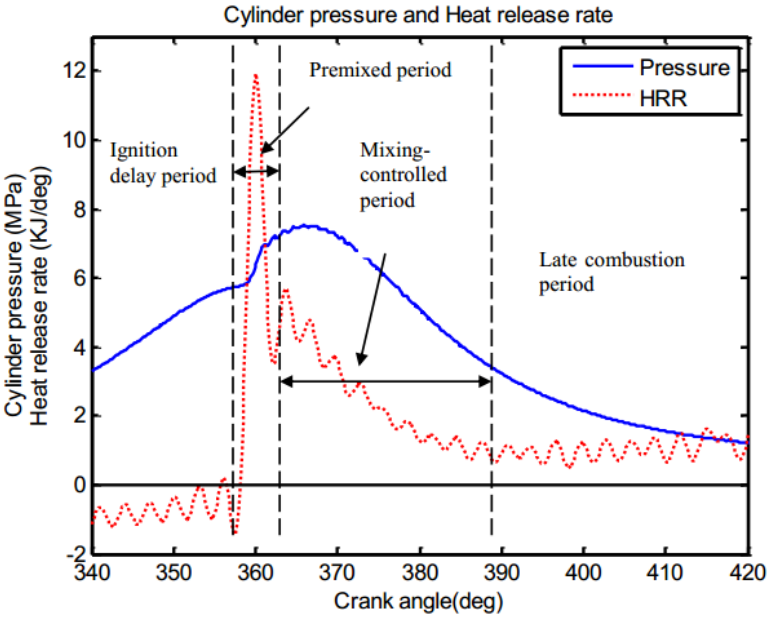

Figure 2- 3 Typical CI engine heat-release-rate diagram identifying different diesel combustion phases [17].

Ignition delay. This is the period between the start of fuel injection into the combustion chamber and the start of combustion (ignition).

Premixed combustion period. In this phase, the combustion of the fuel which has mixed with air to reach combustible limits during the ignition delay period occurs quickly in a few crank angle degrees. When the burning flame spreads to the fuel which becomes ready for burning and burns rapidly during this period, the high heat-release rates characteristic, also known as high pressure rise rate, can be resulted in the premixed period.

Mixing-controlled combustion period. Once the premixed fuel-air mixture has been consumed, the burning rate will be controlled by the mixing rate at which mixture becomes available for burning.

Late combustion period. There are several reasons for the lower rate of heat release in the power stroke. A small fraction of the fuel has not yet been burned. Moreover, a fraction of the fuel energy contained in fuel-rich combustion products can still be released gradually. The intensity of the final burnout processes becomes lower as the gas temperature falls during volume expansion.

During the premixed combustion period, the rise rate of combustion pressure reaches the maximum value of the overall operating cycle, whose frequency content has been proven to be high enough to cover the first few mode frequencies of liner structures. In addition to the rapid rise of combustion pressure itself, combustion oscillations are another serious threat to the structure of cylinder liners. The combustion oscillation occurs in the form of large amplitudes and high frequency (from 3000 Hz to 6000 Hz) pressure waves and heat release fluctuations, which can lead to the structural vibrations of cylinder liners as well as to relevant structural damages[18]. To avoid the harm of structural vibrations caused by combustion shocks, many studies have been performed to understand the generating mechanism of the dynamic responses of cylinder liners to the combustion shocks. R.A. Huls et al. [19] studied the correlation between combustion shocks and the dynamic responses of the surrounding liner structure, revealing that the more severe combustion instabilities can lead to increased sound pressure levels in the combustion chamber and can result in an increased excitation on the liner structure. This means that severe combustion behaviours can exacerbate structural fatigues, which limits the service life span of cylinder liners.

Furthermore, Xiaoyu Wang and Kazuhide Ohta [20] proposed that the dynamic responses of a cylinder liner excited by combustion shocks and piston slaps can contribute to the emergence of cavitation in lubricant film between pistons and cylinder liners. W.W.F. Chong and M. Teodorescu[21] et al. found that the cavitation occurring in lubricant film can usually survive as a confined bubble at the leading edge after the reversal of the piston movement direction near the combustion top dead centre (TDC). Although these cavitation regions only sustain for a brief period, together with a very low entrainment motion and high normal loads, the shock-induced cavitation still lead to thinner films and higher friction forces. These studies showed that combustion shocks can directly and indirectly affect the structural vibration and tribological characteristics.

In fact, the cylinder liner undertakes not only the harsh combustion shocks but also the strong piston slaps, which might affect the frictional behaviour and oil consumption of cylinder assembly while it contributes significantly to engine vibration and noise emissions.

2.2.2 Analysis of Piston Slap Phenomenon

Piston slap is a common knock phenomenon existing in IC engines. Piston slap excites the cylinder liner and manifests itself in the form of surface vibrations, which are eventually radiated as airborne noise emissions in the vicinity of the engine. In addition to the perceived benefits for engine noise, vibration and harshness (NVH) performance monitoring, a good understanding of the generating mechanism of piston slaps can be helpful for revealing the causal relationship between the piston movements and cylinder vibrations [22].

Bradbury, Meier and Hempei [23] were among the first to study the mechanism of vibration and noise generation in IC engines. Their work showed the importance of piston slap as a major excitation source of cylinder vibrations in the majority of operating conditions. Ungar and Ross [24] also studied the effects of piston slaps in reciprocating machines and found that the piston slap-induced noise accounted for approximately 40% of the total noise emissions. It is essential to investigate the causal relationship and correspondences between the piston slaps and structural responses.

To summarise, a basic dynamic model of piston lateral movement based on earlier research can be established and drawn as shown in Figure 2-4. In addition to the direct impact on the cylinder wall, combustion force can also drive the piston assembly to move along the cylinder with a relatively constant angular speed mainly maintained by the flywheel. Due to the periodically changing pendular angle of the connecting rod, a periodically changing side-thrust force can be decomposed from the longitudinally acting combustion force and inertial force of the moving piston assembly. This side-thrust force pushes the piston assembly from one side of the cylinder wall skipping onto the other side, thereby leading to the unceasing slap impacts on the cylinder liner [25].

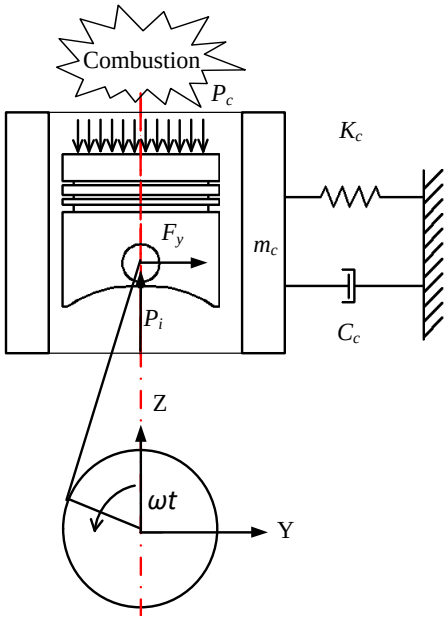

Figure 2- 4 Dynamic model of cylinder assembly

Mainly maintained by the flywheel, the crankshaft can be considered to be rotating at an unvarying speed, i.e., ω is constant. Based on this assumption, the specific expression for the piston lateral displacement x_p in terms of the crank angle ωt can be derived as [26]

$$x_p = r_c(1-\cos\omega t) + l(1-\sqrt{1-\lambda^2\sin^2\omega t}) \qquad (4.1)$$

where $\lambda = r_c/l$, r_c is the crank radius and l is the length of the connecting rod.

Furthermore, Eq. (4.1) can be simplified into a first-term approximation form [25]

$$x_p \approx r_c(1-\cos\omega t) + \frac{1}{2}\lambda^2\sin^2\omega t \qquad (4.2)$$

As illustrated in Figure 2-4, the side-thrust force of the piston assembly toward the cylinder wall can be decomposed from the longitudinally acting combustion force P_c and the inertial force of the moving piston assembly $P_i = m_1 r_c \omega^2(\cos\omega t + \lambda\cos 2\omega t)$ (m_1 is the equivalent mass of the piston assembly). Along with the periodically changing pendular angle of the connecting rod, the side-thrust force is also periodically changing, with a

periodic term $\sin \omega t / \sqrt{1+(\lambda \sin \omega t)^2}$, which pushes the piston assembly to skip from one side to the other side. Finally, the piston side-thrust force can be derived as[25]

$$\begin{aligned} F_y &= (P_c - P_i)\lambda \sin \omega t / \sqrt{1+(\lambda \sin \omega t)^2} \\ &= P_c \times \lambda \sin \omega t / \sqrt{1+(\lambda \sin \omega t)^2} + P_i \times \lambda \sin \omega t / \sqrt{1+(\lambda \sin \omega t)^2} \\ &= F_c - F_i \end{aligned} \qquad (4.3)$$

By introducing the engine parameters and in-cylinder combustion pressure F_c measured from the test engine QCH1110 into Eq. (4.3), the side-thrust force at 1800 rpm and 40 Nm can be calculated as shown in Figure 2-5.

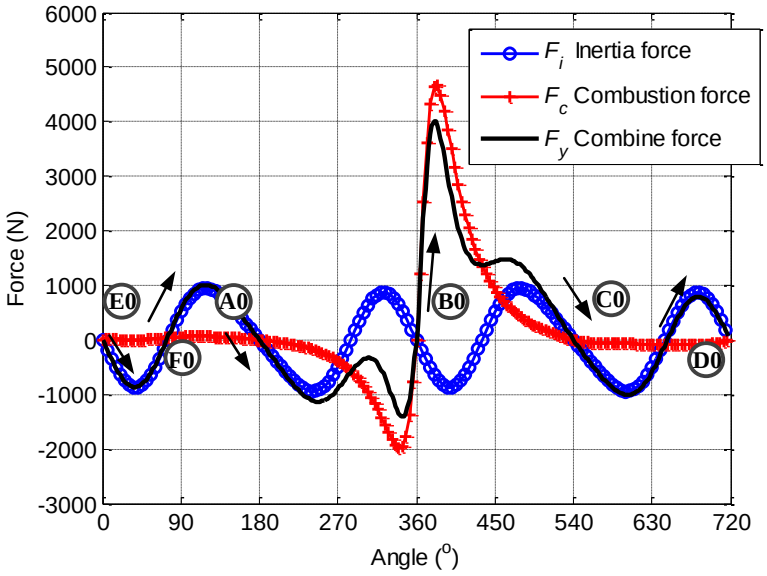

Figure 2- 5 Composition of the piston lateral force

In Figure 2-5, it shows a typical characteristic of the side-thrust force, obtained based on the engine in this study. Every time the combined side-thrust force F_y passes zero and changes direction (from positive to negative, or vice versa) means a possible occurrence of piston-slap impact on a definite position along the cylinder wall. In this instance, there are 6 slap impacts occurring in the four-stroke working cycle, which are denoted as Impact Ⓐ0 – Ⓕ0 respectively as illustrated in Figure 2.5 [22], [27]. Obviously, the force amplitude of

Impact ⑧⓪ occurring around the power TDC at 360 ° is the most significant one. It will results in a higher impact and appears in the similar angular position to the combustion shock, making it difficult to separate these two effects in measured responses.

However, due to the overlapping excitation sources, strong noise background, time-varying transfer properties, severe reverberation and dispersion, neither the occurrence time nor the frequency range of combustion-induced and piston slap-induced dynamic events can be precisely identified and located from measured vibration signals. In addition, there is a certain phase delay between the numerical predictions and observed events in measured signals cannot be well explained just by the sign changes of piston side-thrust force [27]. This shows that the characteristic of excitation source (sign change of piston side-thrust force) alone is not sufficient to predict and characterize the influence of piston slaps on structural response.

To seek a quantitative correspondence between the piston slaps and structural responses, based on the calculated piston side-thrust force, many researches have been carried out to better understand the number and location of observable events induced by piston slaps in measured vibration signals. In earlier research, mathematical models of piston dynamics have usually neglect its tilting motion around the piston pin [24] or have just applied constrained Lagrangian dynamics to consider the partial reactions due to piston tilting [28]. The structural analysis of cylinder liners has been reported using finite element analysis (FEA) [29]–[31]. The static deformation, forced response analysis and frequency response analysis of cylinder liners have been undertaken based on finite element models, for impact force calculation and liner response analysis [30]. These studies have led to in-depth understandings of the correspondence between the excitations and the dynamic response of liners.

As stated, the lateral movement of piston assembly is driven by a component force decomposed from the combustion force and inertial force of piston assembly itself,

indicating that any change in the combustion status is bound to affect the piston side-thrust force and response characteristics of cylinder liners.

Due to the different physicochemical properties, the combustion of alternative fuels can cause many differences in the burning characteristics and subsequent piston side-thrust force, thereby resulting in obvious changes in the dynamic responses of cylinder liners. Therefore, an in-depth understanding on the influence of the usage of alternative fuels on the vibration characteristics of IC engines is clearly needed.

2.3 Impacts of Alternative Fuels on Engine NVH Performance

The type of fuel used in an IC engine directly affects the noise, vibration and harshness (NVH) performance of its structure. Although the frequency range of the dynamic response is mainly determined by the structural properties, the vibration intensity produced depends on the details of the explosion inside the cylinder chamber and therefore on the type of fuel burned [32].

The realisation of dwindling fossil fuel supplies and their adverse environmental impacts has accelerated a great deal of research and development activities in the domain of renewable energy sources and technologies. It has been shown by many researches and small-scale applications that the use of alternative fuels such as biodiesel, ethanol and methanol blends can be feasible as burning such fuels in a diesel engine can produce the desired power and an emission level similar to that of petroleum diesel. In the meantime, it has also been observed that there are many significant differences of using such fuels in terms of combustion behaviours, burning residuals, vibration and noise emissions, which might be attributed to their significant differences in physical and chemical properties.

These differences may be clear evidence that alternative fuels can result in many effects on engines, which includes their influence not only on power output performance and emission levels but also on the changes in the dynamic processes of critical components, friction losses, overall service life spans and associated maintenance activities. It is

essential to understand the physical and chemical characteristics of alternative fuels in depth.

To guarantee the representation of alternative fuels selected in this study, this chapter examines two types of alternatives to diesel: biodiesel and methanol-diesel blended fuel, which have been tested to be able to produce the required power and emissions, to study the potential effects of alternative fuels on the engine NVH performance.

2.3.1 Biodiesel

The application of biodiesel in internal combustion engines has a history as long as the diesel engine. When Rudolf Diesel launched his prototype of the compression ignition (CI) engine for the first time in Augsburg, on 10 August 1893, the fuel supplied for the first CI engine was nothing but peanut oil.

Biodiesel generally means a vegetable oil or animal tallow-based alternative fuel to diesel consisting of long-chain alkyl esters. Biodiesel is designed to be used in standard compression ignition engines as an alternative fuel to diesel. Compared to low sulphur diesel fuels, biodiesel possess promising lubricating properties and cetane numbers. The low calorific value of biodiesel is about 37.27 MJ/kg, which is 12% lower than standard fossil diesel. Biodiesel has a density of about 0.88 g/cm ^{3}, higher than fossil diesel (~ 0.85 g/cm ^{3})[33]. The physical and chemical properties similar to diesel make it possible to fuel CI engines with biodiesel without modifying engines.

Since diesel engines are not specifically designed for biodiesel fuel, the impact of burning biodiesel on the NVH performance and the operating condition of diesel engines need to be analysed. Biodiesel has a higher cetane value, which means that it is much easier to ignite after being injected into the combustion chamber. Advanced ignition or earlier premixed combustion can effectively shorten the ignition delay period, thus reducing the peak of pressure rise rate. It can be inferred that the burning of biodiesel may be helpful to reduce the dynamic responses of engines.

In fact, many experimental studies have partially confirmed the inference about the vibration performance of burning biodiesel. Erinç Uludamar et al. [34] proposed that, due to the high oxygen fraction, the combustion quality of biodiesel is better than conventional fossil diesel. The average of engine vibration fuelled with biodiesel decreased by 3.72% compared with fossil diesel. Smoother combustion with the usage of biodiesel means lowering the vibration emissions of the engine body.

However, as Ahmad Taghizadeh Alisaraei et al. [35] found, with an increase of the operating speed, especially at high-load conditions, the blended fuel consisting of biodiesel and diesel with a blending ratio from 20% to 40% (biodiesel in blended fuel=20% to 40%) shows much more intense vibration and noise emissions than the diesel under high speed operating conditions. This can hardly be explained just by the combustion characteristics of biodiesel, whether the shorter ignition delay or higher flammability.

2.3.2 Methanol-Diesel Blended Fuel

Methanol, also known as methyl alcohol, is a chemical with the formula CH_3OH (often abbreviated to MeOH). Methanol is produced from fossil or renewable resources such as coal, natural gas, residual oil and biomass, and is considered as one of the favourable alternative fuels to fossil fuels with its advantages of low price and high oxygen content.

Methanol-diesel is a blended fuel composed by methanol, diesel and relevant additives. However, due to the difficulty in forming a stabilised blend fuel of methanol and diesel, few reports of previous work have been found on the experimental investigation of methanol-diesel blends in a compression ignition engine. As the solvent polarity of methanol (0.762) is much greater than that of diesel (less than 0.2), the methanol can be infinitely dissolved into the water rather than the diesel. The high proportion of methanol in diesel blended fuel can hardly be prepared and kept for the long term. Z. Huang[36] and C. Sayin[37] investigated the influence of methanol–diesel blended fuels usage on the power performance and exhaust emissions of engines. It was shown that brake specific fuel consumption (BSFC) increased while mechanical efficiency decreased with the

blending ratio of methanol in diesel. Nagafi and Yusaf [38] found that the effective power and torque of an engine fuelled with methanol-diesel blends were higher compared to standard fossil diesel fuel. These studies indicate that the combustion of methanol-diesel blended fuel can intensify the combustion behaviours in combustion chambers, which may lead to the deterioration of engine vibrations.

To fully understand the impact of methanol fuel properties on combustion behaviours, many research works have been done on the combustion characteristics of methanol-diesel blended fuel. Zuohua Huang et al. [39] investigated the basic combustion behaviours of a CI engine fuelled with methanol-diesel blended fuels. Their research illustrated that increasing methanol mass fraction in methanol-diesel blends resulted in the growth of the pressure rise rate in the premixed combustion period and the shortening of the combustion duration of the mixing-controlled combustion period. To explore the chemical kinetic mechanism behind these combustion behaviours, Li et al. [40] established an enhanced multi-disciplinary model embedded with a basic chemical kinetics mechanism to study the combustion characteristics of methanol-diesel blended fuel burned in a compression ignition engine. Their simulation results indicated that, with an increase in the fraction of methanol, the smaller cetane number of methanol resulted in extended ignition delay and higher burning rate at the premixed combustion period, increasing the peak of pressure rise rate and combustion intensity. The phenomenon of retarded ignition timing, or extended ignition delay, has been confirmed by the studies of Zhang[41] and Wang et al. [42]. Their investigations indicated that the ignition delay of engine combustion fuelled with methanol-diesel blended fuel increased gradually with an increase in the methanol mass fraction in blends. Both the maximum cylinder pressure and the maximum rate of pressure rise, showed an obvious increase along with an increase of the methanol fraction. As in the above mentioned exploration and the case analysis, the maximum rate of pressure rise and the maximum heat release rate of the compression ignition engine can be increased by increasing the methanol fraction. Based on these theoretical researches, methanol had been regarded as an alternative fuel would produce much more vibration and noise emissions.

Nevertheless, the NVH performances of a CI engine fuelled with methanol-diesel blend fuels are often reported to produce less vibration and noise emissions under higher operating speeds [43]. Ioannis Gravalos et al. [44] constructed an algorithm for studying the effects of the rapid burning characteristics of methanol-diesel blended fuel on the engine vibrations. Their study showed that the vibration amplitude of the engine block fuelled with the methanol-diesel blended fuel was lower at low frequencies around 1500 Hz compared to the fossil fuel. Most researches have claimed that the improved NVH performance, or weakened vibration emission, of engines fuelled with methanol-diesel blends should be attributed to the shortened ignition delay period as a result of the combustion-supporting characteristic of the high oxygen fraction, as seen in the formula CH_3OH[45]. As another oxygenated fuel, although biodiesel possesses relatively less oxygen fraction compared with methanol, it produces even worse NVH performances than the methanol-containing fuels. It indicated that the NVH performance of methanol-diesel blended fuels cannot be well interpreted simply by a single property of the fuel.

These complex nonlinear relationships between the engine NVH performance and fuel types hinder the researchers from reaching a full understanding of the influences from the combustion characteristics of alternative fuels on the engine vibrations. It further restricts an in-depth investigation into the potential impacts of alternative fuels on the dynamic deformations of liners and their consequent effects on the friction characteristics.

To study how the combustion of alternative fuels affects the tribological characteristics of cylinder liners in a direct way, it is essential to first survey the possible influence of liner deformations, as a medium, on the friction behaviours of the cylinder assemblies.

2.4 Influences of Liner Deformations on Cylinder Friction

The first modelling and calculation on the lubrication between the piston ring and cylinder liner was achieved by Castleman [46]. In the 1950s, Eilon and Saunders [47] estimated the oil film thickness on the cylinder wall based on a balance of forces acting radially on rings. They first estimated the mean oil film thickness at around 0.5~10 microns. Ting and Mayer [48], [49] established a mathematical model for describing the friction and lubrication behaviour based on hydrodynamic lubrication theory for an internal combustion engine in a whole operation cycle. They introduced the piston ring geometric and elastic characteristics into the lubrication model and got a good agreement between the predicted and measured results. But, they work did not take account the surface roughness into their lubrication model.

Patir and Cheng [50], [51], Greenwood and Tripp [7] improved the average Reynolds equation for the consideration of surface roughness between matched surfaces. They proposed the pressure and shear flow factors based on a series of numerical flow simulations. Based on the researches done by their predecessors, Priest and Taylor [52] investigated the friction behaviours of the engine cylinder with a special emphasis placed on surface topography and found that the film thickness ratio and the surface topography can drastically affect the friction and wear characteristics of piston-cylinder pairs.

More and more factors are considered in the modelling of cylinder lubrication, pushing the numerical evaluations even closer to the experimental results. However, since most theoretical models for estimating the oil film thickness and friction forces have been developed based on the assumptions that the surfaces of the rings and liners are smooth on macrostructure and have good circumferential conformity[23], the potential impacts of liner deformations, especially the structural modes-related dynamic deformations, to the friction characteristics of piston-cylinder pairs have not been well investigated.

In fact, no cylinder liner is perfectly cylindrical or of nominal bore radius along its entire length. The liner distortion leads to loss of conformity between the piston rings and cylinder liner. As a result of liner deformation, the drop of piston ring follow-up

performance can cause the uneven contact and increased friction[53]. Therefore, it is essential to quantitatively study the deformation of cylinder liners. Chittenden and Priest [54] first proposed that the non-circularity of the engine cylinder liner can be represented by a Fourier series:

$$R(\phi) = \sum_{i=0}^{i=n} (A_i \cos\phi + B_i \sin\phi) \qquad (4.4)$$

where:

$R(\phi)$ = radial co-ordinate

ϕ = angular co-ordinate

A_i, B_i = amplitude constants

i = order

n = highest order distortion to be considered

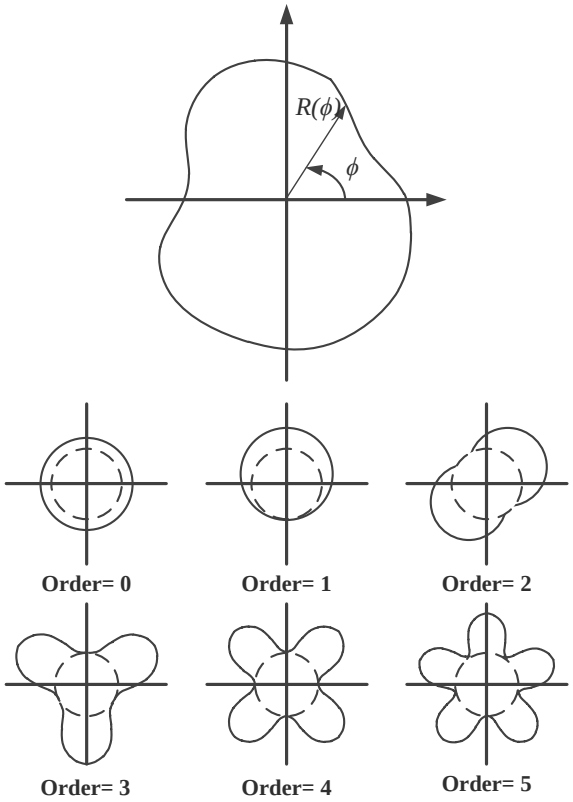

Figure 2- 6 Cylindrical coordinate system and Fourier orders

The coordinate system and various Fourier orders of liner distortion have been drawn in Figure 2-6. There are several reasons for the non-circularity of the cylinder liners. The machining precision of the cylinder liner is defined, or limited, within an allowed difference between the maximum and minimum diameters of the liner, which may be from 10 to 100 times the film thickness between piston rings and liner. Thus, the nonconformity arising from machining tolerances is likely to impose a substantial effect on the friction characteristic of the piston-cylinder assembly. The zero-order and first-order liner distortions, as a function of the size and location tolerances of the cylinder liner [54], have been drawn in Figure 2-6. As these deformation components are circular, they have little consequence to conformity between piston rings and liners.

The assembly constraints of cylinder assembly can cause significant deformations in the liner. One typical case is the tightening of the cylinder head bolts. Chittenden and Priest

pointed out that[54] the tightening of four cylinder head bolts is the main reason for the occurrence of the fourth-order distortion approximately 25 microns in a distorted cylinder liner of a light-duty engine.

Insufficient cooling or over-cooling of cylinder liner may lead to expansion deformations around the circumference of the cylinder and along its length, which leads to the distortion of the cylinder liners [54]. Reipert and Voigt[55] proposed that the magnitude of the thermal expansion is greater by far than the distortion caused by the clamping of cylinder head bolts. But the thermal expansion is primarily a quasi-static deformation, with good radial continuity, which cannot cause obvious dynamic localised deformation on the liner surface, and therefore cannot cause direct impact on the friction and lubrication behaviour between piston rings and liner surface.

In addition to static deformations, the impulsive gas explosion can also cause evident distortion of the cylinder liner, although it only acts on the liner wall within a restricted area. Furthermore, as Chittenden and Priest [54] pointed out, a significant deformation of the cylinder liner induced by combustion force can only be observed in those heavy-duty diesel engines with thin-walled wet liners. However, they did not make a detailed study of piston slap-induced deformations, which led to them ignoring the effect of dynamic deformations on the friction and lubrication behaviours. To investigate the possible influence of liner deformations on friction and lubrication behaviours between piston and liners, several studies have been carried out. M.T. Ma et al. [11] studied the impacts of liner distortion on the friction forces between the piston rings and cylinder liners. Their simulation results showed that the distortion of the cylinder liner can considerably reduce friction loss by approximately 2% to 5%, but will also drastically increase the net quantity of lubricating oil transported into the combustion chamber. Another study conducted by G. Ali Usman et al. [56] pointed out that a distorted cylinder liner will decrease the viscous friction force of piston ring cylinder liner interface because the average film thickness between ring and distorted liner is much higher than that of circular liner. Lipu Ning et al. [57] conducted a numerical study involving the piston skirt and liner system lubrication considering the thermal and elastic deformation of the cylinder liner due to the combustion

pressure and the piston inertia. The results showed that, when considering the effects of the thermal distortions of the cylinder liner, the piston and liner assembly may run in a safer situation because the minimum oil film thickness (MOFT) is thicker than the original model by up to 20%, and the friction losses are correspondingly decreased by approximately 4% than the original prediction. F.M. Meng et al. [58] further indicated that the vibration of the cylinder liner can result in fluctuations in the dynamic and tribological performances of the piston assembly, especially in the power stroke of an IC engine. Their studies have shown that the vibration-induced friction reduction is closely related to the engine's running speed, structural stiffness, damping characteristics and the mass of the cylinder structure. The experimental study conducted by Michael Gore et al. [59] strongly confirmed the existence of fluctuations in the piston friction force through a direct measurement, as seen in Figure 2-7. Their work suggested that this kind of friction fluctuation may be associated with a multitude of engine structural harmonics.

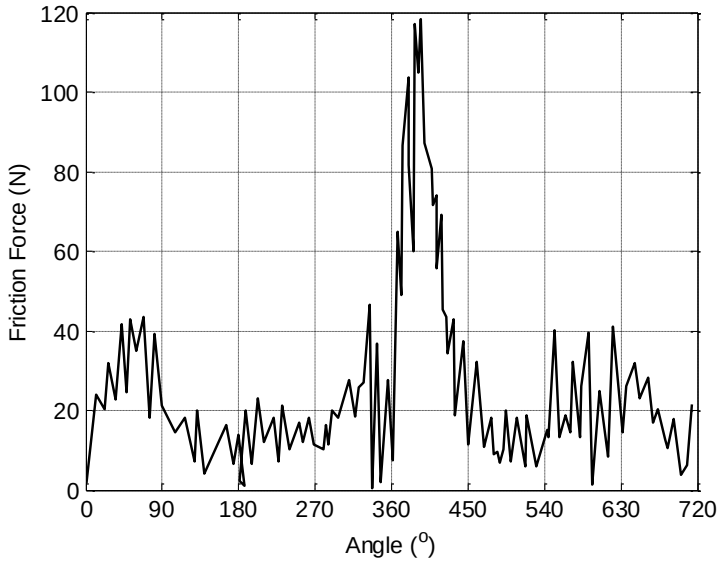

Figure 2- 7 Measured friction under fired conditions at an engine speed of 2500 r/min and a torque of 72 Nm [59]

However, none these experimental and theoretical studies have provided more vigorous evidence or in-depth discussion on the mechanism behind the correspondence between the

structural deformations and friction fluctuations. More in-depth research is needed to determine the exact way in which liner deformations affect the friction forces.

2.5 Vibration-Induced Friction Reduction

As previously mentioned, the dynamic response of the cylinder liner affects the friction and lubrications between the piston rings and liners. To find out whether it is possible to improve the lubrication condition to achieve a reduction in the friction between piston rings and liners, a brief review of vibration-induced friction reduction is presented as follows.

It has been proved that the magnitude and characteristics of the friction forces can be significantly changed by imposing high frequency micro-vibrations on the friction pair. Many researches have been carried out to exploit this phenomenon under various conditions [60]–[64]. The friction reduction has been explored according to changes in the magnitude and frequency of the normal load, or changes in the magnitude and direction of the resultant sliding velocity, including the case of vibration acting parallel or perpendicular to the sliding direction. The impacts of normal vibration on friction behaviour have been studied by Wiercigrocha M and Hess D P et al. [64], [65]. Their studies suggested that the normal dynamic load can cause a reduction in the actual area of contact and a corresponding reduction in friction loss up to 10% for certain situations.

In order to improve understanding of normal vibration induced friction reduction mechanism, D. M. Tolstoi[66] and Douglas Godfrey [67] studied the impact of additional normal vibrations on the friction reduction. It was found that the normal vibrations affect the mean surface separation of matched surfaces, and therefore reduce the real area of contact. More specifically, V. C. Kumar and I. M. Hutchings [68] studied friction reduction in the presence of additional ultrasonic vibrations, in which an obvious reduction approximately 80% in the friction force was observed with amplitude of additional vibration up to 10 micrometres at 20 kHz. Their research showed that when an ultrasonic

movement in the contact surface plane is perpendicular to the sliding direction, it can lead to variations in the direction of total relative movement, and accordingly cause the reduction of time-averaged friction forces in the sliding direction to a certain extent. Their study showed that, as one of vibration actuator, ultrasonic vibrator can effectively reduce the friction loss between contacting surfaces without filling of lubricating oil.

In addition to normal vibrations, the influence of tangential vibrations acting on the surfaces has also been studied. Oscillatory normal force components always accompany the real oscillatory friction force, thus yielding bending waves and transverse vibrations in the matched surfaces. In [68], experiments on samples of aluminium alloy, copper, brass and stainless steel sliding against tool steel were conducted. The experimental results indicated that tangential vibrations can also induce an observable reduction in friction forces. Good agreement was obtained between the measured friction forces and the predictions of the two theoretical models for the influences of longitudinal and transverse additional vibrations in contact surfaces. It has been concluded that the longitudinal additional vibration can produce a greater reduction up to 80% in the friction force than the transverse one approximately 40% under the same exciting amplitude and frequency.

More specifically, the impacts of additional vibrations on the tribological characteristic of the cylinder structure have been preliminarily studied in recent years, although mostly based on a pneumatic cylinder. Dongkyun Lee et al.'s [69] study has shown that the superimposition of ultrasonic excitations can reduce stagnation-related static friction or stiction, particularly in microscopic mechanical contacts. The ultrasonic excitations can release a stuck surface from bonds or junctions. A comprehensible interpretation is that the vibration pulses deliver additional momentum and vibration energy, thereby prompting the micro-junctions between contact surfaces to release them from serious stuck status. It also imparts energy to the liquid filled in asperities, to enable them to have micro-flowing and redistribution. Cheng Tinghai et al. [70], [71] investigated the static friction reduction using ultrasonic vibrations in a pneumatic system with a cylinder as the actuator. Their study showed that the ultrasonic vibrations can reduce static friction by approximately 40%, compared with the non-excitation case.

As stated above, theoretical and experimental investigations about vibration-induced friction reduction indicate that the friction loss of matched surfaces can be dramatically reduced by applying additional vibrations, which is promising for guiding the optimisation design aiming at an improvement of mechanical efficiency. However, the present studies used to be conducted within limited prototypes or mechanical test benches, rather than machines in actual operations. Especially for the cylinder liners used in IC engines, experimental studies on the influence of additional vibrations on friction reduction have not been studied or published, so far.

2.6 Observations from a Review of the Literature

The observations from reviewed articles point to combustion-induced dynamic responses of cylinder liners and their consequent impacts on the friction and lubrication characteristics of cylinder assemblies. It seems certain that the dynamic responses of cylinder liners affect the frictional and lubrication characteristics between the piston rings and liners, and that the changes in combustion behaviour caused by the usage of alternative fuels may further diversify these friction characteristics. Therefore, it is essential to study the influences of alternative fuel usage on the dynamic responses and tribological characteristics of cylinder liners in depth by coupling the hydrodynamic lubrication models with structural vibration effects, for improving the mechanical efficiency, NVH performance and service-life span of IC engines fuelled with alternative fuels.

The review of the literature has also shown that few investigations on the correspondences between in-cylinder combustion behaviours and the dynamic responses of liners have been performed for revealing the effects of fuel properties on the friction behaviours. It is the lack of an in-depth understanding of the dynamics mechanism of cylinder vibrations, especially on the dynamic deformations induced by combustion shocks and piston slaps, that has hindered further research on the influence of structural vibrations on cylinder frictions. This is why the existing studies only mentioned or confirmed the existence of

impacts from structural vibrations on the tribological characteristics of cylinder liners, but did not provide more vigorous evidence or in-depth discussion on the mechanism behind them. Moreover, the question of whether an additional vibration with proper characteristics can help to achieve a reduction in friction forces, has yet to be studied based on the practical operations of IC engines.

Therefore this research work aims to reduce this gap and develop a series of validated numerical models for revealing the influences of alternative fuel burning on the dynamic responses and tribological characteristics of liners in a single-cylinder diesel engine.

Chapter 3

Development of a Finite Element Model for Predicting Dynamic Responses of Cylinder Liners

This chapter describes the establishment of a finite element dynamic model of piston-cylinder assembly to predict the dynamic responses of liners under two main excitation sources. The model takes into account both the characteristics of structural modes and nonlinearities of assembly constraints when selecting optimal elements for efficient computation of the responses under both the highly nonlinear combustion pressure excitations and its subsequent piston slap impacts. Then, based on the established model, the causal relationship and correspondences between the localised response features with the excitation sources were analysed. The analysis results show that the dynamic responses of cylinder liner are highly relevant to modal characteristics of the liner structures and its mounting to the cylinder body.

3.1 Introduction

The piston assembly is one of engine's subsystems that determine the performances of friction, lubrication, noise, vibration and hence service lifespan. Previous studies showed that 80% of the total engine vibration and noise emissions can be attributed to the dynamic process of cylinder liners excited by the in-cylinder combustion and its consequent piston slaps [14]. Moreover, this high fraction of vibration implies that dynamic interactions are rather intensive amongst mixture combustions, hydrodynamic lubrication, and liner dynamics. Therefore, active researches have been carried out in order to improve the dynamic behaviours of cylinder liners.

Structural analysis of cylinder liners has been reported using finite element analysis (FEA) [29]–[31]. The static deformation, forced response analysis and frequency response analysis of cylinder liners were undertaken based on finite element models, for impact force calculation and liner response analysis [30]. However, the majority of these FEM-based studies were performed based on a quasi-static model which the modal characteristics and reaction upon piston of cylinder liners were neglected. Obviously, such models may not be able to reflect the phenomena of true contacts between piston and cylinder due to inventible elastic deformations under dynamic forces.

Compared to shell elements, solid elements can better describe the geometric details of liner flanges, to facilitate the modelling of more realistic boundary conditions, although it comes at the cost of longer solution time [72]. To enhance the computing efficiency, Jafari et al. [31] derived the dynamic response of cylindrical shells using mode superposition method, which is recognized as the most powerful method to solve the equation sets of linear system considering the required solution time. While the contact constraint widely existed in cylinder assembly is a typical nonlinear kinematic pair, which cannot be handled by the mode superposition method [73]. To compensate, based on a direct Newmark integration method, Hirotaka Murakami et al. [30] implemented the structure analysis of piston-cylinder assembly, coupling with multi-body dynamics analysis. However, due to

excessive requirement for computational sources, numerical prediction of cylinder dynamic responses contain modal frequencies has not yet been achieved.

To gain an in-depth understanding of the dynamic responses of cylinder liners to in-cylinder combustion shocks and piston slaps, a finite element dynamic model was established in this chapter, which takes into account both structural modal characteristics, nonlinearities of assembly constraints and time-varying exciting forces.

3.2 Establishment of Finite Element Model of Cylinder Assembly

3.2.1 Meshing and Solution Algorithm

Compared with shell elements, solid elements can better describe the geometric details of liner flanges in achieving a more realistic boundary condition, although it comes at the cost of longer solution time. For the balance between better accuracy and efficiency, hexahedral elements are adopted for three-dimensional meshes. To obtain the localised instantaneous deformations on the flanges at top end and the overall cylindrical shell, the model was configured to have 7121 hexahedral isoparametric solid elements using ANSYS Workbench. This finer element mesh arrangement is also taken into account that the vibration can have frequency contents as high as 20kHz which was estimated based on an analytic analysis when the liner is assumed to be an uniform cylindrical shell [74]. To reduce the need for solution time and computing sources, the external surface of the liner and the other components were treat as rigid body in modelling.

For dynamic simulations, modal superposition method is the most powerful method to solve the set of equations considering the required solution time. But, this method cannot handle the nonlinearities when the contact constraint is applied to the cylinder assembly[73]. Thus, the Newmark implicit integration method was used to solve nonlinear model in the cylinder dynamic simulation[75]. To improve the computing efficiency, the reduced method, one subclass of Newmark implicit integration method, was adopted to solve the motion equations of dynamic process.

3.2.2 Material and Boundary Conditions

Wet liners, or sleeves, are widely used in heavy-duty diesel engines, which allow engines to undertake high combustion loads without overheating because the coolant is in direct contact with the sleeve. A wet sleeve is essentially a stand-alone cylinder, supported at the top and bottom by the block, and surrounded by the water jacket.

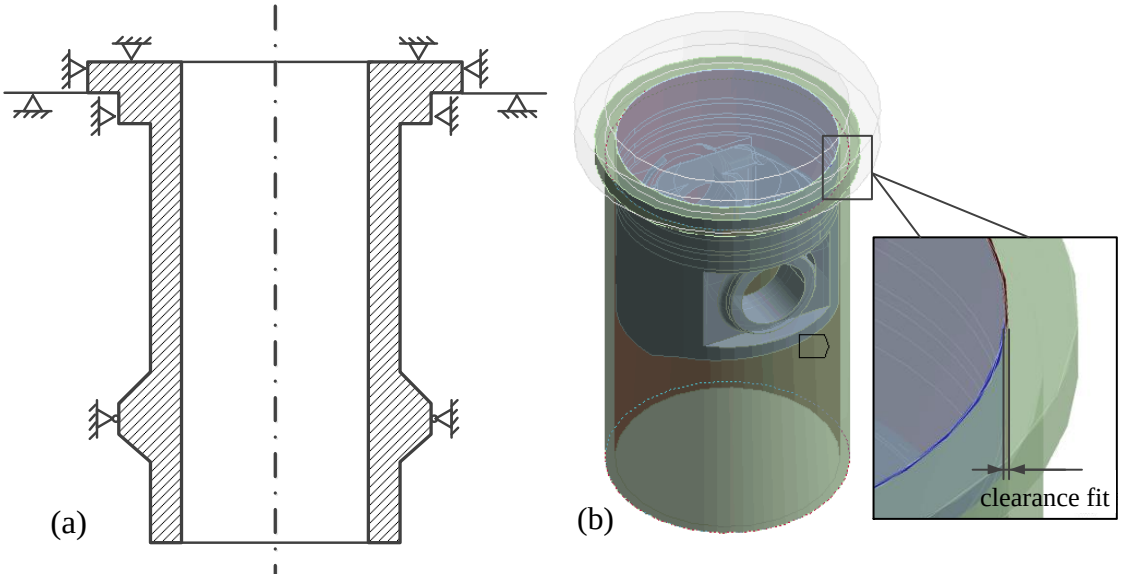

Figure 3- 1 Boundary constraints of cylinder liner

In Figure 3-1(a), it shows the boundary conditions of a cylinder liner, being a nonuniform cylindrical shell and end-flanged cylindrical shell structure. To avoid changing modal characteristics of the cylinder liner caused by improper extra-constraints, the modelling of fixed joints and clearance fits has not been achieved by constraining the degree of freedom, but through constructing a series of frictionless contact pairs as seem in Figure 3-1(b), which avoid the errors induced by over-simplification and inappropriate mathematical equivalent in the modelling and analysis of cylinder dynamic process [76]. By defining boundary conditions in this way, slight changes in modal characteristics of the cylinder liner, induced by variations in local constraint status as the result of the dynamic deformation of matched surfaces, can be more accurately taken into account in the simulation.

The cylinder liner studied in this research was made of ductile cast iron QT600-3 [77]. The material parameters for this material are listed in Table 3-1.

Table 3- 1 Material properties of QT600-3

Density (kg/m^-3)	Young's Modulus(Pa)	Poisson's Ratio	Bulk Modulus (Pa)	Shear Modulus (Pa)
7120	1.69e+11	0.286	1.316e+11	6.5708e+10

3.2.3 Excitation Configurations

Axial movement of the piston is controlled by the crankshaft and connecting rod mechanism. The driving force for piston lateral movement is defined by side-thrust force calculated in Section 3.3 and Eq. (3.1). The last one translational degree of freedom of piston, which is perpendicular to the moving plane, is set as free to avoid over-constraint, as shown in Figure 3-2(a). To simplify the calculation, besides the rotational DOF along the piston tilting motion is set as free, all the other rotational freedoms of piston are ignored.

The pressure data from the in-cylinder pressure sensor were taken as the combustion excitation. Theoretically, the instantaneous pressure value needs to be applied to the cylinder liner uniformly and dynamically at each time interval (crank angle) in order to obtain the full responses of the linear for an entire engine cycle. However, considering much higher pressure rise rate in the combustion process, only the pressure amplitudes are applied corresponding to the major combustion duration which is around combustion TDC and varying with combustion conditions due to different operating conditions. To speed up simulation process, only 1800 sampling points were calculated to show the compression and power strokes, which was resampled from 3600 points of the raw cylinder pressure signal using a polyphase implementation. And the force applying zone was equivalently confined to the top zone of liner inside surface, as shown in Figure 3-2(b). The zone has a

height of 15mm, being allowed to simulate the effective contacting areas at the moment when the combustion shock occurs.

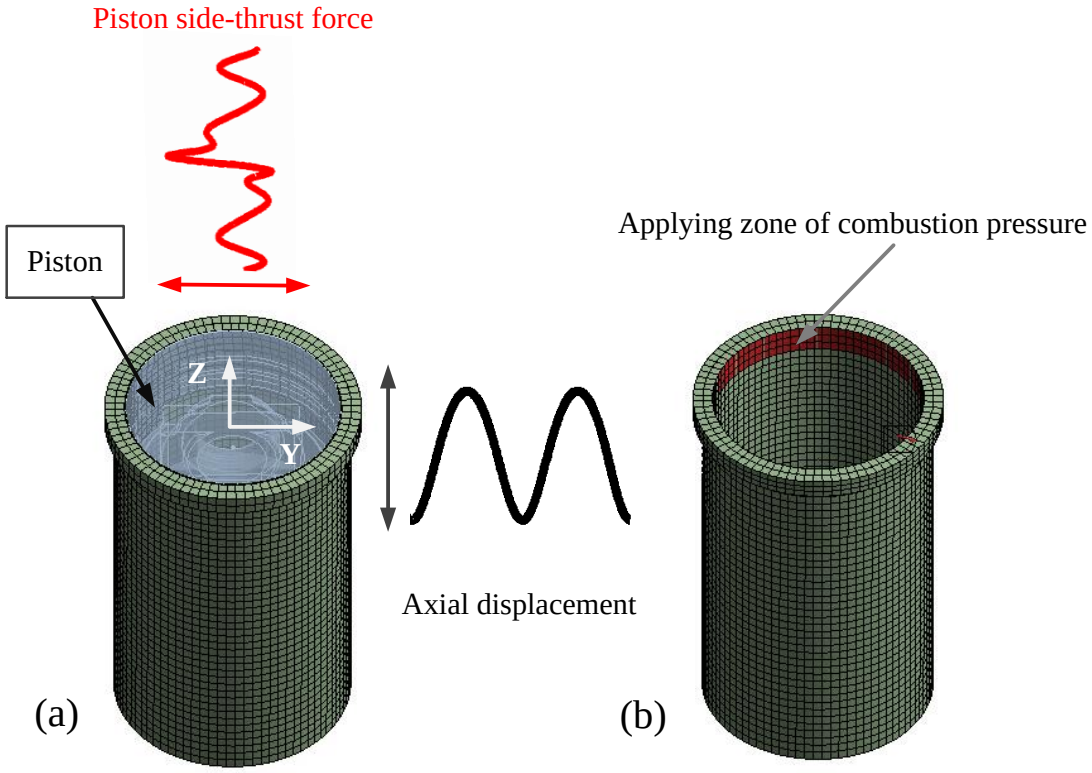

Figure 3- 2 Excitation configurations of cylinder model

3.2.4 Calibration of Finite Element Model

To verify and calibrate simulation parameters of the FE model, a modal test was conducted to obtain the free-free modal responses of the liner. Then modal frequencies from both the modal test and finite element analysis are compared to confirm the accuracy of the FE modelling.

As shown in the Table 3-2, the simulated modal frequencies agree well with the measured ones, with an error less than 3% except the first mode. This shows that the configuration of material parameters and simplified geometric shape are appropriate for the modelling, and

sufficient to represent and characterise the dynamic response features of cylinder liner under 10kHz. The first sixteen mode shapes of cylinder liner are given in Table 3-3. It should be noted that during the modelling process, some geometric details on the outer surface of the studied liner were neglected. These details are close to and relevant to the first mode shape of liner. The neglect of geometric details leads to the decrease of the first mode frequency in simulation.

Table 3- 2 The simulated and measured mode frequency of cylinder liner

No.	**Simulated Freq.(Hz)**	**Measured Freq.(Hz)**	**Error (%)**	**No.**	**Simulated Freq.(Hz)**	**Measured Freq.(Hz)**	**Error (%)**
1	929.0	974.7	4.62	9	6673.2	6569.7	1.58
2	1229.7	1217.5	1.04	10	6979.5	6896.1	1.21
3	2567.3	2584.8	0.68	11	7926.9	7872.2	0.69
4	3128.7	3195.2	2.08	12	8732.6	8559.4	2.02
5	4191.4	4117.7	1.78	13	9011.1	8956.7	0.61
6	4301.5	4324.5	0.53	14	9321.0	9177.1	1.57
7	4847.0	4711.5	2.88	15	9879.4	9760.0	1.22
8	5832.1	5785.3	0.81	16	9939.9	10012.5	0.72

Table 3- 3 The first sixteen mode shapes

No.	1	2	3	4
Mode shapes	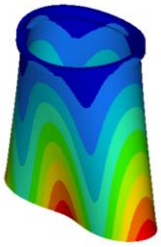	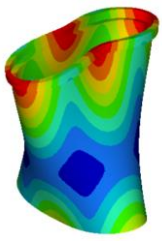	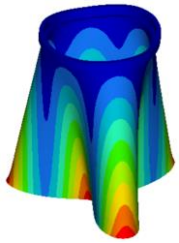	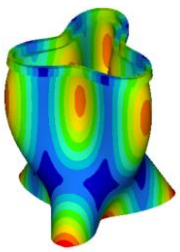

No.	5	6	7	8
	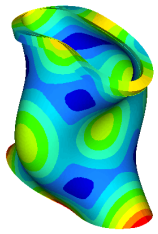	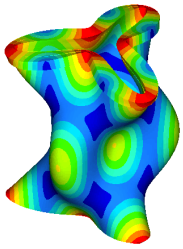	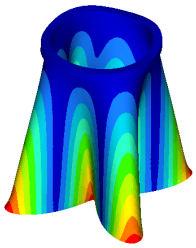	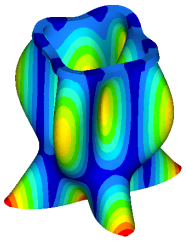
No.	9	10	11	12
	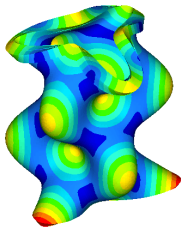	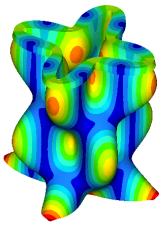	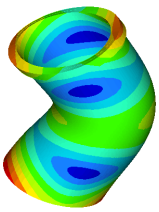	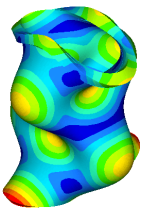
No.	13	14	15	16
	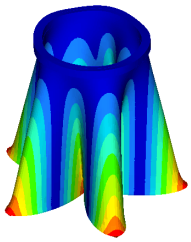	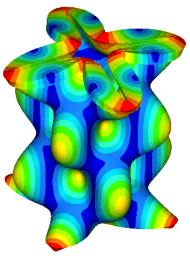	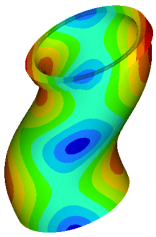	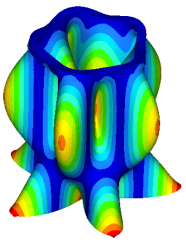

3.3 Vibration Excitations of Cylinder Liners

According to engine operation process, combustion and piston side-thrust forces are regarded to be two major excitation sources that induce the dynamic responses of cylinder liners. Other possible excitations such as the frictions of rings are much smaller in amplitudes and not considered in this study.

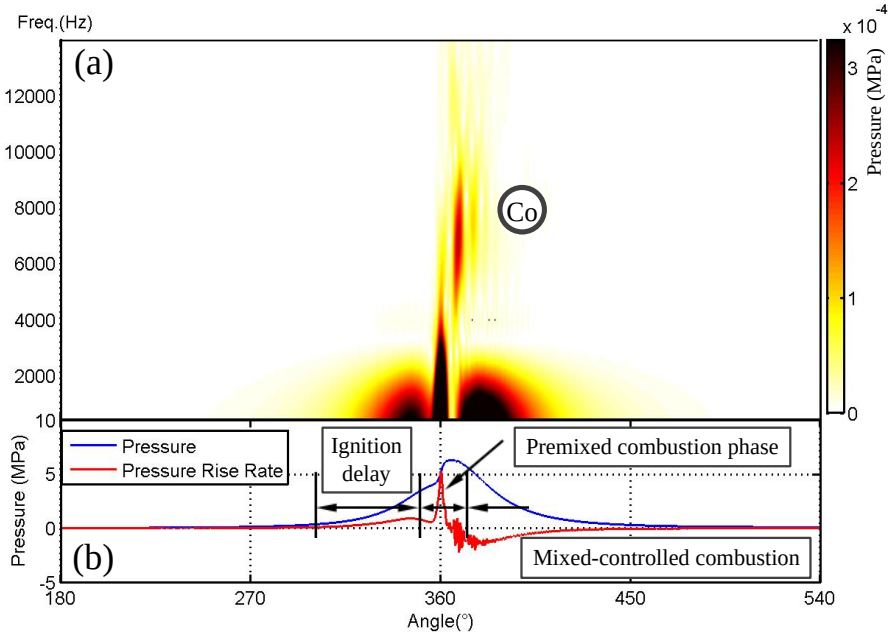

Figure 3- 3 The STFT of measured in-cylinder pressure

During premixed combustion period, both the peak pressure and pressure rise rate will reach their maximum values and the pressure profile can also accompany with high frequency oscillations due to unstable combustions. These time-varying pressures are directly applied to the inner surface of the liner, formalising combustion excitations. To understand the time-frequency characteristics of in-cylinder pressure, a short-time Fourier transform (STFT) result of measured in-cylinder pressure under the operating condition of 1800rpm engine speed and 40Nm torque is presented in Figure 3-3(a). Meanwhile, the raw pressure signal and pressure rise rate (PRR) in Fig 3-3(b), are also provided to facilitate the analysis of the STFT result.

It can be seen in Figure 3-3(a), during the premixed combustion period, there are a series of oscillations can be clearly observed in the frequency range of 4000-8000Hz immediately after the peak of pressure at a crank angle of about 360 °, marked as Ⓒo. These pressure oscillations are caused by unstable turbulent movement of gas in the combustion chamber and special inhomogeneity of combustion [78]. Moreover, it falls in

the range of mode frequencies and thereby induces high frequency responses on the liner correspondingly.

In addition to this direct excitation of combustion pressure oscillations, the combustion force also drives the piston to move laterally and impact the liner due to the kinetic motion of the piston-connecting rod mechanism. As mentioned in Section 2.2.2, the side-thrust is decomposed from the longitudinally acting combustion force and inertial force of the moving piston assembly, which pushes the piston assembly from one side of the cylinder wall skipping onto the other side, so as to induce an unceasing slap impact on the cylinder wall [27]. Mathematically, this side-thrust force F_y can be calculated by

$$\begin{aligned} F_y &= (P_c - P_i)\lambda \sin\omega t / \sqrt{1+(\lambda \sin\omega t)^2} \\ &= P_c \times \lambda \sin\omega t / \sqrt{1+(\lambda \sin\omega t)^2} + P_i \times \lambda \sin\omega t / \sqrt{1+(\lambda \sin\omega t)^2} \\ &= F_c - F_i \end{aligned} \qquad (4.5)$$

where $\lambda = r_c/l$, r_c is the crank radius and l is the length of the connecting rod. The m_l is the equivalent mass of the piston assembly. Figure 3-4 shows a typical characteristic of the side-thrust force, obtained based on the engine in this study.

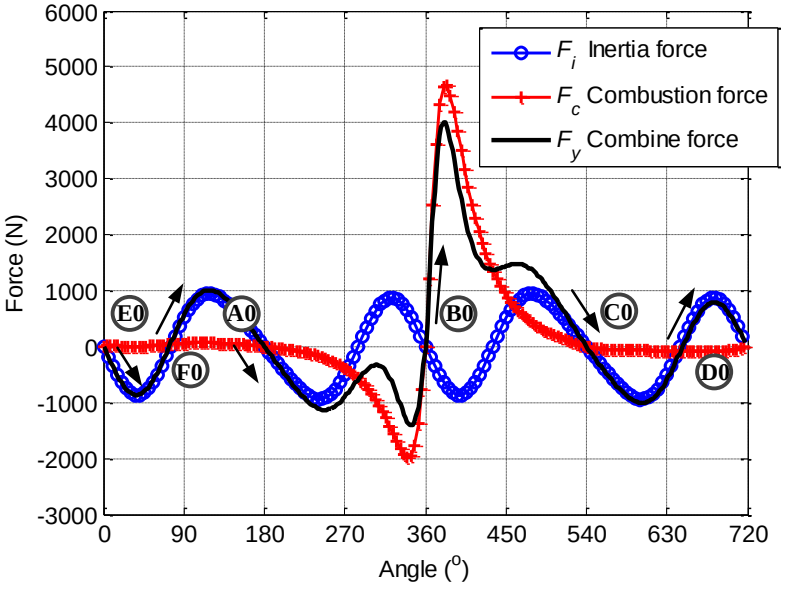

Figure 3- 4 Composition of the piston lateral force

The combined side-thrust force F_y; every time passes zero and changes direction (from positive to negative, or vice versa) means an possible occurrence of piston-slap impact on a definite position along the cylinder wall. In this instance, there are 6 slap impacts occurring in the four-stroke working cycle which are denoted as Impact Ⓐ – Ⓕ respectively as illustrated in Figure 3-4. As N. Dolatabadi et al. [22] pointed out, based on the sign change of piston lateral force, six events should be distributed across the four engine strokes, following a pattern of 3, 0, 2 and 1 events (starting at the intake stroke and ending with the exhaust stroke). Obviously, the force amplitude of Impact Ⓑ occurring around the power TDC at 360 °is the most significant one. It will results in a higher impact and appears in the similar angular poisons to the combustion shock, making it difficult to separate these two effects in measured responses.

3.4 Numerical Evaluations

To gain an understanding of vibrations responses upon the two excitations, a numerical analysis was carried out based on the model under an input of either the combustion force or piston slap force. Figure 3-5 presents two typical responses respective to the combustion shock and piston slap, at crank angle of 370 °, under the same operating condition of 1800rpm and 40Nm.

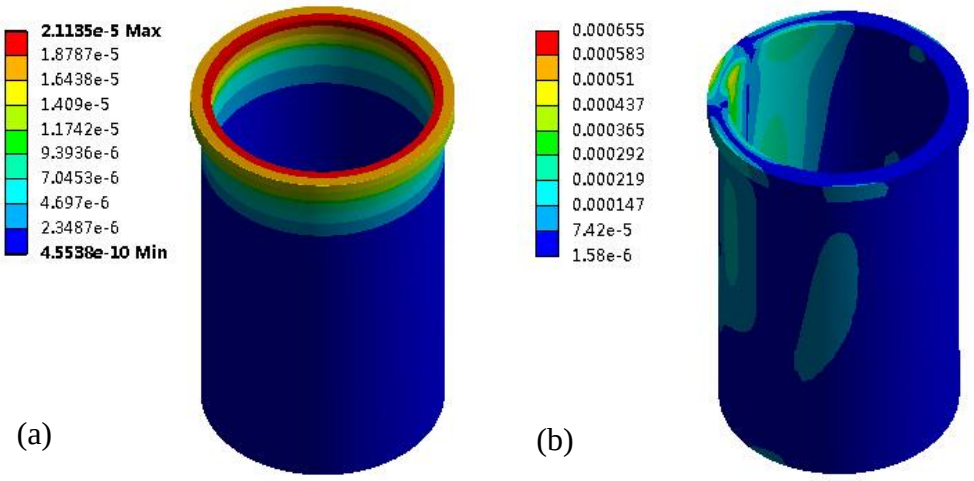

(a) Response to combustion shock (b) Response to piston slap

Figure 3- 5 Total deformation of cylinder liner (Unit: mm)

It can be seen in Figure 3-5(a) that the significant deformation response to combustion shock is mainly appeared and concentrated in the top portion of the liner, while the response to piston slap extended throughout the entire liner structure, as seen in Figure 3-5(b). After removing translation movement and quasi-static deformations, especially that of Figure 3-5(b), the magnitude information of high-frequency local deformations can be obtained. The predicted amplitude of local responses is in the order of 0.02 microns due to the combustion shock, which may be negligible in predicting lubrications between the piston ring and the liner as it far less than the roughness magnitudes of the lubricated surfaces. However, piston slaps can lead to deformation as high as 0.1 micron, being about 20% of roughness amplitude. Therefore, it needs to be taken into account in analysing the lubrication conditions.

To understand more the difference of dynamic responses between the combustion shock and the piston thrust slap, only examined is the radial displacement response at the node on the anti-thrust side of liner outer surface in order to correspond to the measured results. In addition, STFT analysis is used to highlight the time-frequency characteristics of the clean prediction, rather than the wavelet analysis used for the noisy measurements.

3.4.1 Dynamic Responses to Combustion Forces

Figure 3-6 shows the predicted responses to the pressure force measured from the test engine, detailed in Section 5.2.1, fuelled with standard diesel under an operating condition of 1800rpm speed and 40Nm torque output. It can be seen in Figure 3-6(b) that the predicted displacement response shows a profile close to the combustion pressure. The significant responses appear around the combustion TDC. In addition to the quasi-static response, there clearly exist series of high-frequency responses sustained for a relative long duration, which are more obvious in the predicted acceleration responses. As seen in Figure 3-6(a), after the combustion TDC, there is a significant dynamic response event located in the frequency range of 5000 to 8000Hz, marked as Ⓒo. As the frequency location and attenuation pattern show a high similarity to the combustion oscillations shown in Figure 3-2(a), this event is primarily the forced response caused by high frequency oscillations of in-cylinder pressure.

Moreover, clear oscillating components can be observed in frequency band of 8000-12000Hz, denoted marked as Ⓒs, It starts at about 365°, immediately after the peak of the combustion pressure. As there is no such frequency contents in the pressure profile and the oscillation sustains for a long period, which exists even when the input pressure is very low, it is regarded as the modal responses of the liner. A further examination has found that the frequency band is close to 8559-10012Hz of the 8th -12th modes identified by modal experiment as shown in Table 3-2.

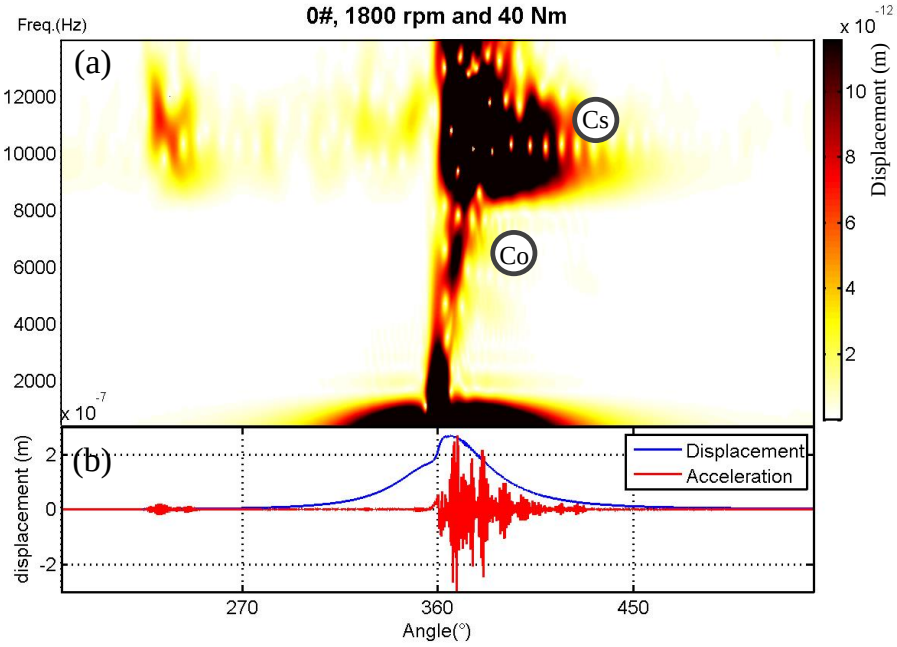

Figure 3- 6 STFT of predicted displacement response to combustion under 40Nm and 1800rpm

The simulation result indicates that in-cylinder combustion process can activate high-frequency modal responses of liner structure, which might be attributed to the rapid rise rate of pressure during the premixed combustion period.

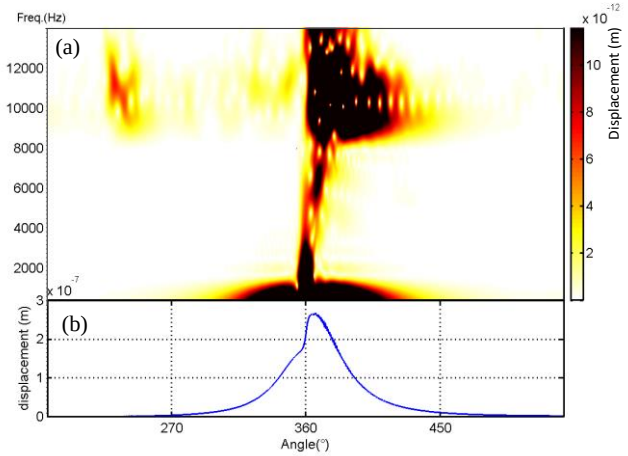

(a) 1800rpm and 40Nm, max. amplitude: 0.015μm

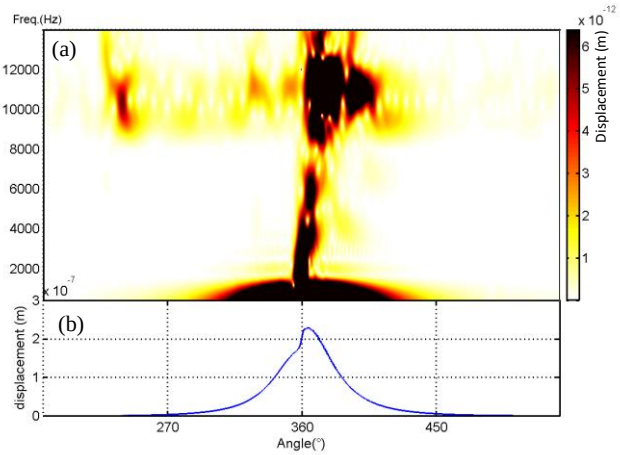

(b) 1800rpm and 10Nm, max. amplitude: 0.01μm

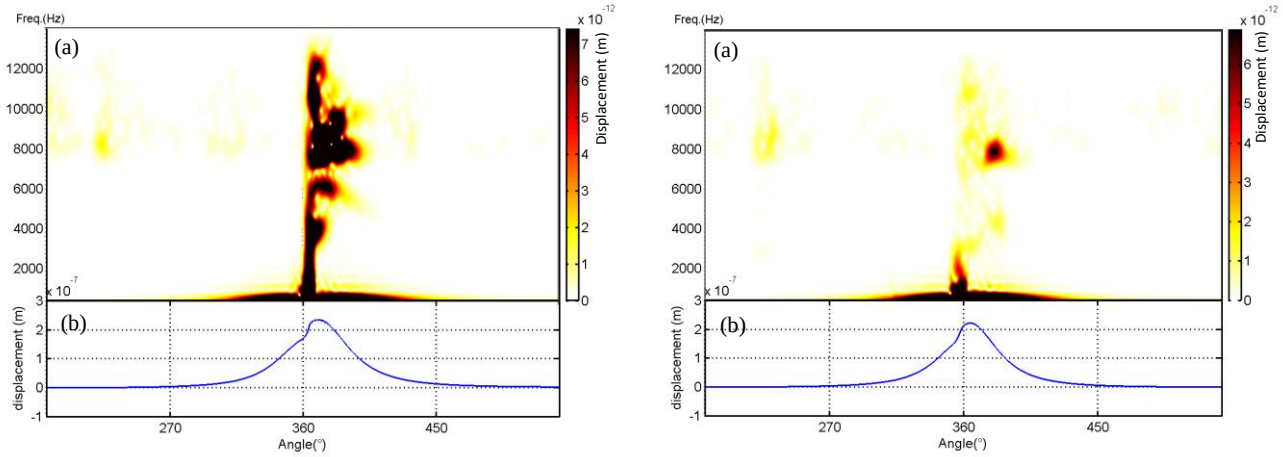

(c) 1000rpm and 40Nm, max. amplitude: 0.005μm (d) 1000rpm and 10Nm, max. amplitude: 0.004μm

Figure 3- 7 STFT of predicted displacement response to combustion shocks (Unit: m)

As shown in Figure 3-7(c) and (d), under the low-speed conditions, sustained angular of dynamic responses excited by combustion pressure is shorter than that of high-speed conditions, and more concentrated in frequency band of 6 kHz and 10 kHz. In high-speed conditions, the sustained angular of responses can be extended to 40-60 degrees. The dynamic response moves to higher frequency band of 8 kHz and 12 kHz, and contains more high-order modal components, indicating that sharper and faster combustion pressure is prone to activate more high-frequency modal responses. As the load increases, these trends are more pronounced.

After being processed by high-pass filter, a preliminary study on the amplitude of dynamic deformations has been carried out. With the increase of operating speed and load, the deformation magnitude of measuring node increased from 0.004 to 0.015 microns. The predicted amplitude of local responses is less than 3% of the surface roughness amplitude, which may be negligible to affect lubrications.

3.4.2 Dynamic Responses to Piston Slaps

In the case of piston lateral slap being considered alone, the dynamic response of the liner at corresponding measuring point shows more complex and abundant patterns in STFT results as shown in Figure 3-8 (a), which corresponds to the piston side-thrust force in Figure 3-8 (b) obtained under the operating condition of 1800rpm and 40Nm. In Figure 3-8 (a), six distinctive transient responses can be clearly observed corresponding to the peaks and troughs of piston side-thrust force [22], which are marked by Ⓐ to Ⓕ. Obviously, these responses mainly appear at the first three modes, especially for the responses to the slaps away from combustion. The 4th modal response can only be observed around the combustion event.

Moreover, three more dynamic events, marked as Ⓖ, Ⓗ and Ⓘ, can also be observed in Figure 3-8 (a). These events correspond to the secondary impact events induced by sustained high-amplitude side-thrust force, rather than by any particular force peak or trough, showing that the sustained high-amplitude side-thrust force may also cause additional impacts.

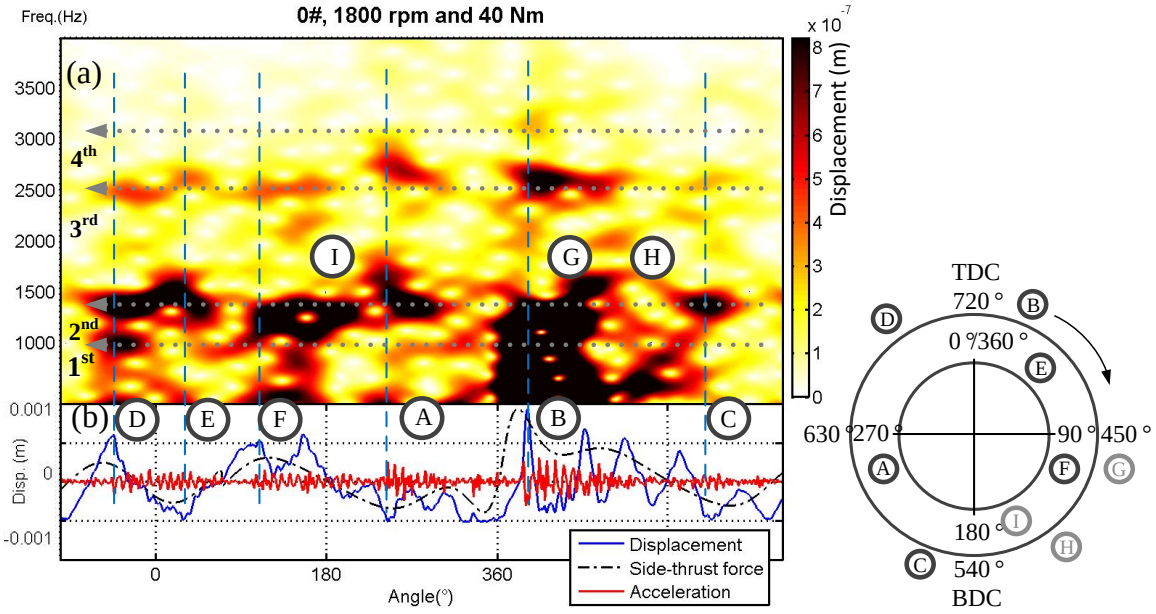

Figure 3- 8 STFT of responses to piston slaps under 40 Nm and 1800Nm

Previous studies [22], [27], [79] tend to select a common frequency range of 500-3000Hz, as a rule of thumb, for the detection and analysis of piston slap events. As shown in Figure 3-8, the distribution of dynamic responses in the frequency domain shows that the experience-based selection of frequency domain has certain rationality. The origins of this rationality may lie in the inherent mode characteristics of liner structures. As illustrated in the simulation of this study, the dynamic responses excited by piston slaps are mainly concentrated in the frequency range of 600-3500Hz, being close to the frequency band of the first four modes. It means that the dynamic responses of cylinder liners may be highly relevant to their structural modes.

N. Dolatabadi et al. [22] suggested that, based on the sign change of piston lateral force, six events should be distributed across the four engine strokes, following a pattern of 3, 0, 2 and 1 events (starting at the intake stroke and ending with the exhaust stroke), as seen in Figure 3-4. However, the simulated events caused by sign changes of piston lateral force show a different pattern of 2, 1 1 and 2 events over the four engine strokes. With the addition of events Ⓖ, Ⓗ and Ⓘ, distribution pattern of slap events eventually becomes even 3, 1, 2 and 2. This indicates that the sign changes cannot well characterise the occurrence of slap events.

It is true that change of sign in driving force does lead to the occurrence of the piston slap, but as to the timing of occurrence, more practical factors such as the clearance, surface stiffness, geometric shapes and material properties, are required to in-depth understand the impact process. It demonstrates again the necessity and rationality of the selection of FE-method in dynamics modelling for this study.

It should be noted that, the slap-induced events appeared at different angular positions show significant differences in both frequency components and patterns. The main causes of these variations are varying impact position and unilateral measuring method.

As seen in Figure 3-8, the differences existed in degree and patterns of slap-induced responses at different angular positions cannot be well interpreted by differences in

magnitude of side-thrust force. For example, there is not much difference in the amplitude of three peaks Ⓓ, Ⓔ and Ⓕ from 630 ° to 720 °, then to 180 ° of next cycle, while their dynamic responses show great differences in frequency characteristic. To fully understand the causes, dynamic deformations of cylinder liner at each slap moment have been selected and organized as the Table 3-4.

Table 3- 4 Deformations caused by slap events at different angular position (Unit: mm)

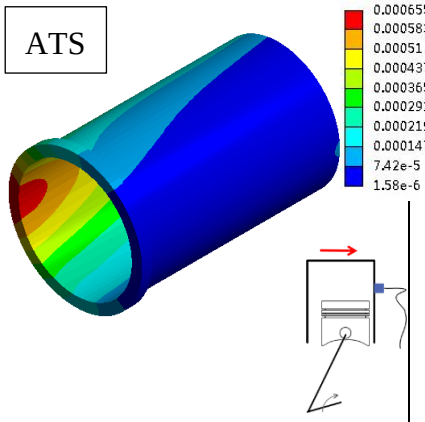	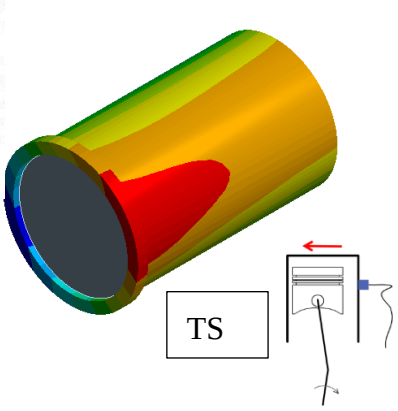	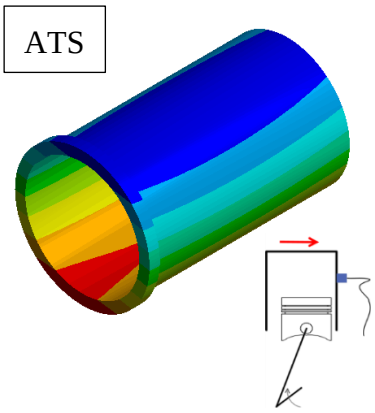
Ⓐ (245 °)	Ⓑ (after combustion TDC, 385 °)	Ⓒ (570 °)
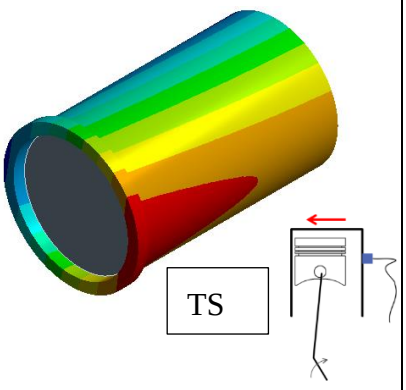	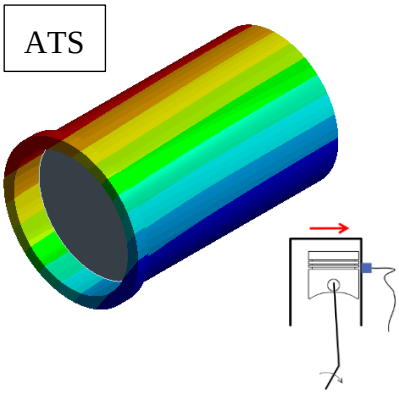	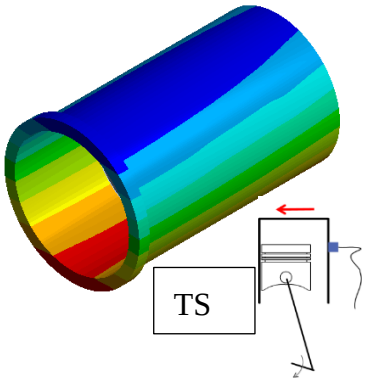
Ⓓ (700 °)	Ⓔ (after exhaust TDC, 35 °)	Ⓕ (95 °)

(1) The frequency range of dynamic responses excited by piston slaps is highly relevant to the slap position, i.e. the location of collision occurred. When the slap position is close to the deformation region of a mode shape, the slap event is prone to excite more frequency components related to this mode. When piston slap occurred near the top flange of liner,

the deformation trend of cylinder liner is close to the modal shape of the second mode, as seen in Table 3-3. This explains why the slap-induced events, Ⓑ, Ⓓ and Ⓔ, show more intense second-order modal features than the others. In contrast, when the slap position move down to the bottom end of cylinder liner, cylinder wall will show a deformation trend similar to the first and third-order modal shapes, as Ⓐ and Ⓕ events seen in Figure 3-8.

As seen in Figure 3-8 and Table 3-4, although the slap position is close to the lower part of cylinder liner, the deformation of liner at event Ⓒ shows more second-order modal features rather than the first or third-order modal response. The most probable reason of this phenomenon is that at this moment the piston exactly knock at the bottom portion of liner where is surrounded by the lower edge of the water jacket. It is similar to the situation of knock occurs at a stationary point in harmonic vibrations, that most of odd-order modal responses have been suppressed in this case.

(2) When piston slap occurs at different sides of cylinder liner, i.e. the thrust side (TS) and anti-thrust side (ATS), the dynamic responses measured at the same measuring point will present obvious differences in the modal components. When the measuring point is located at the deformation region of a mode shape, the response frequency of this mode is much easier to be measured. As shown in Figure 3-8, the deformations of liner at different moment of Ⓐ, Ⓒ and Ⓔ show more second-order modal features than the other modal components.

(3) The number of observable slap-induced events does not only depend on the number of sign changes but also on the contact parameters and piston movement parameters. As it can be seen from the Figure 3-8, after the combustion TDC, in addition to dynamic event Ⓑ, there are two weaker dynamic events can be observed from 450 ° to 495 °, which can well correspond to the peaks of piston lateral displacement in Figure 3-8(b). Once the impact Ⓑ occurred, in the process of leaving from liner surface, the piston was pulled

back to the liner surface again by the sustained high-amplitude side-thrust force, leading to secondary slap events.

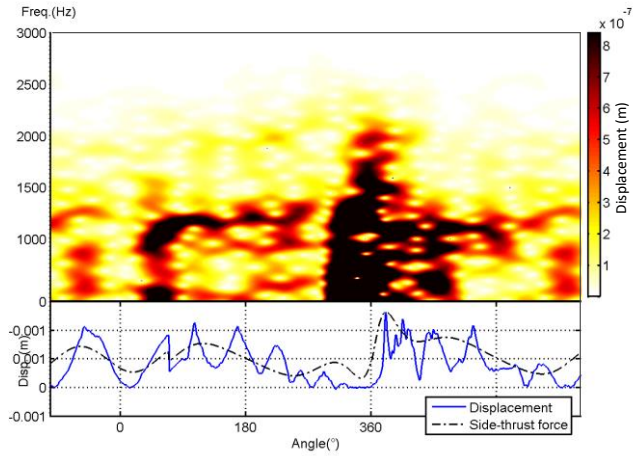

(a) 1000rpm and 10Nm, magnitude= 0.02-0.10μm

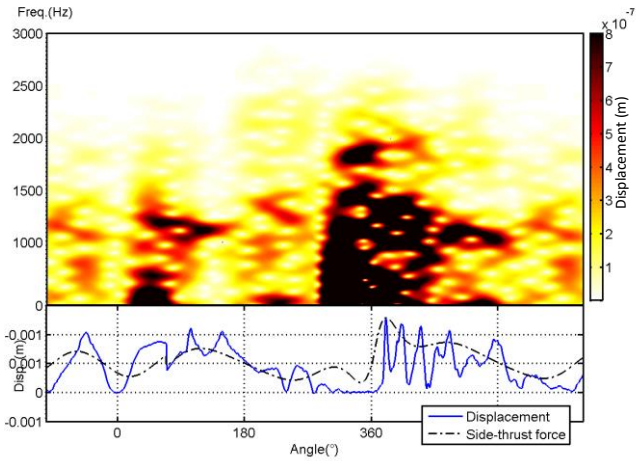

(b) 1000rpm and 40Nm, magnitude=0.02-0.10μm

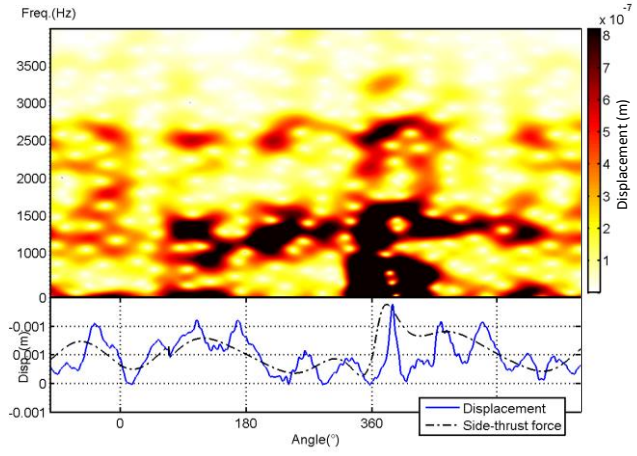

(c) 1800rpm and 10Nm, magnitude=0.04-0.15μm

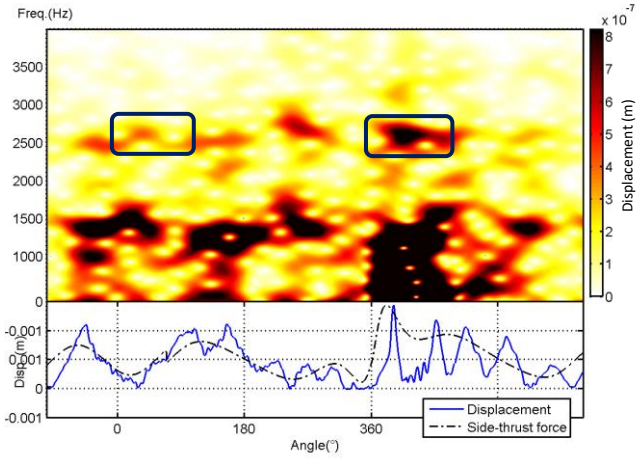

(d)1800rpm and 40Nm, magnitude=0.04-0.15μm

Figure 3- 9 The STFT of dynamic displacements at different operating conditions (Unit: meter)

As seen in Figure 3-9(a) and (b), under the low-speed conditions, there are only two major dynamic events could be observed around the combustion TDC and exhaust TDC

separately. With the increasing of operating speed and load, there are more dynamic events appeared on the time-frequency spectrum of dynamic responses, accompanied by more high-frequency modal components.

In summary, the vibration responses are composed mainly of the contributions of various liner modes due to the very non-stationary excitations of combustion shock and piston slaps.

The predicted amplitude of liner deformation is in the order of 0.02 microns due to the combustion shock, which may be negligible in predicting lubrications between the piston ring and the liner as it far less than the roughness magnitudes of the lubricated surfaces. However, its influences on resultant friction need to be further investigated.

In the meantime, piston slaps can lead to deformation as high as 0.1 micron, being about 20% of surface roughness amplitude, which may cause changes in formation and distribution of lubricating oil film between piston rings and liners. Therefore, it needs to be taken into account in analysing the tribological characteristics of cylinder assemblies.

.

Chapter 4
Dynamic Responses of Cylinder Liners to Combustion of Alternative Fuels

Changes in in-cylinder combustion force and piston side-thrust force induced by the combustion of alternative fuels: biodiesel and M15 are compared and analysed in this chapter. Then the dynamic responses of cylinder liners to different excitation sources are predicted using the FE model to quantify the differences of vibrations between different fuels. It can be concluded that a fuel like biodiesel with a high cetane number can cause more intense vibration of cylinder liners due to its extension of the mixing-controlled combustion period.

4.1 Introduction

It has been shown by many researches and small scale applications that the use of alternative fuels such as biodiesel, ethanol and methanol blends can be feasible as burning such fuels in a diesel engine can produce the desired power and an emission level similar to that of petroleum diesel. In the meantime, it has also been observed that there are many significant differences in using such fuels in terms of combustion behaviours, burning residuals, vibration and noise emissions, which might be attributed to their significant difference in physical and chemical properties.

These differences may be clear evidence that such fuels can result in potential negative effects on engines, which includes the influence not only on the power output performance and emission levels but also changes in the dynamic processes of critical components, friction losses, overall service life spans and associated maintenance activities. However, the research subjects related to these influences have been found not to have been investigated adequately. Particularly, the influence of burning alternative fuels on the changes in the dynamic responses of cylinder assembly, which is the decisive factor affecting the vibration and noise emission, friction and lubrication process of the entire engine, has not yet been fully understood.

Compared with fossil diesel, biofuel, with a higher cetane number, has been proved to possess a softer combustion process and advanced ignition phase. Theoretically, these characteristics should be helpful in the reduction of vibration and noise emissions. However, Ahmad Taghizadeh Alisaraei et al. [35] found that a compression ignition engine fuelled with biofuel-diesel blended fuel (biodiesel/diesel= 20:80) produced even more intense vibration and noise emissions than the diesel under certain operating conditions, which can hardly be explained just by the advanced ignition delay phase of biodiesel. Analogously, by reason of the lower cetane number and higher latent heat, methanol is regarded as an alternative fuel would produce much more vibration and noise emissions. Nevertheless, the NVH performance of the CI engine fuelled with methanol-diesel blend fuels is often reported to produce less vibration and noise emissions under

higher operating speeds. Most researchers claimed that the improved NVH performance, or weakened vibration emission, of an engine fuelled with methanol-diesel blends should be attributed to the shortened ignition delay period as a result of the combustion-supporting characteristic of high oxygen fraction, as seen in the formula CH_3OH[45]. While, as another oxygenated fuel, although biodiesel possesses less oxygen compared with methanol, it produces even worse NVH performance than the methanol-containing fuels. All of these complex phenomena show that the vibration and noise emissions of engines cannot always be well interpreted just by the physicochemical properties of alternative fuels.

These complex nonlinear relationships make it difficult to gain a general assessment of potential influences of such fuels upon different engine systems such as lubrication process straightforward. To overcome the difficulty, this chapter focuses on an investigation into the characteristics of dynamic responses of cylinder linear respective to different fuels. Ultimately the characteristics will be included into more advanced tribological models to achieve a quantitative assessment.

4.2 Physicochemical Properties of Alternative Fuels

In order to investigate the influence of differences in fuel physicochemical properties on the dynamic responses of liners, two representative alternative fuels to fossil diesel with different combustion characteristics, biodiesel and methanol-diesel blended fuel, were chosen for a comparative study of their induced dynamic responses upon cylinder liners.

The basic physical and chemical properties of the alternative fuels and standard diesel have been shown in the Table 4-1. Methanol is considered to be one of the favourable alternative fuels to fossil diesel with its advantages of environmental friendliness and high oxygen content. It is prepared from fossil or renewable resources such as natural gas, residual oil and biomass. The energy content of methanol is lower than the fossil diesel. So in order to obtain the same amount of power as that of diesel-fuelled engine, more methanol fuel is needed to be injected into combustion chamber. Its high oxygen content and high H/C ratio may be beneficial to improving the combustion and to reducing the

soot and particulate emissions. Compared to diesel fuel, methanol has higher latent heat of vaporisation, which extracts more heat in the evaporation process. As a result of the cooling effect, the emissions of nitrogen oxides can also be reduced. Methanol has poor ignitability due to its low cetane number, high latent heat of vaporisation and high ignition temperature, which eventually caused the extended ignition delay[80].

Table 4- 1 Physical and chemical properties of alternative fuels

	Methanol	**Biodiesel**	**Diesel**
Density (20℃) /(g ċm^{-3})	0.788	0.884	0.831
Heat of vaporisation /kJ ƙg^{-1}	1178	320.2	250
Lower heating value /(MJ ƙg^{-1})	19.7	37.4	42.6
Kinematic viscosity (20℃) /mm2 s^{-1}	0.58	5.2	2.6
Surface tension (20℃) /(mN/m)	18.8	30.4	31.1
Cetane	3	59	55
Polarity	0.762	-	0.25

Biodiesel has promising lubricating properties and cetane number compared to low sulphur diesel fuels [48]. The lower heating value of biodiesel is about 37.4 MJ/kg, which is 9% lower than regular fossil diesel. It has been claimed that biodiesel gives better lubricity and more complete combustion thus increasing the engine energy output and partially compensating for the higher energy density of fossil diesel.[51] Biodiesel has a higher oxygen content (usually 10wt% to 12 wt%) than fossil diesel, resulting in lower pollution emissions. Due to the higher viscosity and surface tension, droplets produced by biodiesel during atomisation are greater in diameter than the traditional fossil diesel.

Biodiesel has higher cetane values, resulting in better ignition. The higher cetane number a fuel possesses, the more easily the fuel can combust in a compression ignition engine. Faster premixed combustion can effectively shorten the ignition delay period, reducing the peak of pressure rise rate. Therefore, higher-cetane fuel is usually considered to cause an engine to run more smoothly and quietly.

4.3 Influences of Alternative Fuels on Vibration Excitations

Differences in the physical and chemical properties of alternative fuels will lead to changes in the combustion process, which manifest principally as a variation in in-cylinder pressure or force. As the driving force for piston movements, the combustion pressure can lead to corresponding changes in piston side-thrust forces, which in turn will affect the response characteristics of the cylinder liners.

4.3.1 Impacts on In-cylinder Combustion Behaviours

In this study, methanol-diesel blended fuel (Methanol 15 wt%, co-solvent: isopropanol 8wt%, diesel 72wt%, M15), pure biodiesel (BD), and pure fossil diesel (0#) were prepared and based on for investigating the influences of alternative fuels. The biodiesel was produced from waste cooking oil based on ASTM D6751-09 standard[81]. In-cylinder combustion pressures of alternative fuels at four different operating conditions were acquired from a single-cylinder diesel engine. The measured pressure curves and calculated pressure rise rates are presented in Figure 4-1.

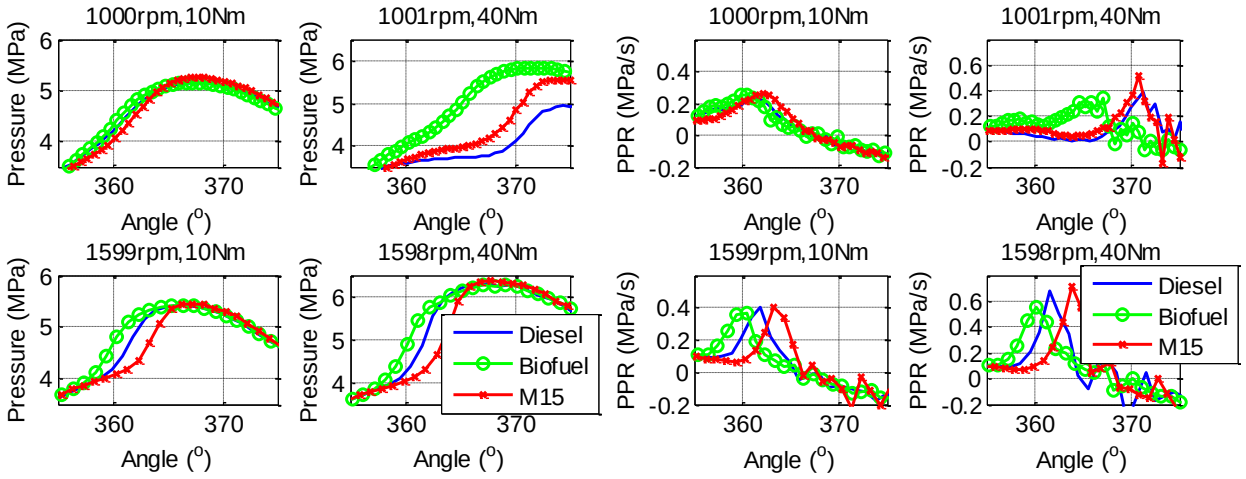

(a) Measured in-cylinder pressure; (b) Rise rate of in-cylinder pressure.

Figure 4- 1 In-cylinder pressure curves and pressure rise rates

Compared with other fuels, biodiesel always shows a pre-ignition phenomenon in different operating conditions, as seen in Figure 4-1. A higher cetane number of biodiesel means

faster in-cylinder burning velocity. The faster the premixed combustion, the shorter the ignition delay period and the lower the peak of pressure rise rate. This also explains why biodiesel possesses a lower magnitude in the peak of pressure rise rate than the others.

In contrast, the in-cylinder combustion behaviour of methanol-diesel blended fuel exhibits more complicated behaviour. In most operating conditions, the ignition timing of M15 is delayed compared to the other fuels. This mainly depends on the unique physicochemical characteristic of methanol and the in-cylinder thermodynamic state. The low cetane number and the poor flammability of methanol, combined with the high latent heat of vaporisation will lead to a low temperature in the combustion chamber, and result in the postponement of the combustion phase. Under high load conditions, the in-cylinder thermodynamic state has been improved, the influence of vaporisation endothermal on the combustion process is weakened, and hence the difference between the alternative fuels is lessened. The prolonged premixed combustion period, caused by the lower cetane number of methanol, eventually resulted in higher pressure rise rates, as shown in Figure 4-1(b).

In the operating condition of 1000rpm engine speed and 40Nm torque output, all three fuels exhibit substantial delays in the peak of combustion pressure. With the engine load going up, the increased fuel delivery per cycle will significantly enhance the heat release of the premixed combustion phase, and enlarge the in-cylinder pressure. In the meantime, the increased proportion of premixed combustion can cause phase delay in the whole combustion process, resulting in the appearance of a significantly delayed pressure peak. This is benefited from the enhanced in-cylinder thermodynamic state in that the influence of the vaporisation endothermal of methanol to the combustion process is weakened. The booster effect of oxygen content in M15 on the combustion process is strengthened, resulting in advanced combustion.

4.3.2 Impacts on Piston Side-Thrust Forces

As mentioned above, the periodically changing side-thrust force can be decomposed from the longitudinally acting combustion force and inertial force of the moving piston assembly. Therefore, the lateral driving force of the piston that applies to cylinder liner is

bound to be affected by variations in combustion force determined by the combustion characteristics of alternative fuels.

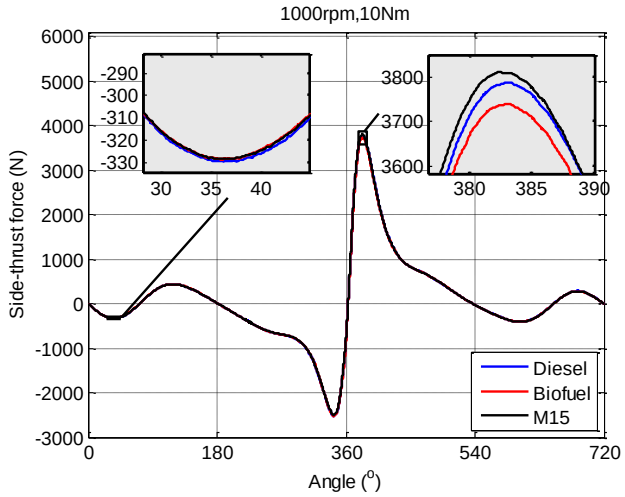

(a) 1000rpm and 10Nm;

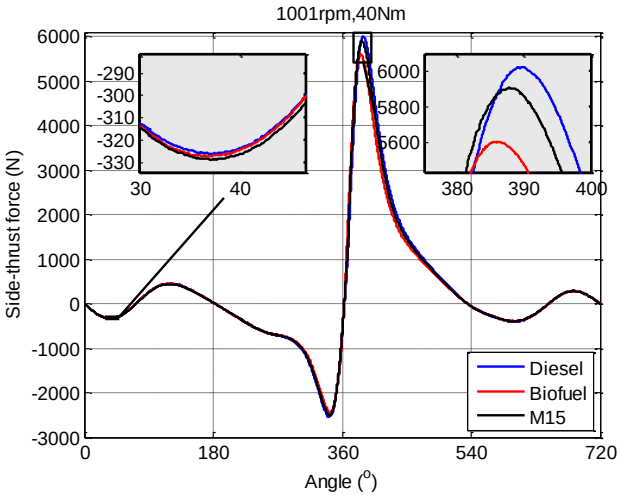

(b) 1000rpm and 40Nm;

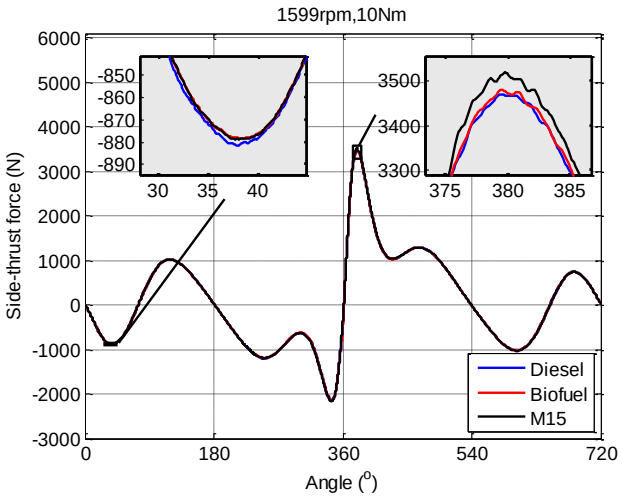

(c) 1600rpm and 10Nm;

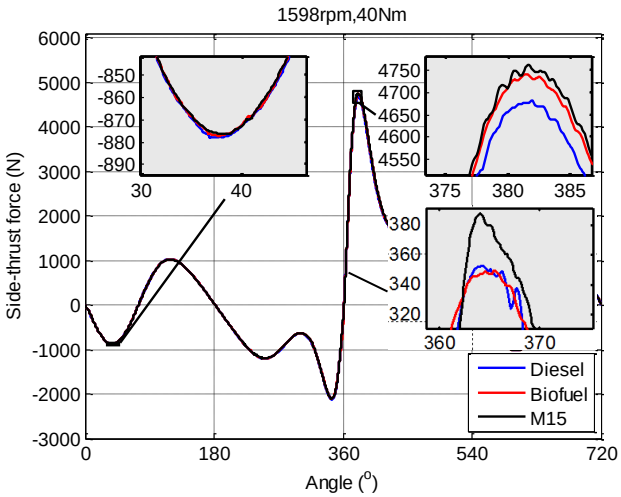

(d) 1600rpm and 40Nm.

Figure 4- 2 Piston side-thrust forces of alternative fuels under different operating conditions

The impact of alternative fuels on the piston side-thrust force mainly manifests clear differences in its peak value and associated phase. With the running speed increasing, the peak value of the side-thrust force burning M15 after combustion TDC increases faster than with any other fuel. Under high speed and high load conditions, this trend is even more pronounced.

Under low speed conditions, the peak value of the side-thrust force after combustion TDC burning biodiesel is lower than with other fuels, which might be attributed to the lower pressure peaks. In high speed condition of 1600rpm and 10Nm, the peak value of biodiesel is slightly larger than that of diesel, after the M15. As the load increases, the peak value of biodiesel becomes higher and closer to the methanol-containing fuel M15. This is because biodiesel has lower energy content than diesel fuel. Therefore, more fuel is injected into the combustion chamber to obtain the same amount of power as that of the diesel-fuelled engine, resulting in a longer period of high-pressure in-cylinder state, i.e. prolonged mixing-controlled combustion phase. A delayed mixing-controlled combustion phase (combustion centre) can lead to a separation between the peaks of the combustion force and the longitudinal inertia force of piston assembly. The combustion force acting on the piston head is not completely cancelled, thereby resulting in a greater lateral force, around the crank angle of 382 °.

The phase characteristic of combustion pressure has a direct impact on the piston side-thrust force in terms of magnitude and rise rate. The magnitude of the side-thrust force depends on the combination of the combustion force and inertia force. Under the low-speed and high-load condition of 1000rpm and 40Nm, the peak value of M15 after combustion TDC is smaller than that of diesel fuel, although the pressure rise rate of M15 is greater than the others, as shown in Figure 4-2(b), due to the high oxygen content of M15, which promotes the premixed combustion process, resulting in pressure peak in advance. When the pressure peak moves close to the combustion TDC, i.e. the angular position of the inertial force peak, the driving effect of the combustion force to the piston can be correspondingly weakened.

It can be concluded that the piston side-thrust force, from the waveform to the time of occurrence, is sensitively changing with different coupling effect of the combustion force and inertia force of the piston assembly, reflecting different combustion processes determined by the physicochemical properties of alternative fuels.

4.4 Numerical Evaluations of Liner Responses to the Combustion of Alternative Fuels

Figure 4-3 shows the predicted dynamic responses to the combustion force measured from the test engine, detailed in Section 5.2.1, fuelled with biodiesel, methanol-blended fuel M15 and diesel under an operating condition of 1800rpm speed and 40Nm torque output. Similarly, the predicted displacement response shows a profile close to the combustion pressure as seen in Figure 3-3. The significant responses appear around the combustion TDC. In addition to the quasi-static response, there clearly exists a series of high-frequency responses sustained for a relative long duration, which are more obvious in the predicted acceleration responses. Both of the forced responses to the oscillations of in-cylinder pressure and modal responses related to the liner structure, located mainly in two frequency bands from 5000 to 8000Hz, and 8000 to 12000Hz respectively, can be clearly observed in the STFT plots of Figure 4-3.

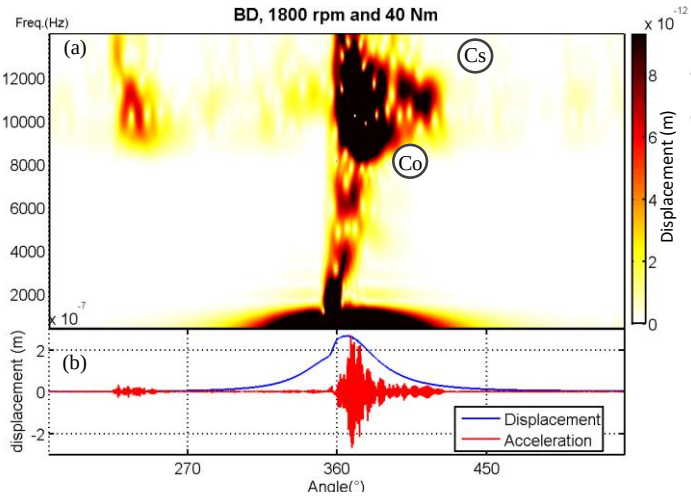

(a) STFT of dynamic responses, biodiesel, 1800/40

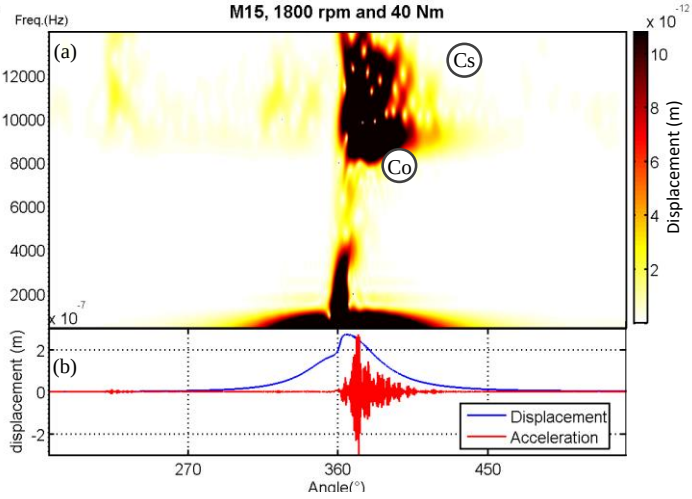

(b) STFT of dynamic responses, M15, 1800/40

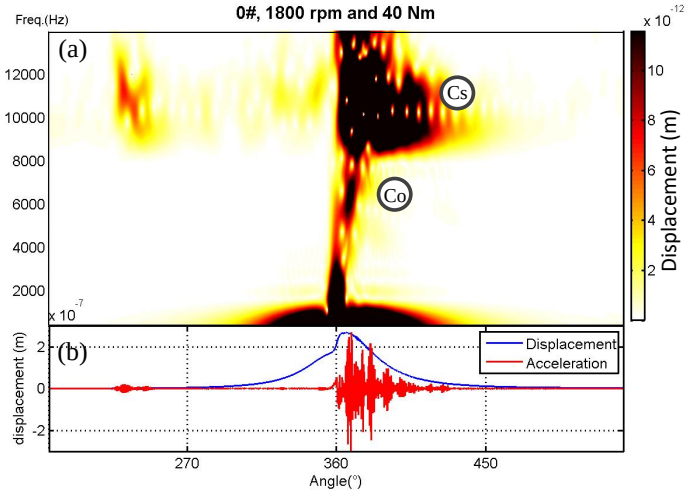

(c) STFT of dynamic responses, diesel, 1800/40

Figure 4- 3 The STFT of dynamic responses to the combustion of alternative fuels (Unit: m)

As seen in Figure 4-3, the modal responses of biodiesel sustains for a longer period than those of other fuels, which can be attributed to the longer duration of mixed-controlled combustion period. Because of the lower calorific value of biodiesel, a much larger amount of fuel delivery was needed to inject into combustion chamber, in order to output the same mechanical power, thereby resulting in a longer combustion duration. However, by the contrast between magnitudes, M15 shows more intensive modal responses than the others, which is fully consistent with the faster rise of in-cylinder pressure fuelled with methanol-blended fuels.

In the case of the piston lateral slap being considered alone, the dynamic responses of the liner fuelled with alternative fuels show the similar complex patterns in STFT results as shown in Figure 4-4, under the operating condition of 1800rpm and 40Nm. As seen in Figure 4-4(a), the overall energy distribution of slap-induced responses fuelled with biodiesel are significantly reduced compared with that of diesel in Figure 4-4(c). This shows that the piston movement driven by the smoother combustion excites fewer mode components in low frequency ranges. In contrast, due to the sharper side-thrust force of piston assembly drove by a rougher combustion of methanol-blended fuel M15, STFT

results in Figure 4-4(b) shows more intensive responses in the frequency band of 2000 to 3500Hz, which are close to the 3rd and 4th mode frequencies.

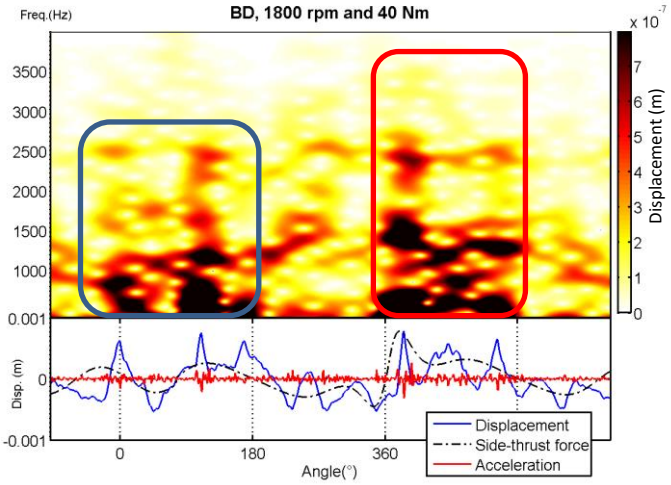

(a) STFT of liner vibrations fuelled with BD

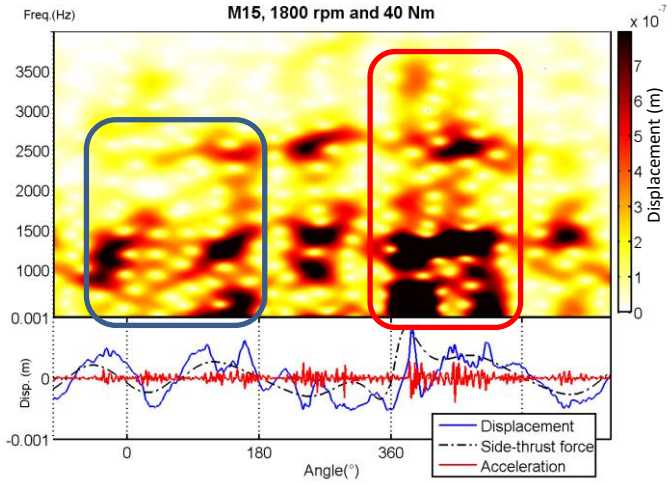

(b) STFT of liner vibrations fuelled with M15

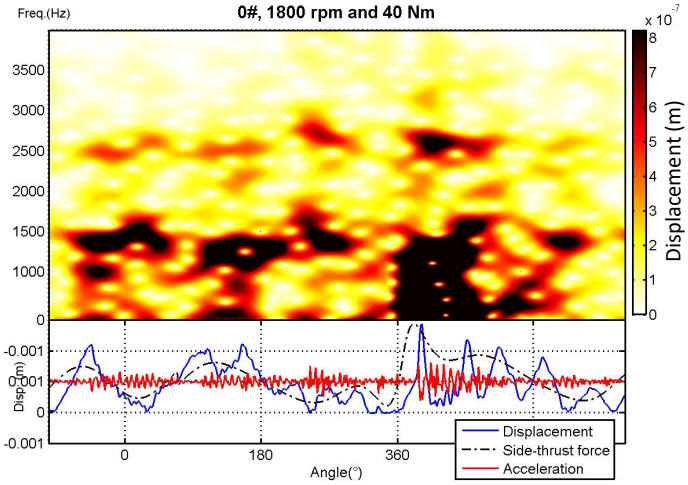

(c) STFT of liner vibrations fuelled with diesel

Figure 4- 4 The STFT of dynamic responses to piston slaps of alternative fuels (Unit: m)

It should be noted that distinguishable differences in local response features between the two fuels can be clearly observed around the combustion TDC and exhaust TDC, marked with red and blue rectangles in Figure 4-4. The STFT result of biodiesel shows much more localised dynamic responses about the exhaust TDC compared with those of M15. Conversely, the methanol-blended fuel M15 presents more intense dynamic responses

around the combustion TDC than the other fuels. These complex and even reverse trends of local features can hardly be interpreted using the differences in the physical and chemical properties of alternative fuels. Therefore, it is necessary to perform some contrastive and diagnostic analyses on these features under different operating conditions to understand the generating mechanisms behind them in depth.

To achieve the diagnostic quantitative analysis for different operating conditions, the RMS results of four local responses, respectively marked as C_o , C_s, the blue rectangle and red rectangle in the above figures, have been calculated and drawn as in Figure 4-5 and Figure 4-6.

Figure 4-5(a) presents the RMS results of local features in regard to the oscillations in combustion pressure and the simulated responses to combustion oscillations C_o. It can be clearly seen that the changing trends of simulated dynamic responses C_o are highly proportional to those of combustion oscillations. This consistency provides clear evidence that this event C_o primarily is the forced response caused by the high frequency oscillations of in-cylinder pressure.

The RMS results of modal responses C_s induced by different fuels, show more abundant information. As seen in the upper plot of Figure 4-5(b), under the low load conditions, the RMS result of M15 shows a dramatic rise, which concurs with the increasing trend of pressure rise rate fuelled with the methanol-blended fuel, due to the improvement of the in-cylinder thermodynamic state along with the increase of running speed. However, under the higher load conditions, the RMSs of the two alternative fuels show the opposite tendencies as shown in the bottom plot of Figure 4-5(b). Under high load conditions, with the fuel injection quantity increasing, the atomisation of biodiesel during the premixed combustion phase deteriorated significantly, thereby resulting in a reduction of the shock strength and the consequent dynamic responses. In contrast, due to the improvement of the in-cylinder thermodynamic state, the booster effect of the oxygen content in M15 on the

combustion process is strengthened, furthermore stimulating more intense modal responses.

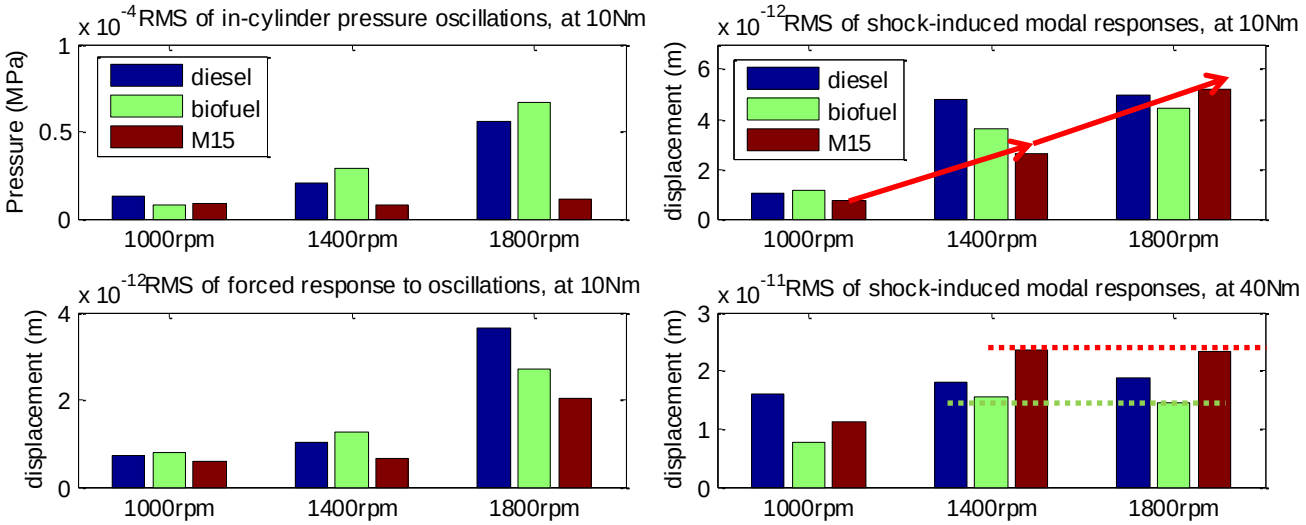

(a) RMS results of pressure oscillations and C_O events (b) RMSs of modal responses C_S under different loads

Figure 4- 5 The variation trends of combustion shock-induced events

To analyse the variation trends of dynamic responses to piston slaps, the RMS results of local responses around two TDCs, marked with blue and red rectangles in Figure 4-4, have been calculated and drawn as shown in Figure 4-6.

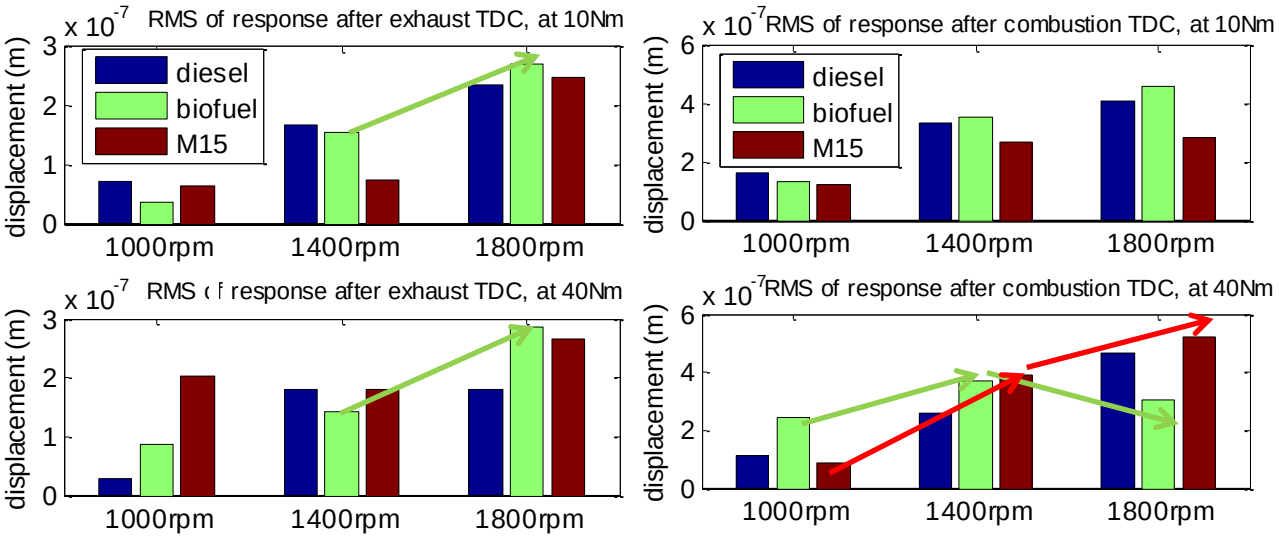

(a) RMS-after Exhaust TDC (b) RMS- after Combustion TDC

Figure 4- 6 The variation trends of combustion piston slap-induced events

As shown in Figure 4-6(a), under low load conditions, almost all of the RMSs of dynamic responses to slap events after the exhaust TDC increase steadily with the running speed rising. The upward trend of RMSs fuelled with biodiesel shows the most rapid rise, which may be due to the prolonged combustion duration as a result of the larger amount of biodiesel injection (biodiesel possesses a lower calorific value). The delayed mixing-controlled combustion phase can cause a relative increase in the kinetic energy of piston side slaps in the exhaust stroke, thereby resulting in the rise of RMSs around the exhaust TDC.

The RMS results of three fuels after combustion TDC show more complex variation tendencies as shown in Figure 4-6(b). Under low-load conditions, with the increase in the operating speed, all three fuels show similar trends with to the forced responses Co of combustion oscillations, indicating that the slap-induced responses around the combustion TDC are basically consistent with the in-cylinder combustion behaviours under low-load conditions.

Under high-load conditions, as explained above, the booster effect of methanol is strengthened by the improved in-cylinder thermodynamic state. The more intense combustion behaviour of M15 resulted in the higher peaks of piston side-thrust forces, and then caused a sharp increase in the RMSs of M15, as seen in the bottom plot of Figure 4-6(b).

However, the RMS result of biodiesel shows a clearly decreasing tendency after an increase, which cannot be well interpreted by the combustion characteristics of biodiesel itself.

To reveal the reasons for this trend, it is necessary to understand in depth the formation mechanism of the piston side-thrust force, especially about the effects of combustion pressure on the peak value of piston thrust force around the combustion TDC. In Figure 4-7, it shows a typical characteristic of the piston side-thrust force, combined with the longitudinally acting combustion force P_c and axial inertia force of piston assembly P_i, obtained based on the engine in this study.

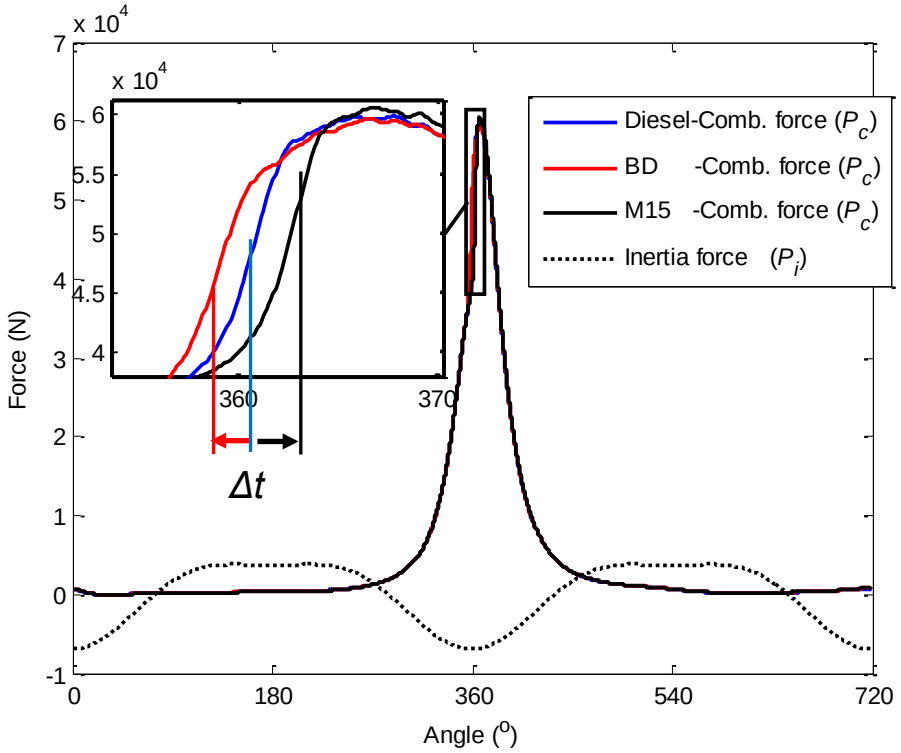

Figure 4- 7 The decomposition of combustion force and axial inertia force

As stated above, the piston side-thrust force is decomposed from the longitudinally acting combustion force and the inertia force of the moving piston assembly, which pushes the piston assembly from one side of the cylinder wall skipping onto the other side [27]. Mathematically, this phenomenon can be expressed by the following equations:

$$F_y = F_c - F_i = (p_c - p_i) \times \lambda \sin \omega t / \sqrt{1 + (\lambda \sin \omega t)^2} \tag{4.5}$$

$$\begin{aligned} F_i &= P_i \times \lambda \sin \omega t / \sqrt{1 + (\lambda \sin \omega t)^2} \\ &= m_1 r_c \omega^2 (\cos \omega t + \lambda \cos 2\omega t) \times \lambda \sin \omega t / \sqrt{1 + (\lambda \sin \omega t)^2} \\ &= m_1 \cdot a_{lateral} \end{aligned} \tag{4.5}$$

$$a_{lateral} = r_c \omega^2 (\cos \omega t + \lambda \cos 2\omega t) \times \lambda \sin \omega t / \sqrt{1 + (\lambda \sin \omega t)^2} \tag{4.5}$$

where ω is the rotating speed of the crankshaft. As seen in Eq.(4.5), the side force F_i is the lateral component of the resultant force combined with the combustion force and the vertical inertia force of the piston assembly.

The inertia force of piston assembly is roughly proportional to the square of the crankshaft speed, which means that the inertia force will grow rapidly with the increase of the running speed. Due to the opposite sign, when the increment of the inertia force is greater than that of the combustion force, the cancellation between the combustion force and inertia force will lead to a decrease in the peak value of the side-thrust force, as seen in Figure 4-2(d), thereby resulting in a decreasing trend after an increase, as shown in Figure 4-6(b).

Principally, with the increase of running speed, the piston inertia force of the entire work cycle increased significantly, which results in a corresponding rise in the kinetic energy of piston slaps. Therefore, the RMS result of the liner dynamic response rises steadily with the increase of running speed, represented by the RMSs of local responses near the combustion TDC, as shown in Figure 4-6(a).

The influences of alternative fuels on the dynamic responses can be summarised as follows:

- Due to the cancellation, or offsetting effect, between the combustion force and inertia force, the rise rate of the piston thrust force near the combustion TDC shows a nonlinear decrease with increasing in engine speed.
- The advanced ignition caused by the high cetane number of biodiesel can have a significant contribution to the cancellation effect on the piston side-thrust force, thereby resulting in a nonlinear trend of the RMSs of local response near the combustion TDC.
- However, due to the opposite effect of methanol on ignition delay, the cancellation effect to the piston side-thrust force is weakened. The RMS result of methanol-blended fuel M15 shows a relatively rapid increase in the local responses to slaps after combustion TDC.

In summary, there is clear difference in the physical and chemical characteristics of alternative fuels from standard diesels, which will cause inevitable deviations of combusting such fuels. Based on FE model predictions, a clear difference of vibration responses at cylinder linear has been found between different fuels. Obviously, this difference will alter the tribological behaviours between the piston rings and cylinder liners. However, the significance and directions of such alternations needs to be further clarified.

Chapter 5
Establishment of Experimental Systems

This chapter details the test facility employed for this study. In addition to the construction of a single cylinder engine bench and associated control systems, intrusive installations of pressure sensor and vibration sensor are also depicted in conjunction with a high speed dynamic data acquisition system. The establishment of these facilities provides a generic and rational basis for conducting various tests required in this study.

5.1 Introduction

To validate the simulation investigation, an engine test system has to be developed to suit various tests required for confirming and evaluating conclusions drawn from Chapter 3 and 4 and paving ways for further investigation.

In addition to the consideration that the test results are valid for commonly used engines, the test system, particularly the testing engine, should meet the easy modification of test components, less consumption of oils and fuels, and easy installation of all transducers. In the meantime, the measured dynamic data have less interference, allowing accurate quantify the dynamic responses of interests.

Based on these objectives and considerations, this chapter depicts the full test system with a rigorous description of the vibration measurement system and measurement procedures, in which the rationality is addressed against various objectives.

5.2 Test Rig Construction

The test facilities and instruments are presented in this section; particularly, the test engine specification, the measurement instruments and the data acquisition system. The test engine is a single-cylinder, four-stroke, water-cooled diesel engines for power generation, and for this research, it is locally tailored for the installation of an accelerometer on the external surface of the liner, the aim of which is to collect the vibrational responses of liner as accurately as possible. All of the measured data were recorded and thereafter processed offline for making corresponding comparisons with FE model predictions.

5.2.1 The Test Engine Specification

The engine used for this study is a single-cylinder, four-stroke, water-cooled diesel engine with a bore of 110 mm, a stroke of 115 mm, a displacement of 1.093 litre and a compression ratio of 18. Figure 5-1 shows an overview of the test rig. The major specifications of the engine are described in Table 5-1.

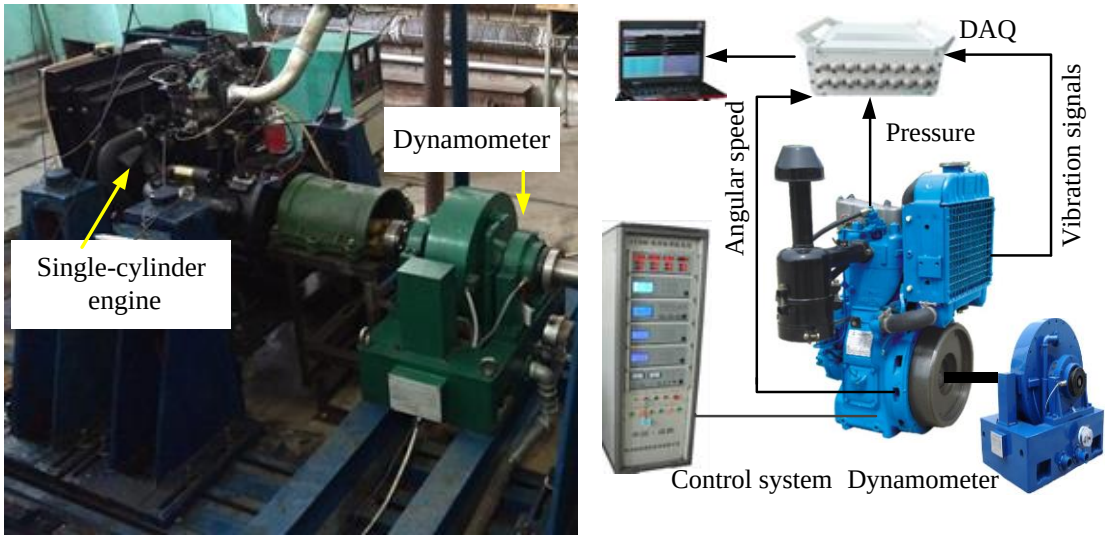

Figure 5- 1 A photograph of the diesel engine test rig

Table 5- 1 Specification of the test engine

Manufacturer	Quanjiao Power Co., Ltd., PR. China
Engine type	QCH1110
Number of cylinders	One
Combustion system	Direct injection, toroidal combustion chamber
Bore/stroke	110/115 mm
Displacement volume	1.093 L
Compression ratio	18:1
Cylinder liners	Cast iron replaceable wet liner
Start of fuel injection	14±2 °BTDC
Rated power	14.7/2400 kW/r/min

The test bench is controlled by an ET2000 Control and Data logging System. ET2000 is an advanced, fully integrated, Windows operating system based engine test system fabricated by ChengBang Company to meet the function and delivery testing needs of various diesel engines, gasoline engines, and gas engines. The ET2000 has adopted digital increment voltage-control technology to make speed and torque of the engine shift without disturbance. It is integrated with high speed data acquisition, dynamometer management and a throttle control system.

5.2.2 Measurement Instrumentation

To acquire accurate test data for the diagnostic analysis of liner vibrations, the test bench was elaborately set up to allow the in-cylinder pressure variation and the changes of vibrations on the cylinder liner under different operating conditions to be measured. Figure 5-1 shows the schematic diagram for the test rig and the measurement equipment used in this study. The test signals were acquired by the following transducers:

- Accelerometer
- Pressure transducer
- Angle transducer

The cylinder pressure signal is used to provide the input source for the dynamic model; in particular, to provide the driving force for the calculation of the piston lateral movement. A Hall shaft encoder was used to measure the speed of the engine via the gear teeth on the flywheel. There was another Hall encoder connecting to the crankshaft to provide a trigger pulse once per revolution in order to synchronise data collection.

- **Accelerometer**

Accelerometers are a widely used device for measuring the vibration of rotating machinery, and have been used extensively in the analysis of dynamic system behaviour. The accelerometer is typically attached to the outer surface of the machinery for measuring the vibration of the body or the structure to which it is attached. In this research, a piezoelectric accelerometer (model INV9824) is used to measure the vibration of the cylinder liner. Figure 5-2 shows the installation scheme of the accelerometer on the external surface of cylinder liner. Technical specifications of the accelerometer are shown in Table 5-2.

Table 5- 2 Technical specification of the accelerometer

Manufacturer	China Orient Institute of Noise & Vibration
Model	INV9824
Axial sensitivity (20±5℃)	5mV/g
transverse sensitivity	≤5%
Frequency range 5%	1 to 15kHz
Mounting resonance frequency	40kHz
Polarity	Positive direction
Isolation resistance	>108Ω
Operating temperature range	-40 to +120℃
Shock limit (±peak)	1000g
Magnetic sensitivity	2 g/T
Base strain sensitivity	0.6 mg/με
Weight	18g

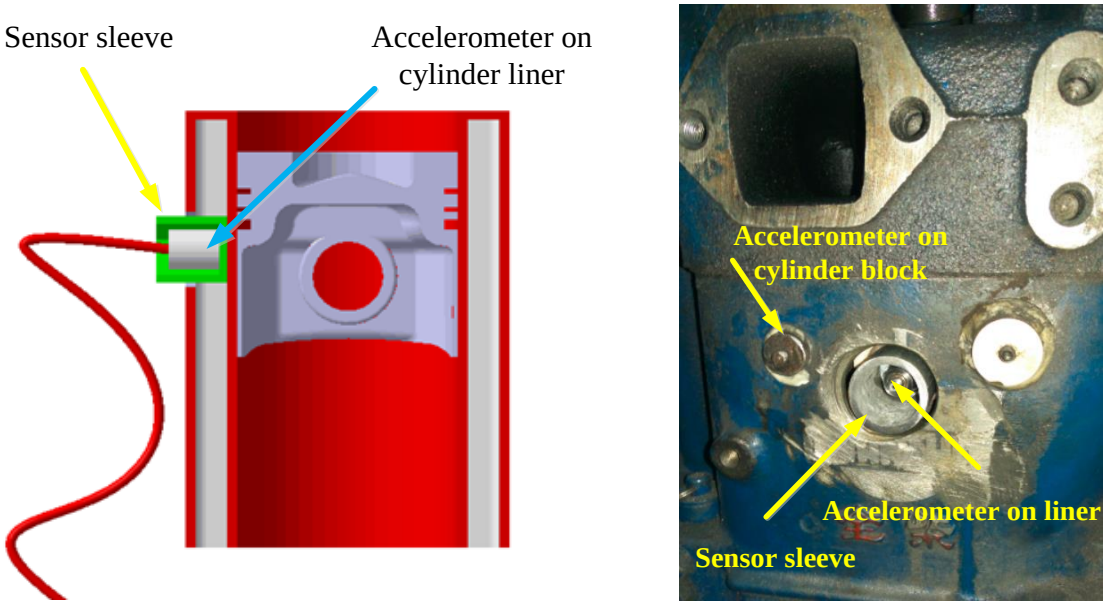

Figure 5- 2 The installation scheme of the accelerometer on the cylinder liner

A special accelerometer installation method was designed and implemented for the purpose of measuring the liner vibrations directly with minimum interference. As shown in Figure 5-2, a through-hole with diameter of 30 mm was drilled on the engine block.

Passing through the water jacket, a tailored copper sensor sleeve was fixed on the outer surface of the cylinder liner using heat-resistant super glue. Then, an accelerometer for measuring liner vibrations was installed directly on the external surface of the liner through the waterproof adapter.

- **Pressure transducer**

The in-cylinder combustion pressure was measured using a 601CBA series pressure sensor (Kistler Instruments Ltd.) as shown in Figure 5-3. The sensor was fixed in the combustion chamber with the help of a copper adaptor. The transducer has a combination of high accuracy, high overload, excellent stability and a fast dynamic response. With its operating pressure ranging from 100 mbar and 250 bar gauge, it has also been specifically designed to work at high temperatures for precision measurement in internal combustion engines. To prevent leakage of the water coolant, and to facilitate the disassembly of the sensor, a mounting sleeve for the pressure sensor installation was designed as seen in Figure 5-3(a). To achieve the effective pressure seal, the actual sensor bore can be machined accurately in the sleeve, which is another advantage of sleeves.

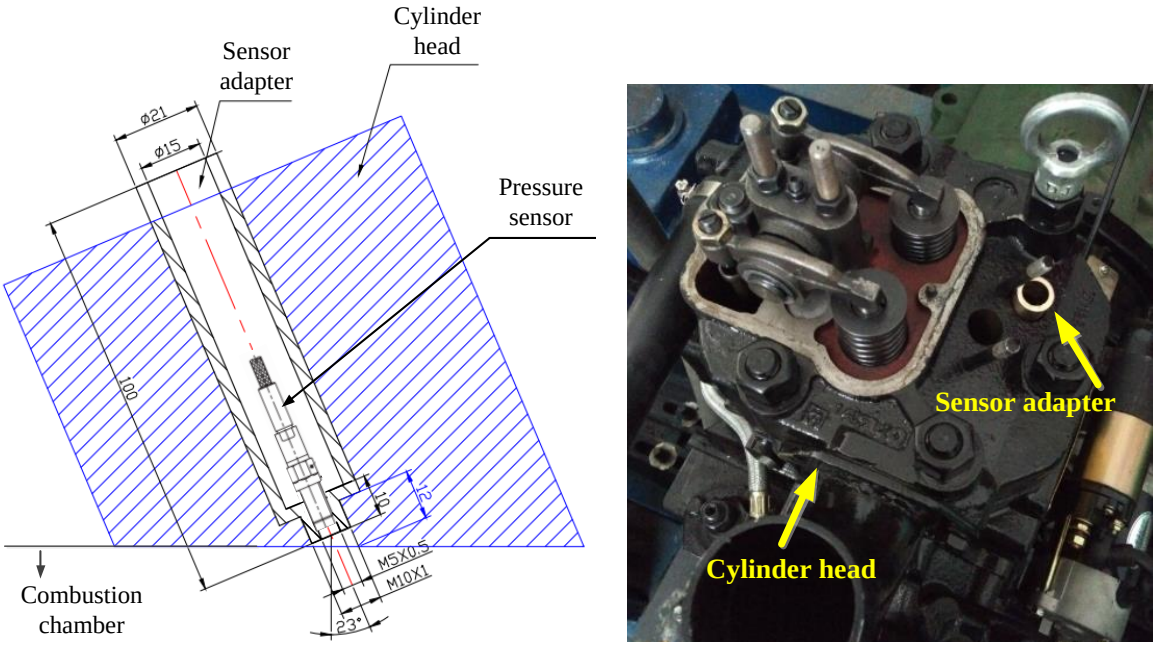

Figure 5- 3 The installation scheme of the pressure sensor

- **Calibration of transducers**

Precision measurements depend on accurate and repeatable sensor calibration methods. Standardization of calibration test equipment and measurement techniques ensures more accurate and repeatable measurements. In this thesis, the calibration of accelerometer was achieved based on the back-to-back (BTB) comparison method which has been widely accepted as a laboratory standard. The accelerometer was mounted upon a reference accelerometer that has been previously calibrated by a recognized laboratory. The calibration method of pressure transducer is similar to that of accelerometer. The pressure transducer to be calibrated was mounted on a pressure generator in parallel with a reference transducer that has been previously calibrated. By contrast, the calibration approach of Hall shaft encoder is relatively simple which is mainly achieved by adjusting the distance between the sensor head and gear tooth on the flywheel.

5.2.3 Data Acquisition System

The dynamic data was acquired by a YE6232B data acquisition system from Sinocera Piezotronics, Inc., which is a general purpose dynamic data acquisition system (DAQ). The DAQ has built-in signal conditioners and able to collect the data from sensors measuring vibration, in-cylinder pressure, temperature and operating speed, and sends them into a PC for post processing and analysis. A photograph of the data acquisition system is shown in Figure 5-4 and its main specifications are contained in Table 5-3.

Figure 5- 4 Data acquisition system used for tests

Table 5- 3 YE6232B DAQS specifications

Manufacturer	Sinocera Piezotronics, Inc.
Model	YE6232B
Number of Channels	16 (selectable)
A/D Conversion resolution	24 bit
Sampling rate (maximum)	96kHz per channel, Parallel sampling
Input range	±10 V
Gain	×1, ×10, ×100
Filter	Anti-aliasing
Interface	USB 2.0

During tests data are collected based on the maximum sampling frequency of the DAQ, i.e. 96000 samples per second, and each set of dynamic data has been acquired for 30 seconds. For such settings the length of data collected for each set is 30×96000= 2880000 data points. This data acquisition system is equipped with an antialiasing filter which guarantees that the aliased frequencies are not captured. Additionally, the antialiasing filter is also used to automatically adjust the cut-off frequency of another built in low pass filter based on a pre-selected sampling rate[17].

5.3 Test Operations

Testing was carried out based on the QCH1110 test engine. The data was collected using related transducers for future analysis. In order to compare the collected data and to perform the time domain or angular domain average of the signals, a reference point was obtained by using a Hall shaft encoder to measure a special indentation on the front face of flywheel.

For comparison purposes raw signals were collected from the sensors under different operating conditions and fuelled with different fuels, meaning that the engine was running under various operating speeds and loads supplied by diesel, biodiesel and methanol-diesel blended fuel, respectively.

Table 5- 4 Test operating procedure

Fuel	**Speed (rpm)**	**Load (Nm)**
Diesel	1000, 1200, 1400, 1600,1800	10, 40
Biodiesel	1000, 1200, 1400, 1600,1800	10, 40
M15 (Methanol in diesel: 15 wt %)	1000, 1200, 1400, 1600,1800	10, 40

In the experiment, the test engine operated at different loads and speeds in the operating setups as shown in Table 5.4 for different alternative fuels and lubricating oils. In the operating setup, for the speed and load variation, the engine was running at five speeds from 1000rpm to 1800rpm in intervals of 200rpm, with two loads being applied at each speed: 10 Nm and 40 N m. The test engine was fuelled with fossil diesel, biodiesel and methanol- diesel blended fuel M15. M15 represents the mixture of 15% methanol, 10% co-solvent isobutanol and 75% diesel. The rapeseed biodiesel is produced by a transesterification process from 'virgin' oil using methanol. The main physical properties such as the composition, density, lower heating value (LHV) and viscosity are presented in Table 5-5 [93].

Table 5- 5 Properties of biodiesel [93]

Property	**Measured**	**Units**
Composition	77	% C
	12	% H
	11	% O
Density	879	Kg/m^3
LHV, KJ/Kg	38.5	MJ/Kg
Kinematic Viscosity	4.9	mm^2/s

To investigate the influence of changes in oil properties to the dynamic responses of cylinder liner, an extended experiment was designed based on the first operating setup. The test procedure proposed above is still used in this experiment; the only difference is an additional oil replacement operation after completing the entire operation. This test

procedure was repeated three times until all three different lubricating oils were replaced and studied. The dynamic responses of a cylinder liner lubricated by different lubricating oils in the grades of 0W20, 10W30, 20W50 and an used 10W20 oil (about 10000 kilometres, from a Land Rover Freelander II) are measured and analysed. The key properties of the lubricating oils used in the test are detailed in Table 5-6.

Table 5- 6 Main properties of lubricating oils

Property	**0W20**	**10W30**	**20W50**
Viscosity μ_0 /Pa.s	0.0038	0.01	0.02
Modulus E' /$\times 10^9$Pa	1.0969	1.1078	1.1034
Viscosity-pressure coefficient α /Pa^{-1}	2×10-8	3.19×10-8	4×10-8

Chapter 6
Experimental Studies of Cylinder Liner Vibrations

This chapter evaluates predictions in Chapters 3 and 4 against experimental results. To confirm the generality of the results, the evaluation was carried out under different engine operating conditions, two representative alternative fuels and three lubricating oils. As the measured vibration contains random noise and exhibit high non-stationarity, the state of the art continuous wavelet transform (CWT) is used to highlight the dynamic responses localised in both the time and frequency domains.

6.1 Introduction

To evaluate the predictions derived from dynamics simulation, an in-depth time–frequency analysis of measured cylinder vibration is needed to fully understand the interrelations among the response characteristic, operating condition, fuel characteristics and lubricant properties. The vibration signals measured from cylinder liner are noisy and non-stationary with wide frequency band. It is not possible to reveal the instantaneous and non-stationary characteristics of vibration signals effectively just using conventional signal processing methods based on the time or frequency domain. Continuous wavelet transformation (CWT) has the ability to highlight the dynamic responses, present the high frequency band details and can reveal time-frequency characteristics of a non-stationary vibration signal. To confirm the generality of the results, the evaluation was carried out under different engine operating conditions, two representative alternative fuels and three lubricating oils.

6.2 Dynamic Responses to Engine Operating Conditions

As the measured vibration contains random noise and exhibits high non-stationarity, continuous wavelet transform (CWT) was applied to the raw vibration to highlight the dynamic responses localised in the joint time and frequency domains. In addition, the wavelet result was averaged over 80 engine cycles to further suppress noise and random short duration interferences for obtaining reliable results.

Figure 6-1 presents a typical CWT result of the liner vibration under the operating condition of 1800rpm and 40Nm. The complicated time-frequency characteristics in Figure 6-1(a) can be viewed as having the following key patterns:

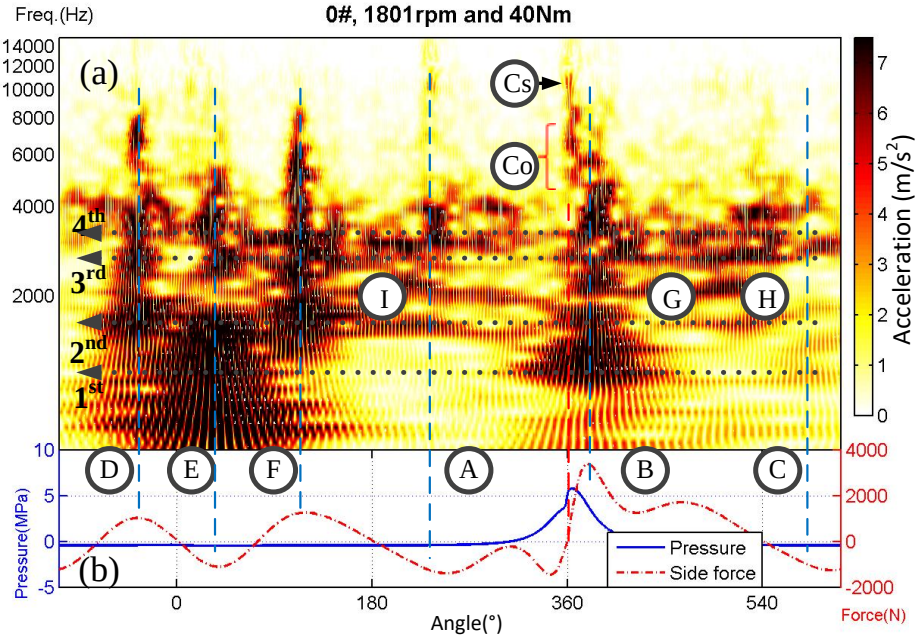

Figure 6- 1 CWT of vibration signal under 40Nm and 1800rpm

The significant responses, marked as Ⓒo and Ⓒs appear around the combustion TDC at 360 °and in the frequency range from 6000Hz to 8000Hz, and 8000 to 12000Hz. Moreover, they can well correspond to the peak of in-cylinder pressure, which is agreeable with the numerical prediction presented in Section 3.4.1 and Figure 3-6.

More distinctive responses, marked as Ⓐ to Ⓕ, correspond to dynamic events induced by piston slaps, being consistent with that in Section 3.4.2 and Figure 3-7. These responses appear in the frequency band from 900 to 4000Hz, which associates with the first four modal frequencies of the cylinder liner.

Furthermore, three more events predicted in dynamic simulation can also be observed in Figure 6-1(a), marked as Ⓖ, Ⓗ and Ⓘ in the frequency range around 2000Hz, showing that the sustained high-amplitude side-thrust force can cause repeated impacts, which agrees with that of the established FE model.

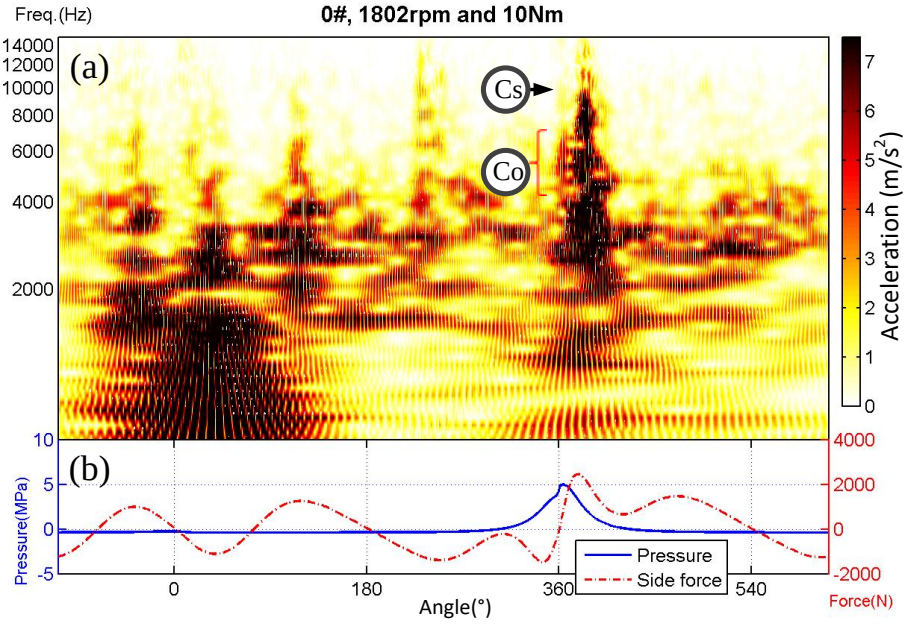

Figure 6- 2 CWT of vibration signal under 10Nm and 1800rpm

Likewise, the time-frequency responses of the liner under a lower load show significant patterns corresponding to the combustion shock which is marked as Ⓒs in Figure 6-2. However, the combustion is smoother when they are in a frequency band from 4000Hz to 7000Hz, which is 2000Hz lower than that of higher load. Moreover, almost all of the slap-induced events above 2000Hz are significantly reduced, showing that the piston movement driven by the smoother combustion is prone to exciting more low-frequency mode components.

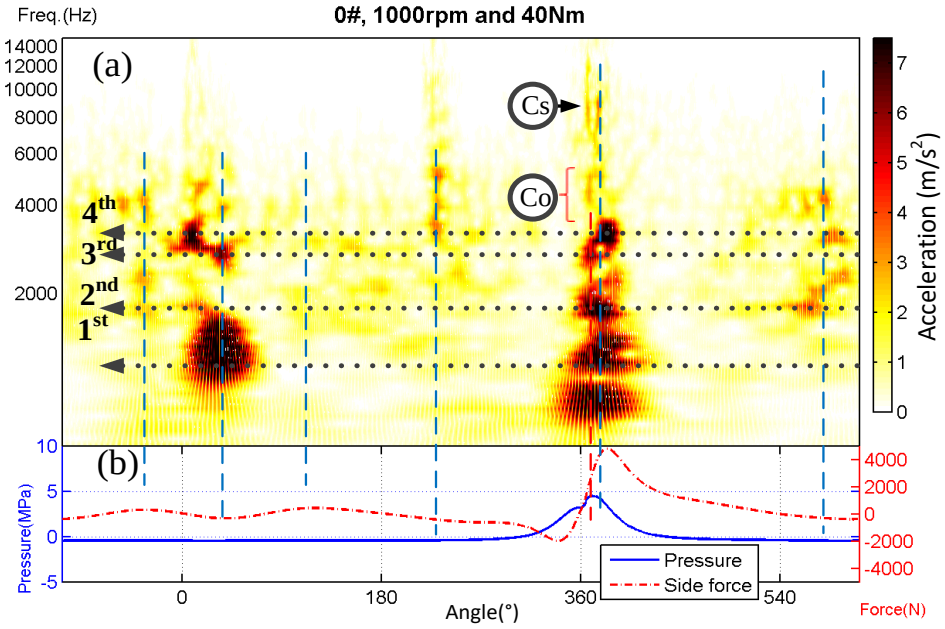

Figure 6- 3 CWT of vibration signal at 40Nm and 1000rpm

At the low-speed of 1000rpm and 40Nm, CWT plots in Figure 6-3(a) show significant reduction of amplitudes for all dynamic events aforementioned. Particularly, only two events around the combustion TDC and exhaust TDC are still significant. The main reason is that, under low-speed conditions, the kinetic energy of the piston lateral movement is low due to the reduced reciprocating inertia force, which leads to a reduction in the frequency content of the piston side-thrust force.

6.3 Dynamic Responses to Alternative Fuels

Understanding of the correspondence between the response characteristics and operating conditions enables a more accurate and in-depth study of the influences of alternative fuels combustion on the response characteristics of cylinder liners.

6.3.1 CWT Analysis

As stated in Section 6.2, under low-speed conditions, the dynamic responses to excitations are less apparent and show fewer components. Therefore, in order to facilitate comparative analysis of the influences of burning alternative fuels on the liner vibrations, only the

CWT of vibration signals at one engine speed 1800rpm with two loads of 10Nm and 40Nm are selected and analysed, as seen in Figure 6.4.

Since the peak pressure and PRR of biodiesel are not as high as those of the other fuels, the combustion shock-induced responses Ⓒo and Ⓒs of biodiesel located in the frequency range from 5000 to 7000Hz and 10000Hz to 12000Hz, slightly lower than the diesel, as shown in Figure 6-4.1. However, in the entire work cycle, biodiesel showed more abundant and intensive response events than the diesel, which is agreeable with the numerical prediction in Section 4.4 and Figure 4-4(a). This may be due to the prolonged combustion duration as a result of larger amount of biodiesel injection (biodiesel possesses a lower calorific value). The extended mixed-controlled combustion phase can cause a relative increase in the kinetic energy of piston side slaps, thereby resulting in the increase in response intensity and the number of observable events.

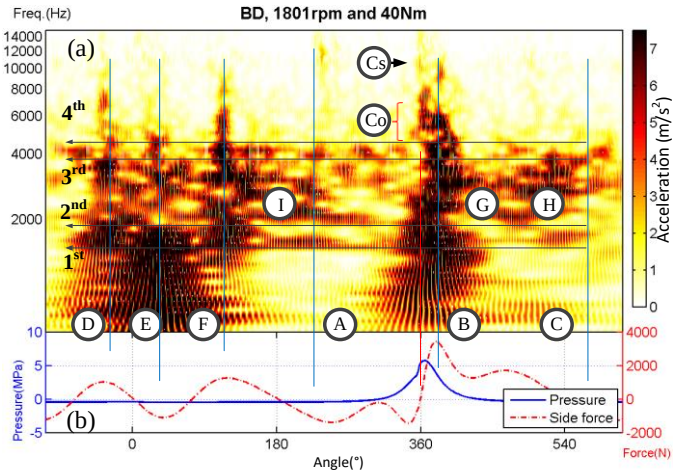

(1)CWT of vibration fuelled with BD, 1800rpm-40Nm

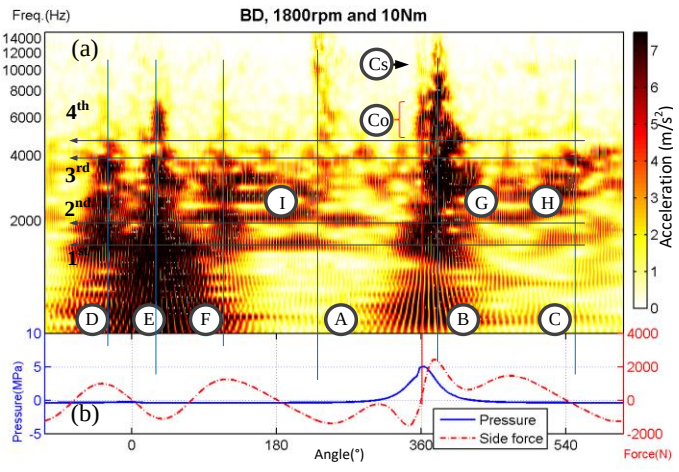

(2) CWT of vibration fuelled with BD, 1800rpm-10Nm

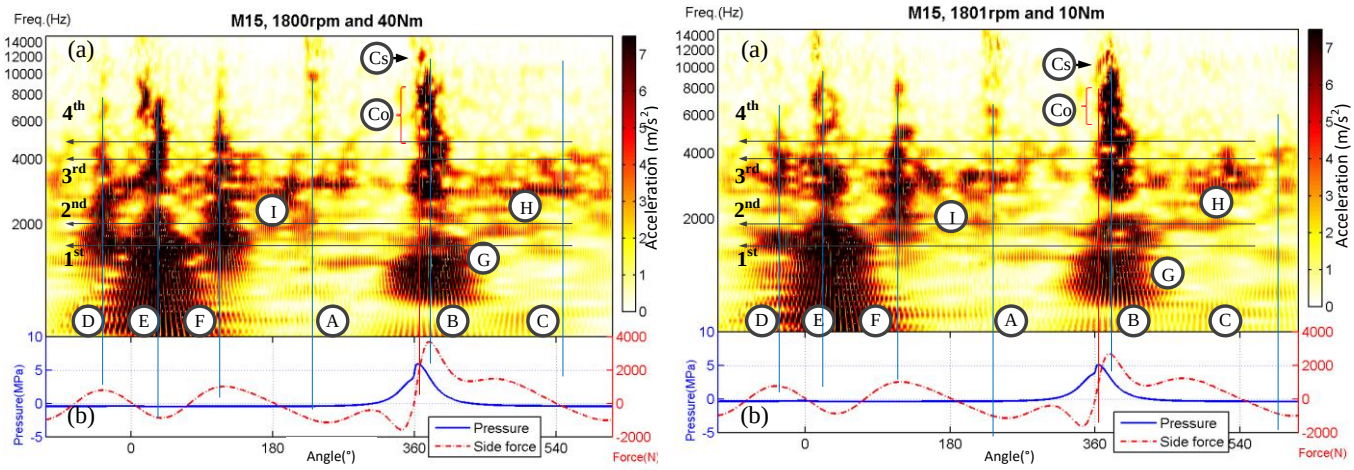

(3) CWT of vibration fuelled with M15, 1800rpm-40Nm (4) CWT of vibration fuelled with M15, 1800rpm-10Nm

Figure 6- 4 CWT of liner vibrations fuelled with alternative fuels under different operating conditions

However, the CWT of methanol-diesel blended fuel M15 shows almost the opposite result. Due to the combustion-supporting characteristic of methanol, M15 has a larger rise rate of pressure, which results in a higher response frequency of combustion-induced event Ⓒs from 6000 to 9000Hz. Correspondingly, the sharp combustion behaviour of M15 causes a higher kinetic energy of piston lateral movement concentrated in the combustion TDC, thus resulting in the uneven distribution of response events over the entire operating cycle. As seen in Figure 6-4.3, the piston slap-induced responses around the combustion TDC show a clearly upward shift to the frequency range of 3000 to 8000Hz. While almost all the other events above the frequency of 2000Hz, especially the secondary events Ⓖ, Ⓗ and Ⓘ, are significantly reduced. This indicates that a rough combustion can cause severe vibrations of the engine around the combustion TDC, as a combined result of the combustion shock and its consequent piston slap.

Under low-load conditions, .as seen in Figure 6-4.2 and Figure 6-4.4, the combustion shock-induced events Ⓒs fuelled with alternative fuels are in the frequency band of 4000 Hz to 7000 Hz, which is 2000Hz lower than that of the higher load. Likewise, all the slap-

induced events above 2000Hz are significantly reduced, showing that the piston movement driven by the smoother combustion is prone to excite more low-frequency mode components.

It can be seen that the dynamic responses of the same fuel under different operating conditions possess a similar pattern in the time-frequency characteristics. In other words, the response patterns of a fuel are definite and unique, corresponding to the physicochemical properties of the fuel itself.

To get a further understanding of these differences in the localised response features fuelled with alternative fuels, it is necessary to perform some contrastive and diagnostic analyses on these features under different operating conditions.

6.3.2 Diagnostic Analysis

In order to study the variation trends of localised dynamic responses to different fuels, several representative local features were chosen to carry out comparative analysis. The root mean square (RMS) results of combustion shock-induced dynamic response Ⓒs have been drawn as shown in Figure 6-5(b). The RMS results of piston slap-induced events Ⓑ and Ⓔ, at combustion TDC and exhaust TDC, under different operating conditions, have been presented in Figure 6-5(c) and Figure 6-5(d).

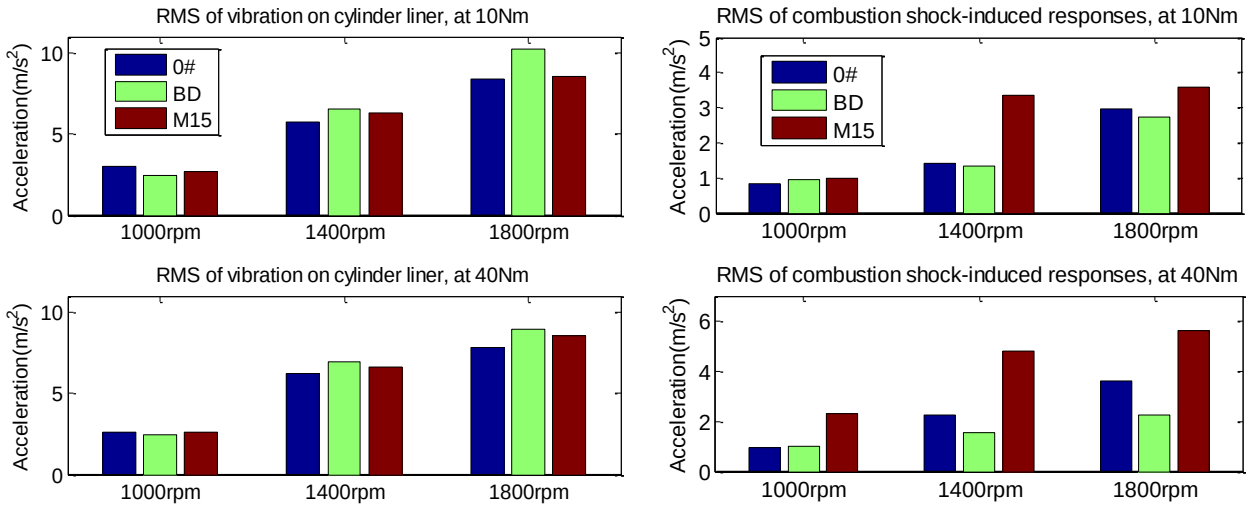

(a) Overall RMSs of liner vibrations

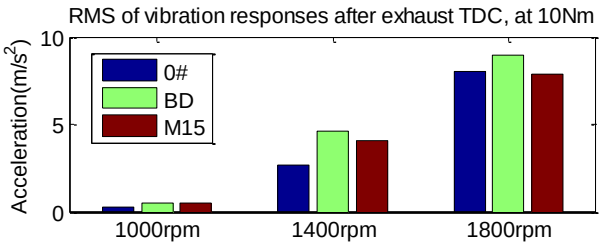

(b) RMSs of localised responses to combustion shocks

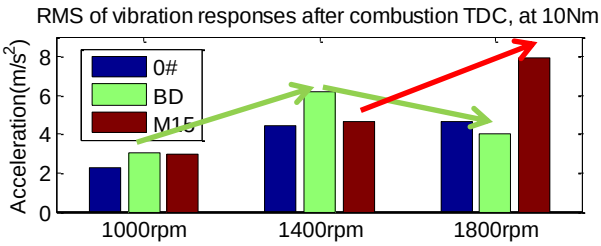

(c) RMSs of local responses after exhaust TDC

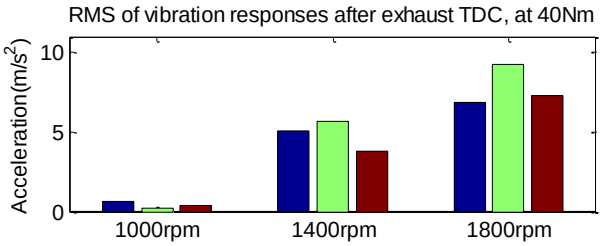

(d) RMSs of local responses after combustion TDC

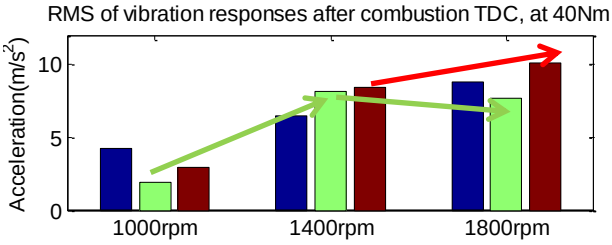

Figure 6- 5 Comparison of characteristic parameters of different fuels

First of all, the overall RMS results of vibrations measured from the cylinder liner have been calculated and drawn as shown in Figure 6-5(a). As the operating speed increases, the RMS value of the vibrations on the cylinder liner gradually increases.

With an increase of the operating speed, the RMS of the liner vibration fuelled with biodiesel shows a greater increment than the other fuels, which might be attributed to the prolonged combustion duration. Due to the lower calorific value of biodiesel, a greater amount of fuel was injected into the combustion chamber, to generate the same mechanical power as the diesel. The extended combustion duration led to a relative increase in the kinetic energy of the piston lateral movement, thereby resulting in a rapid rise in the RMS of the liner vibrations.

Although the methanol can boost the combustion process, the combustion duration of methanol-blended fuel, especially the mixed-controlled combustion phase, is close to the diesel, thus showing a similar trend to that of the diesel in the RMS of vibrations.

To understand the direct influence of combustion shock on the dynamic responses of the cylinder liner, the RMS results of combustion shock-induced vibration Ⓒs have been presented in Figure 6-5(b). With an increasing engine speed, the RMS of combustion shock-induced response shows a proportional increase to the peak value of the pressure rise rate, suggesting that the selected local feature can well characterise the immediate influence of the combustion force to dynamic responses.

The differences between the alternative fuels in combustion-induced responses are even more pronounced than the overall responses. As the speed increases, under both load conditions of 10Nm and 40Nm, the RMS of biodiesel becomes less than that of the diesel, while the methanol-diesel blended fuel M15 shows a dramatic increase, which is even faster than the others. These trends can well correspond to the combustion properties of alternative fuels regarding the peak value of the pressure rise rate. A smaller peak value is reached in the rise rate of pressure due to the smoother in–cylinder combustion of biodiesel, which means the frequency contents of in-cylinder combustion pressure is relatively less and not sufficient to motivate many clear mode responses. Conversely, the PRR peak of M15 is greater than that of the other fuels because of the combustion supporting characteristic of methanol, giving rise to the more intensive responses.

Then, a contrastive analysis on the localised response characteristic is approached by choosing two typical local features after combustion TDC and exhaust TDC respectively, in order to study the influence of piston lateral movement on the cylinder dynamic response characteristics from under different conditions.

The RMS results of piston slap-induced events Ⓑ and Ⓔ, around the combustion TDC and exhaust TDC respectively, under different operating conditions, have been presented in Figure 6-5(c) and Figure 6-5(d). As shown in Figure 6-5(c), the changing trends of RMSs after exhaust TDC correspond well to the previous numerical prediction in Section 4.4 and in Figure 4-6(a). The inertia force of piston assembly is directly proportional to the square of crankshaft speed, as seen in Eq. (3.1). The lateral inertia force of piston assembly

increases dramatically with the square of running speed, from 1000rpm to 1800rpm. Consequently, the kinetic energy of the piston lateral movement shows a rapid growth along with an increase in the running speed, resulting in a sharp increase in the vibrational responses to the piston slap after exhaust TDC.

Differences in the response trends between fuel types show a similar pattern to that of the overall vibrations, which further confirms the earlier proposed explanation that the overall responsive intensity is determined by the combustion duration. The magnitude of the inertial force is more affected by the driving action of combustion force during the late stage of combustion contains part of mixed-controlled combustion phase and late combustion phase. The extended combustion duration of biodiesel can cause a relative increase in the kinetic energy of the piston lateral movement, thereby resulting in a rapid growth in the RMS around exhaust TDC. Because of the similar combustion duration to diesel, the RMS result of M15 shows a rising trend close to that of diesel.

As seen in Figure 6-5(d), the variation trend of dynamic responses after combustion TDC has also shown a high similarity to the numerical prediction in Section 4.4 and Figure 4.6(b). The RMS of biodiesel shows a clear tendency of decrease after an increase, which cannot be well interpreted by the combustion characteristics of biodiesel itself. As the speed increases, the ignition phase of biodiesel advances gradually, resulting in the enhanced cancellation effect between the combustion force and the inertia force of the piston. Since the driving action of the combustion force is substantially offset by the inertia force, the magnitude of the piston side-thrust force drops significantly, eventually leading to the downward trend at high-speed conditions.

On the contrary, as a result of the non-inflammability property of methanol, the ignitions phase of M15 shows a significant postponement, which consequently leads to the separation between the two peaks of gas pressure and inertia force. As the cancellation effect between the combustion force and inertia force gradually weakens, the magnitude of the piston side-thrust force continues to rise along with an increase in the running speed, thereby causing more intensive dynamic responses.

6.4 Dynamic Responses to Changes in Lubricant Properties

John J. Truhan and P. S. Dellis et al. [82], [83] proposed that the differences in the lubricant properties can cause observable changes in the dynamic behaviours of critical kinematic pairs in IC engines. In particular, a lubricant with a higher viscosity may result in a larger damping factor of lubricant film, thereby diminishing the dynamic responses.

As previously noted, the local features associated with mode responses can well reflect the impact intensity between the piston and liner surfaces. To eliminate the interference from combustion behaviours, the local feature of the liner vibration after exhaust TDC and in the frequency range of 1000 to 3500Hz was selected for diagnostic analysis. Figure 6-6 shows the RMS result of local response at exhaust TDC lubricated by four different lubricating oils.

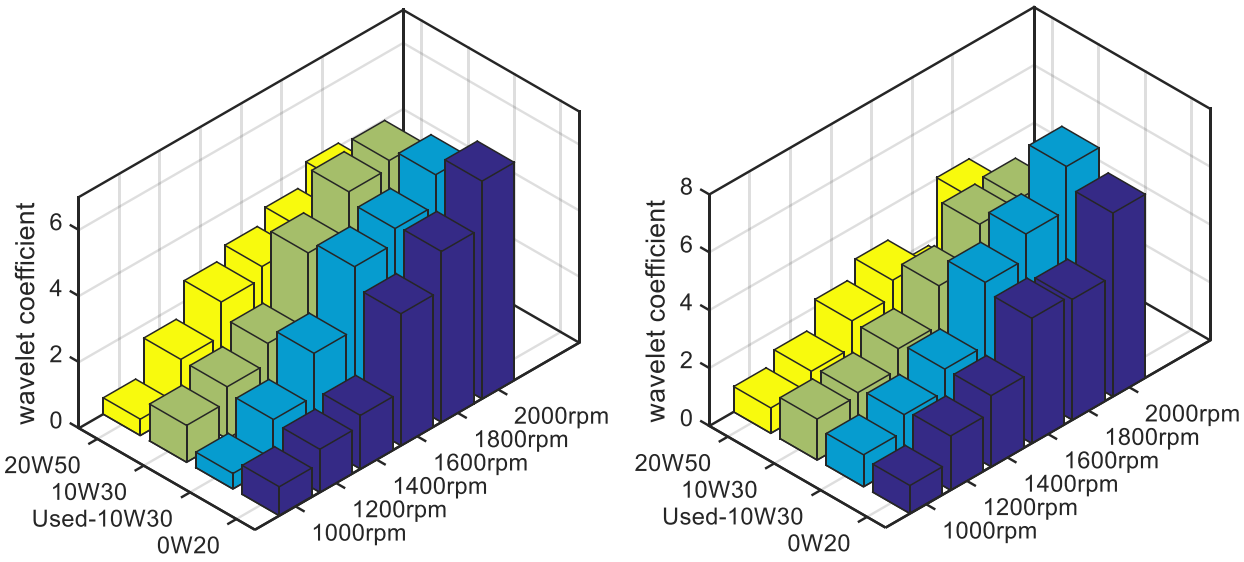

(a) Under operating conditions of 10Nm; (b) Under operating conditions of 40Nm.

Figure 6- 6 RMSs of local responses at exhaust TDC lubricated by four different oils

As seen in the bar plots with the increase of oil viscosity, the magnitude of the impact response basically shows a downward trend. It turns out that the changes in oil properties, and especially in kinematic viscosity, can definitely affect the kinetic parameters of the film, thus affecting the dynamic behaviours between piston and liners.

However, it should be noted that in low-speed conditions, the RMSs of liner response lubricated by 0W20 oil are slightly lower than the other oils. This may be because the severe situation of the oil supply for splash lubrication at low-speed conditions is effectively improved by the high mobility of lubricants, as the result of the lower viscosity of 0W20. High mobility helps more lubricating oil splashing to reach the clearance between piston and liner surfaces, thrown out by the instantaneous rotation of the crankshaft. Sufficient fluid on the liner surface is helpful to achieve fully flooded lubrication, and to form thicker film, thereby reducing the dynamic responses of liners.

Moreover, the used lubricating oil 10W30 shows more intensive responses than the new 10W30 oil, which can be attributed to the degradation of oil properties after long-term usage. The oil properties, and especially the viscosity, constantly worsen over time, which can ultimately lead to the reduction of film stiffness and damping, and cause more intensive dynamic responses. These findings accord well with the previous experimental results [82], [83].

Experimental results show that differences in the lubricant properties can definitely cause observable changes in the vibration responses of cylinder liners in IC engines. A lubricant with a higher viscosity can indeed cause an enhanced damping effect in the lubricant film, thereby diminishing the dynamic responses. However, the variations in oil characteristics such as viscosity reduction will also affect the status of the oil supply, thereby affecting the formation and distribution of film, causing changes in vibration response characteristics. The dynamic characteristics of lubricant film are influenced by many superimposed and coupled factors. These factors relates to multiple disciplines such as tribology, fluid dynamics and multiphase flow, which can hardly be analysed through numerical modelling. Further studies are still needed in the future to understand the in depth linkage between the oil properties and the vibration responses of engines.

In summary, it has been confirmed that the dynamic responses of the cylinder liner, particularly, the vibration responses are sensitive to the operating conditions, fuel

properties and lubricant oils. This shows that it is possible to diagnose any changes caused by using alternative fuels based on external vibration measurements.

Chapter 7

A Dynamic Deformation based Lubrication Model between the Piston Rings and Cylinder Liners

This chapter presents the development of an improved mathematical model of film formation with consideration of the liner dynamic deformations. Based on classic hydrodynamic lubrication theory, the dynamic defamation of cylinder liners is taken into account through a rationally modified shear factors subsequently. The influences of structural deformation on cylinder frictional characteristics are predicted based on the improved model.

7.1 Introduction

In modelling oil film formation and distribution on the cylinder liners, the cylinder wall is often taken as being a perfect cylindrical surface by the majority of researchers[4]–[7]. These studies lead to in-depth understandings of the lubrication process.

In addition to the ring and liner geometrics, ring and liner surface waviness and roughness which is already inclusive in the model, the oil film thickness can also be influenced further by the following factors [84]:

- Ring rigid-body displacement due to eccentricity and piston secondary motion
- Ring deformation
- Cylinder liner deformation

Nevertheless, according to the simulation result in Section 3.4, the amplitude of liner deformations induced by piston slaps is at the order of 0.1 microns, being about 20% of the roughness amplitude; this may affect the distribution of oil film. Consequently, to examine the influences of the deformation on lubrication performance and the friction losses of liners, this chapter improves the existing oil film models by taking into account the deformations obtained in the previous section. Accordingly, frictional fluctuations are predicted based on the improved models.

7.2 Formation and Distribution of Lubricant Film between Piston and Liners

It is widely accepted that the Stribeck curve, as shown in Figure 7-1, generally represents the lubrication regimes for sliding surfaces which are categorised into: boundary friction, mixed friction and hydrodynamic friction.

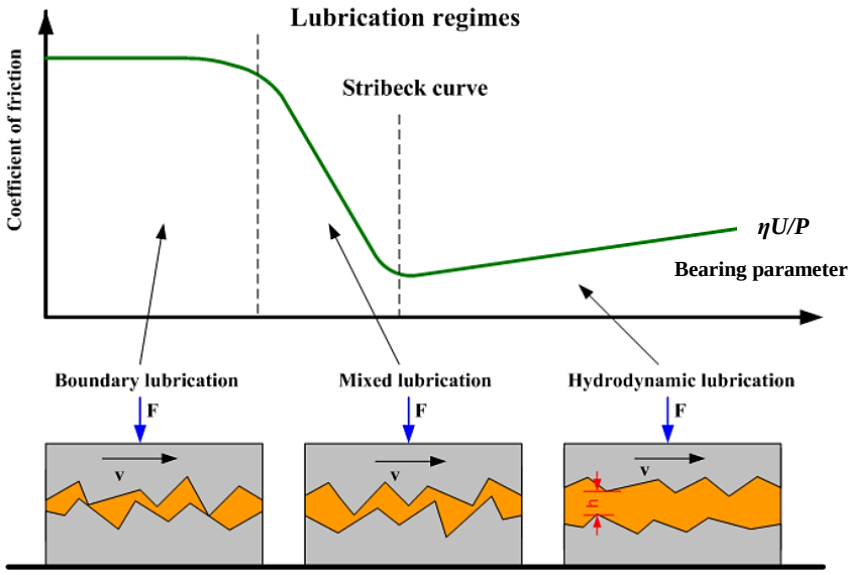

Figure 7- 1 Stribeck curve

On the basis of the Stribeck curve, it clearly shows that the friction coefficient is highest in the cases of boundary lubrication, while the minimum value of the friction coefficient appears in the demarcation between full fluid-film lubrication and the mixed lubrication with a few solid asperity interactions. The friction coefficient during hydrodynamic lubrication shows an obviously ascending trend along with the increase of sliding velocity. Stribeck and other researchers systematically studied the variation of friction between two liquid lubricated surfaces as a function of a dimensionless lubrication parameter $\eta U/P$, where η is the lubricant viscosity, U is the sliding speed and P is the normal load applied on to the matched surface.

In 1886, Osborne Reynolds first proved that the hydrodynamic pressure generated in a viscous liquid can physically separate two sliding surfaces[85]. Reynolds equation describes the hydrodynamic behaviours of thin film between narrow channels. It is derived from Navier-Stokes and continuity equations for incompressible flow under a number of critical assumptions detailed in Table 7.1.

Table 7- 1 Basic assumptions the Reynolds' equation

Assumption	**Comments**
Newtonian fluid	Stress is proportional to the rate of shear
Laminar flow regime	There is no disruption between the parallel flow layers.
Negligible inertia forces	Valid for low bearing speed or high load
No slip condition at fluid-solid interface	Valid, except for rarefied gas films
Fluid density constant	Usually valid for small thermal expansion.
Fluid viscosity constant	Usually uses effective viscosity
Pressure constant across the film thickness	Always valid, since hydrodynamic film is micrometre thickness

Based on these assumptions the Reynolds' equation between two interfacing/matched surfaces can be expressed as

$$\frac{\partial}{\partial x}\left(\frac{h^3}{\eta}\frac{\partial p}{\partial x}\right)+\frac{\partial}{\partial z}\left(\frac{h^3}{\eta}\frac{\partial p}{\partial z}\right)=6U_x\frac{\partial h}{\partial x}+12\frac{\partial h}{\partial t} \qquad (4.6)$$

where $p=p(x,z,t)$ is the oil film hydrodynamic pressure field and $h=h(x,z,t)$ is the distribution of the film thickness. Figure 7-2(a) shows the coordinate system and notation used in this work. The lubricant viscosity and the piston primary velocity are represented by η and U, respectively. The positive direction of the h-axis is chosen to be towards the thrust side of the piston. The x-axis is along the axial direction of the piston. Both terms in the right-hand side of the Reynold's equation affect the hydrodynamic pressure and are of physical significance. The first term represents the so-called lubricant shearing effect due to the motion of the piston along the x direction. The second term is the oil film squeeze action due to the instantaneous motion of the piston in the h direction.

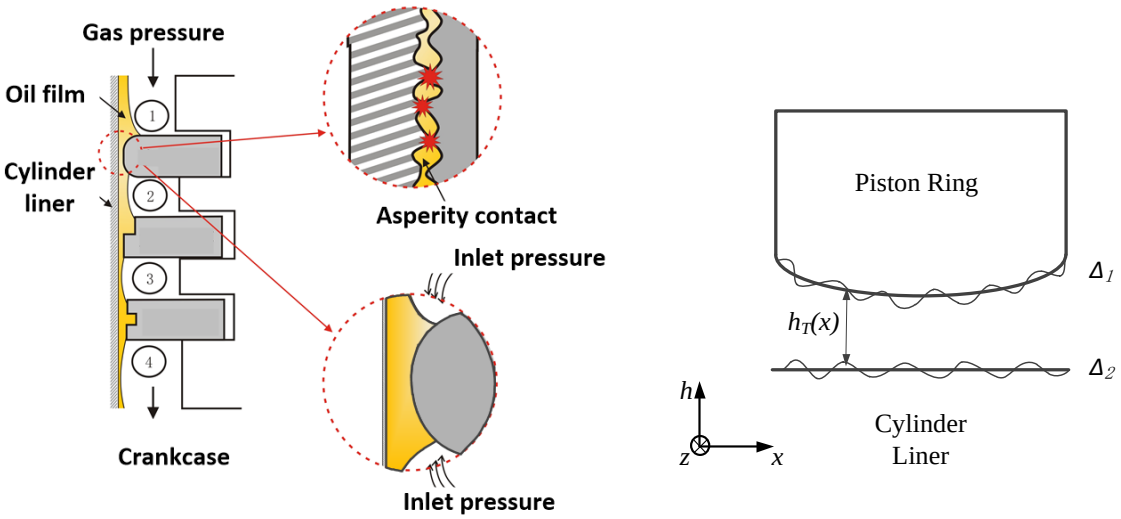

Figure 7- 2 Characteristics of the lubrication regimes between the piston ring and cylinder liner

Due to the secondary motion of the piston, the relative movements between the piston ring and liner wall are mostly in a condition of mixed lubrication. When the hydrodynamic bearing pressure is insufficient to separate the matched surfaces, surface asperities contact occurs. Such a lubricated contact is commonly known as mixed lubrication. Usually a statistical macro-scale method or a deterministic micro-scale method describes mixed lubrication.

Figure 7-2 depicts a conjunction between the piston ring and cylinder liner with surface roughness. Here the function $h_T\ (x)$ describes the local film thickness, including surface roughnesses. The local film thickness h_T is given by

$$h_T = h + \Delta_1 + \Delta_2 \tag{4.7}$$

Where h is the nominal film thickness, Δ_1 is the surface roughness amplitude of piston ring, and Δ_2 is the surface roughness amplitude of cylinder liner. The nominal film thickness $h = h_{min}(t) + h_x(x)$, giving

$$h_T = h_{\min}(t) + h_x(x) + \Delta_1 + \Delta_2 \tag{4.8}$$

For the case of one-dimensional lubrication, the average gap $\bar{h}_T$ is defined as

$$\bar{h}_T = \int_{-h}^{\infty} (h + \Delta) f(\Delta) d\Delta \qquad (4.9)$$

where $\Delta = \Delta_1 + \Delta_2$ is the combined roughness of the ring and liner, and f is the probability density function that describes the statistics of surface roughness Δ.

In a mixed lubrication regime, Patir-Cheng's average Reynolds equation describes the isothermal, incompressible lubricant behaviour between the ring and liner rough surfaces

$$\frac{\partial}{\partial x}\left(\phi_x \frac{h^3}{\eta}\frac{\partial \bar{p}}{\partial x}\right) + \frac{\partial}{\partial z}\left(\phi_z \frac{h^3}{\eta}\frac{\partial \bar{p}}{\partial z}\right) = 6U\phi_c \frac{\partial h}{\partial x} + 6U\sigma \frac{\partial \phi_s}{\partial x} + 12\phi_c \frac{\partial h}{\partial t} \qquad (4.10)$$

where ϕ_x, ϕ_z, ϕ_s are flow factors that depend upon surface roughness conditions. $\bar{p}$ is the mean pressure, and σ is the composite RMS roughness of ring and liner. A contact factor ϕ_c is introduced

$$\phi_c = \frac{\partial \bar{h}_T}{\partial h} \qquad (4.10)$$

to simplify the numerical implementation [86]. The first terms of the right side of equation (4.6) are written as $\partial h/\partial x$ and $\partial h/\partial t$ functions in Eq. (4.10). Surface roughness has a profound effect on fluid flows. Surface roughness can affect flows near the surface, altering boundary layer flows. Flow factors capture the statistical properties of surface topography.

Asperity Contact

Surface asperities contact only when the hydrodynamic pressure is insufficient to separate two matching surfaces. Greenwood-Tripp's rough surface contact model estimated the asperity contact load based on the surface mean separation and other statistical parameters[85]. The average contact pressure P_a was related to the density of asperities μ, the curvature of asperity of radius β, composite surface roughness σ, and composite material modulus E [7].

$$P_a(h) = \frac{16\sqrt{2}}{15}\pi(\sigma\beta\mu)^2 E\sqrt{\frac{\sigma}{\beta}}F_{2.5}(\frac{h}{\sigma}) \tag{4.11}$$

where:

$$F_{2.5}(x) = \frac{1}{\sqrt{2\pi}}\int_x^\infty (s-x)^{2.5} e^{-\frac{s^2}{2}} ds \tag{4.12}$$

$$\frac{1}{E} = \frac{1-\nu_1^2}{E_1} + \frac{1-\nu_2^2}{E_2} \tag{4.12}$$

In equations (4.11) to (4.12), E_1 and E_2 are ring and liner Young's modulus, and ν_1 and ν_2 are ring and liner Poisson's ratio.

Viscous Friction Force

The shearing of asperities and viscous lubricant film generates the friction force in the mixed lubrication regime. Viscous friction is attributed to generated shear stress arising from entraining motion of the lubricant as well as pressure gradient in a converging–diverging wedge [87]. The hydrodynamic component of average friction force F_h can be predicted by an integration of viscous shear stress across the sliding surfaces

$$F_h = \int_A \tau dA = \int_A \left(\frac{h}{2}\frac{\partial p}{\partial x} + \frac{\eta U}{h}\right) dA \tag{4.13}$$

Furthermore, to meet different sliding scenarios, the local shear stress τ can also be expressed in terms of the mean quantities and three empirical shear stress factors ϕ_f, ϕ_{fp} and ϕ_{fs}

$$\tau = \frac{\mu U}{h}\left(\phi_f - \phi_{fs}\right) + \phi_{fp}\left(\frac{h}{2}\frac{\partial p}{\partial x}\right) \tag{4.14}$$

The term $\phi_f = E\left(\frac{1}{h_T}\right)$ accounts for the effect of varying film thickness on the mean shear stress due to the sliding velocity of matched surfaces. It is often treated as a correction factor to be included in the sliding velocity term of the local shear stress expression. ϕ_{fp} is a correction factor for the mean pressure flow component of the shear stress. ϕ_{fs} is the correction factor for the combined effect of sliding roughness[88].

$$\phi_{fs} = V_{r1}\Phi_{fs}(\frac{h}{\sigma}, \gamma_1) - V_{r2}\Phi_{fs}(\frac{h}{\sigma}, \gamma_2) \qquad (4.14)$$

where Φ_{fs} is a positive function of h/a and the γ value of surface. γ is the directional properties of roughness. V_{r1} and V_{r2} are the variance ratios given by:

$$V_{r1} = \left(\frac{\sigma_1}{\sigma}\right)^2, \quad V_{r2} = \left(\frac{\sigma_2}{\sigma}\right)^2 = 1 - V_{r1} \qquad (4.15)$$

Assuming that one of two matched surfaces is smooth, Equations (4.14) (4.14) suggest that the amplitude of the mean shear stress acting on the rough surface is dwindled, while the stress acting on the smooth surface is increased due to the effect of ϕ_{fs}. It is easy to understand this phenomenon if the flow in the valleys is considered. If the rough surface is moving, the fluid in the valleys is carried along with the surface, resulting in a more or less uniform velocity near the surface. The reduction of the shear stress in the valleys overcomes the increase in the shear stress below the asperities, resulting in a net decrease in the mean shear stress acting on the rough surface[88]. Based on this thought, the surface deformations in the order of roughness amplitude might cause a certain degree of reduction in viscous friction. To introduce the surface deformation into the ϕ_{fs} factor, an improved algorithm has been proposed by Jeffrey Jocsak [10].

Asperity Friction Force

The asperity component of friction force is given by Amontons' law

$$F_a = \mu_f W_a \tag{4.16}$$

Here $W_a = P_a A_a$ is the total asperity contact load, A_a is the apparent contact area, and μ_f is the friction coefficient under lubricated contact (boundary lubrication). In numerical practice, W_a is calculated according to the recommendation in [6] and [5]

$$W_a = \int_{-B/2}^{B/2} P_a dx \tag{4.17}$$

where B is the ring axial thickness.

Total Friction Force

The total friction force between the piston ring and the cylinder liner is

$$F_f = F_h + F_a \tag{4.18}$$

Based on these equations, a computational fluid dynamics (CFD) code in Matlab platform was developed to obtain oil film distribution and various friction forces numerically. Figure 7.3 shows the logical flowchart of the established computer program. As shown in the flow chart the multidimensional Reynolds equation is solved iteratively.

The accuracy and convergence of the numerical method and algorithm were validated by comparing the film thicknesses of the starting step and the terminal step between the rings and liners with a closed-form solution. The key parameters used in this study are given in Table 7.2. in which the surface accuracy parameters are obtained from the engine manufacturer. Most of the figures shown in this chapter are plotted against the minimum film thickness-roughness ratio H_m, which is given by

$$H_m = \frac{h_{\min}}{\sigma} \tag{4.19}$$

where $h_{\min}$ is the minimum nominal film thickness. $\sigma = \sqrt{\sigma_1^2 + \sigma_2^2}$ is the composite rms roughness. σ_1, σ_2 are the standard deviations of surface roughness amplitudes Δ_1 and Δ_2.

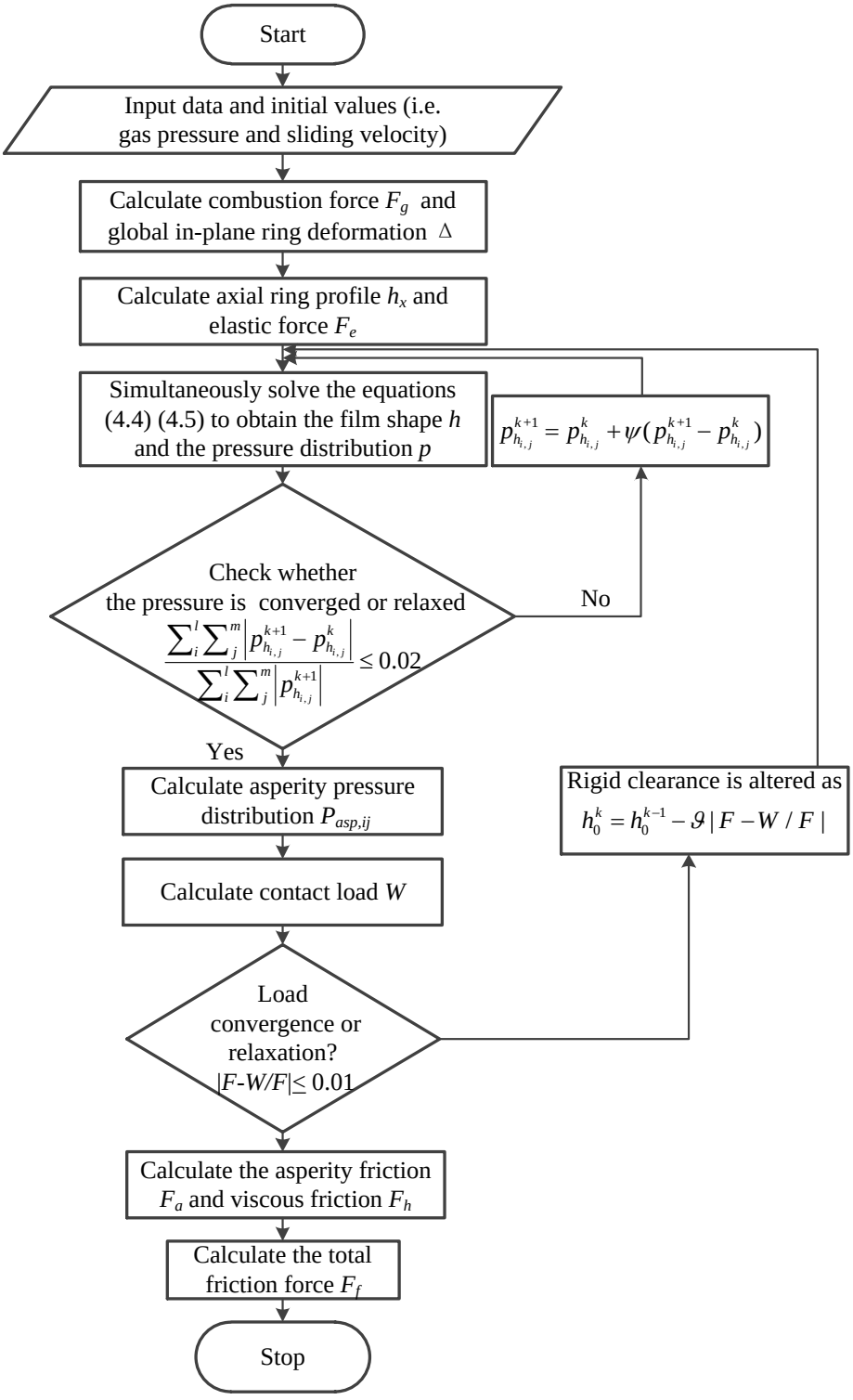

Figure 7- 3 Flowchart of the computation program of cylinder lubrication

Table 7- 2 Key calculating parameters for simulation

Symbol	Name	Value	Unit
σ_1	Cylinder surface roughness	0.8	μm
σ_2	Ring surface roughness	0.4	μm
r	Crank radius	0.057	m
l	Connecting rod length	0.19	m
e_1	Piston ring surface height	0.003	m
B	The axial height of piston ring	0.003	m
ρ	Oil density	890	Kg/m^3
E_1	Liner elastic modulus	122×10^9	Pa
E_2	Modulus of elasticity of piston rings	165×10^9	Pa

After operation throughout the entire working cycle, the minimum oil film thickness H_{min} and friction forces versus the crank angle can be obtained as seen in Figure 7-4.

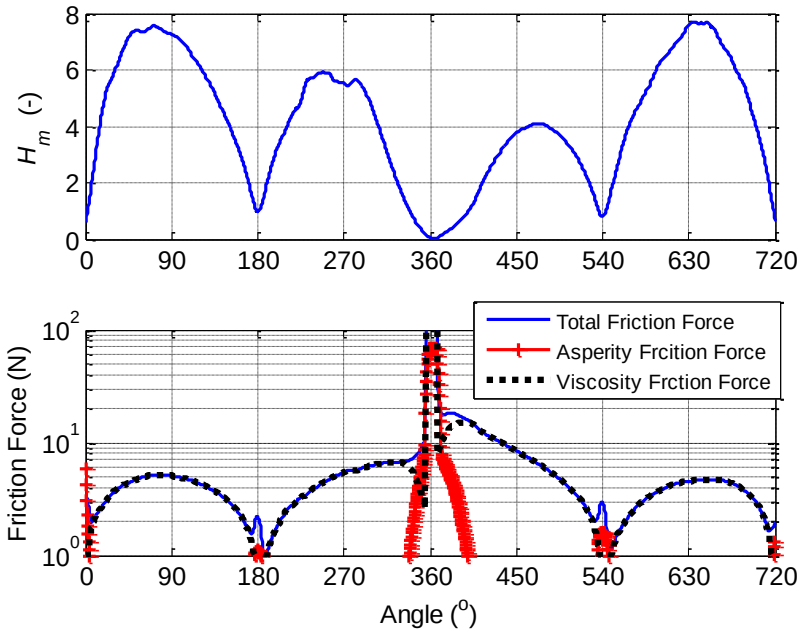

Figure 7- 4 Minimum oil film thickness and friction force of compression ring

Figure 7-4 shows the minimum oil film thickness H_{min} for the top compression ring versus the crank angle. The lowest minimum oil film thicknesses occur in the vicinity of the dead centres which correspond to crank angles of 0, 180, 360, and 540 degrees. This prediction agrees with the wear pattern observed on the cylinder-liner interface, which shows high wear at the top and bottom of the piston stroke[5]. The highest minimum oil film thickness occurs at the maximum piston speed regions, where the maximum hydrodynamic action is attained.

It should be noted that the initial film thickness and film profile are predefined; only the H_m is recalculated and modified for every cycle to achieve a force balance in the normal direction. In other words, the force balance is achieved only by constantly correcting the film thickness. During the computation, the contour of film distribution is changeless; only the thickness of the overall film surface is modified to adjust the bearing capacity of film or asperities for achieving overall force balance.

Since the profile of film distribution can be predefined, it is feasible, to place the dynamic deformations of the liner surface, in the form of a predefined condition, into the calculation, for predicting the dynamic friction behaviours.

7.3 Development of Dynamic Deformation based Lubrication Models

Since there is no data interface between the finite element software ANSYS and MATLAB, the dynamic deformations obtained based on the finite element model cannot be directly introduced into the mathematical model established in Section 7.2. In order to accurately import geometric deformations of the liner surface into the mathematical model, series of transformation processing is needed, which includes spatial reconstruction, geometry extraction, coordinate transformation and partial/local surface fitting.

7.3.1 Geometric Extraction and Coordinate Transformation

The simulation result of ANSYS is generally encapsulated and saved in a packaged file with the suffix '.ret', which cannot be loaded into MATLAB. Moreover, the batch export of time-history results cannot be directly implemented on the user interface (UI) of the ANSYS workbench.

In general, there are two ways to extract and export the simulation results by batch.

The first is that the user can select and export the time-history results of specified nodes in bulk, by writing the specific macrocode in ANSYS APDL. This approach needs to get the accurate name information of the specified nodes first, which is difficult to designate. It is neither intuitive nor convenient to implement. Another, more efficient and easily implemented practice is to import the result file of the ANSYS simulation into the professional post-processing CAE package HyperView. Using HyperView, the time-history results of region of interest, by creating node sets, can be more easily packaged and exported into the numerical computing environment of MATLAB.

It should be noted that, the data packet export from HyperView contains only the node name and its displacement increments, without the information about global coordinate positions of specified nodes. However, before the processing of coordinate transformation in the mathematical model, these nodes should be sorted and rearrange according to their spatial position. Therefore, accompanied with the export of the deformation results, an additional document containing both the node ID and node coordinates should be generated, to facilitate the following rearrangement and coordinate transformation.

Figure 7-5 shows the flowchart of the geometric extraction and coordinate transformation process, from the FE model in ANSYS to the local deformation of the liner surface. After the geometric data has been successfully imported, a three-dimensional cylindrical shell can be drawn based on the spatial positions of the nodes as shown in Figure 7-5(c). The colour of the nodes represents the amplitude of displacement increment relative to the global coordinate system.

To facilitate the modelling and calculation, in the two-dimensional film thickness model presented in Section 7.2, the cylindrical surface of liner was equivalent and converted into a plane. Therefore, before the introduction of deformations into a lubrication model, the selected nodes should be transformed from the spatial coordinate system (x, y, z) into a two-dimensional coordinate system containing the axial and circumferential directions.

As seen in Figure 7-5(d), the magnitude of deformation in the liner surface reached almost 0.1 millimetre, which is inconsistent with the existing simulation results[29], which is in the level of micron. This is because, as illustrated in Section 3.2, there exist noticeable clearances between the external surface of the liner and cylinder block, especially at the bottom rim of the liner contacting with the water jacket. Under the excitation of piston impact force, the liner exhibited significant overall translation, mainly perpendicular to the cylinder axis. It is essential to filter and suppress this unwanted overall translation before the processing of coordinate transformation, to avoid the introduction of significant errors into the local deformations.

Specifically, a cylinder shell should be fitted (extracted) according to the geometric profile of node set in Figure 7-5(c), firstly. Then, by subtracting the coordinate values of the fitted cylindrical shell, accompanied by coordinate transformations, a two-dimensional deformation surface of the liner excluding the overall translation can be obtained as shown in Figure 7-5(e).

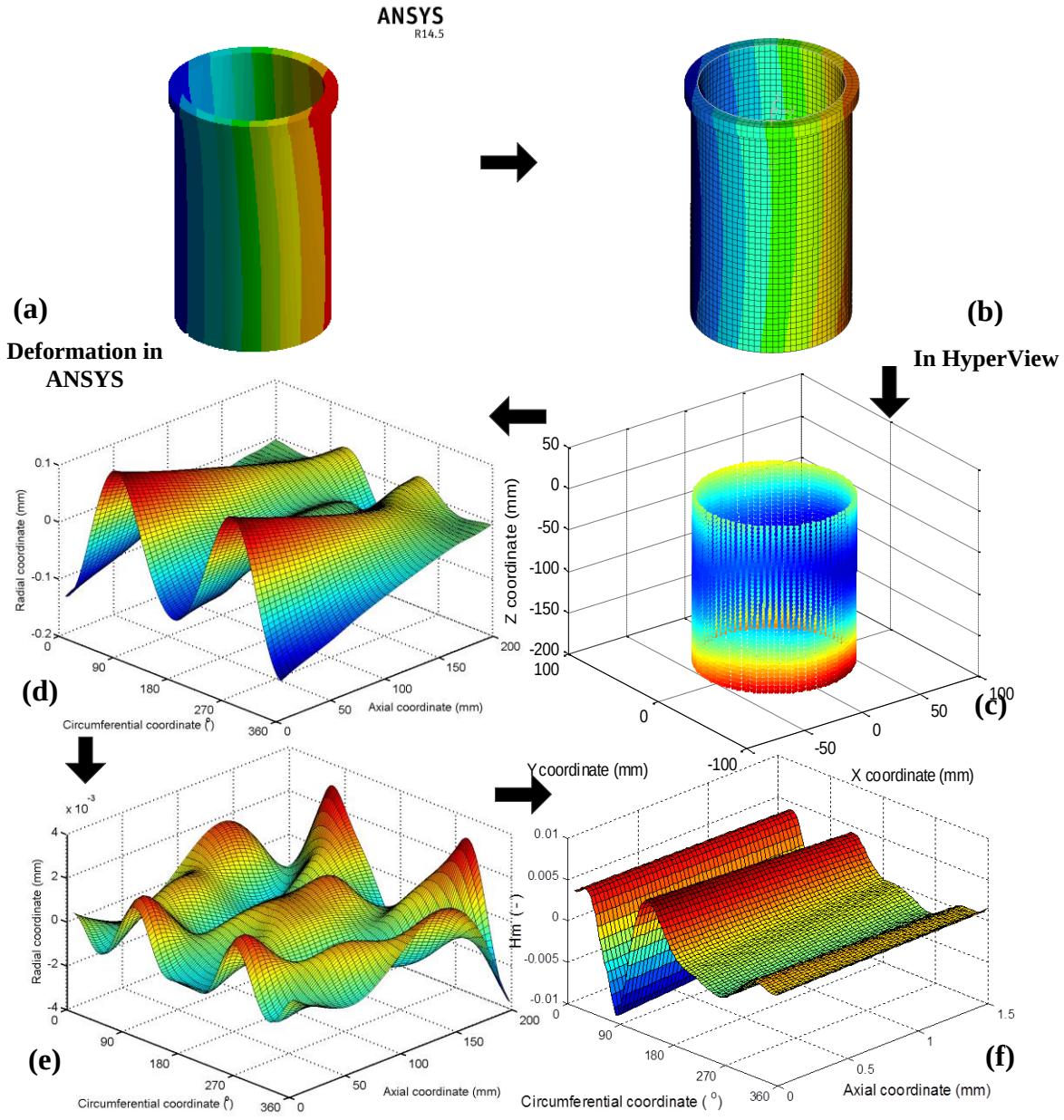

Figure 7- 5 Flowchart of the geometric extraction and coordinate transformation

It should be noted that, compared with the axial length of the liner 19.8mm, the axial height of the piston ring is very small with only 1.5mm, in the studied engine QCH1110. Furthermore, the axial position of the ring is continuously changing along with the crank rotating. Based on the instantaneous axial position of the piston, the deformation region

corresponding to the ring surface can be accurately intercepted and plotted as shown in Figure 7-5(f).

7.3.2 Improved Initial Film Thickness with Consideration of Cylinder Deformation

The deformation of the cylinder has been recognised as one of the most important factors in the film thickness and friction process[11]. As stated in Section 7.2, for the mathematical model, the initial film thickness and film profile are predefined. During the computation, the contour of film distribution is changeless; only the thickness of the overall film surface is modified to adjust the bearing capacity of the film or asperities for achieving overall force balance.

Therefore, placing the dynamic deformations of the liner surface, in the form of a predefined condition, into the calculation, will not change the core algorithm of Reynolds equations, and will not produce any adverse effect on the accuracy of the model.

Figure 7.6 depicts a conjunction between the piston ring and cylinder liner with surface roughness. Here the function $h_T\ (x,)$ describes the local film thickness, including surface roughness.

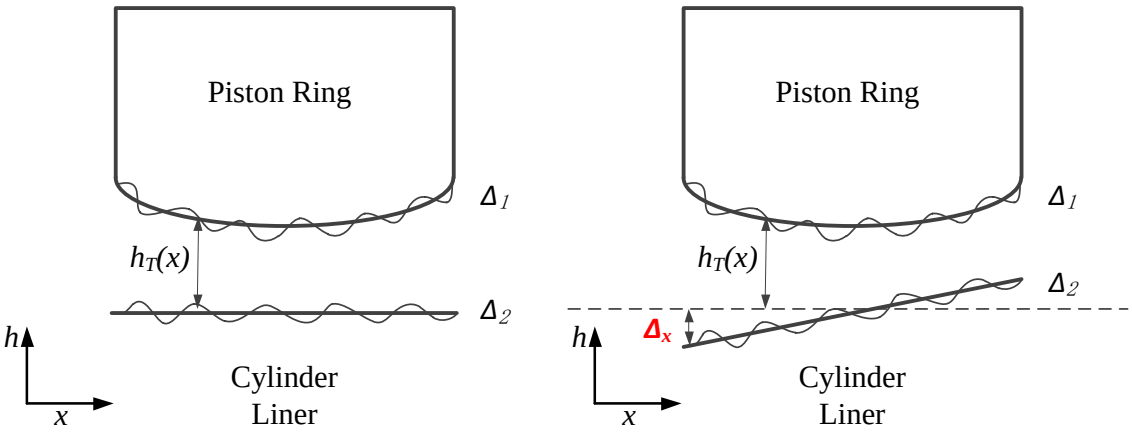

Figure 7- 6 Rough piston ring and cylinder liner conjunction: (a) without liner deformation (b) with consideration of liner deformation

For one-dimensional lubrication, the local film thickness h_T is given by

$$h_T = h + \Delta_1 + \Delta_2 \tag{4.20}$$

where h is the nominal film thickness, Δ_1 is the ring surface roughness amplitude, and Δ_2 is the liner surface roughness amplitude. The nominal film thickness $h = h_{min}(t) + h_x(x)$, giving

$$h_T(t) = h_{\min}(t) + h_x(x) + \Delta_1 + \Delta_2 \tag{4.21}$$

Taking the deformation amplitude of the liner surface Δ_x into account in the film formation model, the nominal film thickness can be improved as

$$\begin{aligned} h_{T\_deforms} &= h_{\min}(t) + h_x(x) + \Delta_1 + \Delta_2 + \Delta_x \\ &= h_T(t) + \Delta_x \end{aligned} \tag{4.22}$$

By analogy, for the two-dimensional lubrication, the film thickness is given by

$$\begin{aligned} h_{T\_deforms}(t) &= h_{\min}(t) + h_x(x) + h_y(y) + \Delta_1 + \Delta_2 + \Delta_x + \Delta_y \\ &= h_T(t) + \Delta_x(t) + \Delta_y(t) \\ &= h_T(t) + \Delta_{deforms}(t) \end{aligned} \tag{4.23}$$

where, the two-dimensional deformation of the liner surface matched with the piston ring is combined with axial deformation Δ_x and circumferential deformation Δ_y.

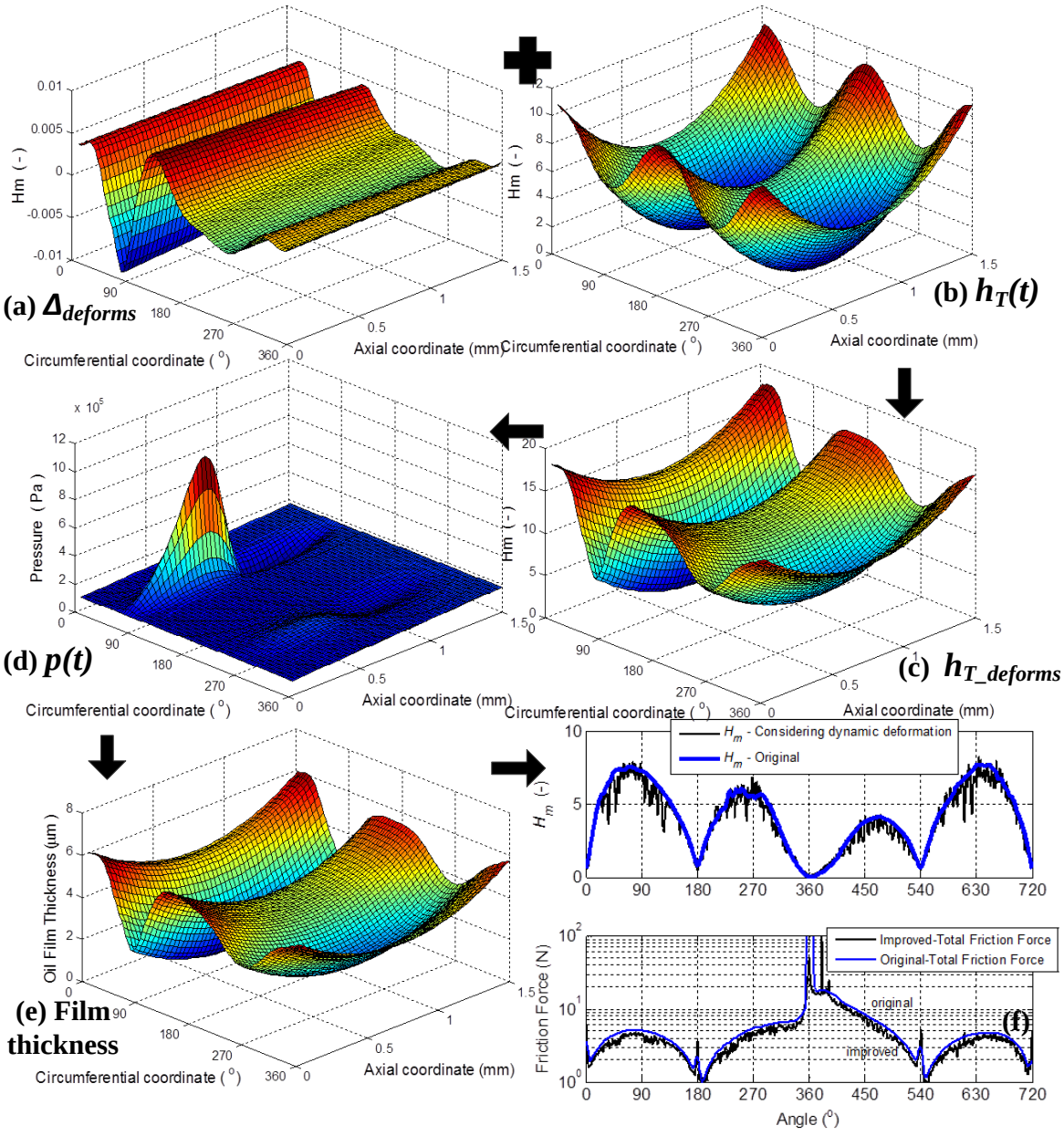

Figure 7- 7 Flowchart of the introduction of liner deformation

Thus, taking the improved two-dimensional film thickness $h_{T\_deforms}$ into the computation program, in the form of a predefined condition, the pressure distribution of the film and its corresponding film thickness with consideration of liner deformation can be calculated and drawn as shown in Figure 7-7(d), Figure 7-7(e)and Figure 7-7(f). After running through the entire computation program, the resulting curves of minimum oil film thickness and

three kind of friction forces considering the influence of liner deformation can be acquired as shown in Figure 7.7(f).

7.4 Friction Responses to Dynamic Deformations of the Liner Surface

For comparing and analysing the influence of liner deformations to friction behaviours, the predicted minimum oil film thickness and friction forces with and without consideration of dynamic deformations, at the operating condition of 1800rpm and 40Nm, are drawn together in Figure 7-8.

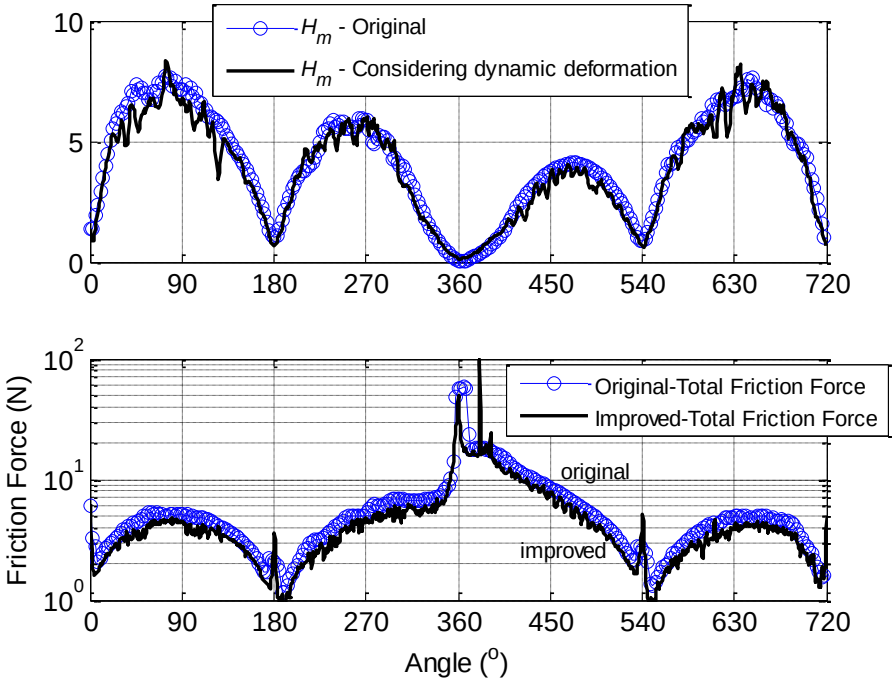

Figure 7- 8 Minimum film thickness-roughness ratio H_m and friction forces considering dynamic deformation

In comparison, the minimum film thickness-roughness ratio H_m considering the dynamic deformation of the cylinder liner shows significant fluctuations throughout the entire operating cycle, especially in the mid-strokes with higher sliding speed, as shown in Figure 7-8(a). And the amplitude of film thickness considering deformations shows an

evident decline compared to the original one. Although the minimum oil film thickness is reduced, the improved total friction force did not increased correspondingly, but shows a significant reduction. The friction curves of the improved model also manifest some obvious fluctuations. The frequency range of these fluctuations, from 1000 to 2000Hz, has been proven to be close to the mode responses of the liner surface. This indicates that the friction and lubrication process of the piston ring-liner pair can indeed be affected by the dynamic deformations of cylinder liners.

The improved minimum film thickness-roughness ratio H_m after combustion TDC is slightly fluctuated around the original one, while its corresponding friction force presents some more complex and significant changes in the power stroke, as shown in Figure 7-9. This may indicate that the actual friction and wear behaviours between piston rings and liners are far more complex than had been previously theoretically estimated.

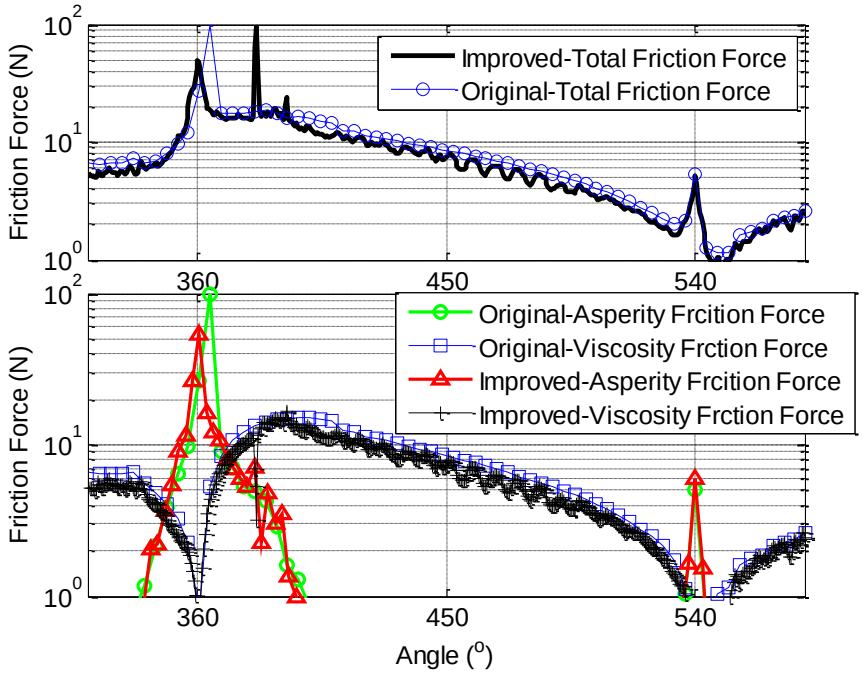

Figure 7- 9 Comparison of friction forces between the improved and original

In the middle of the piston stroke, the improved friction force, mainly the viscous friction force, shows an obviously decline compared to the original one. This kind of friction reduction may be attributed to the changes of shear stress factors ϕ_{fs}, as a result of

instantaneous surface roughness when the dynamic deformations of liner vibration are taken into account.

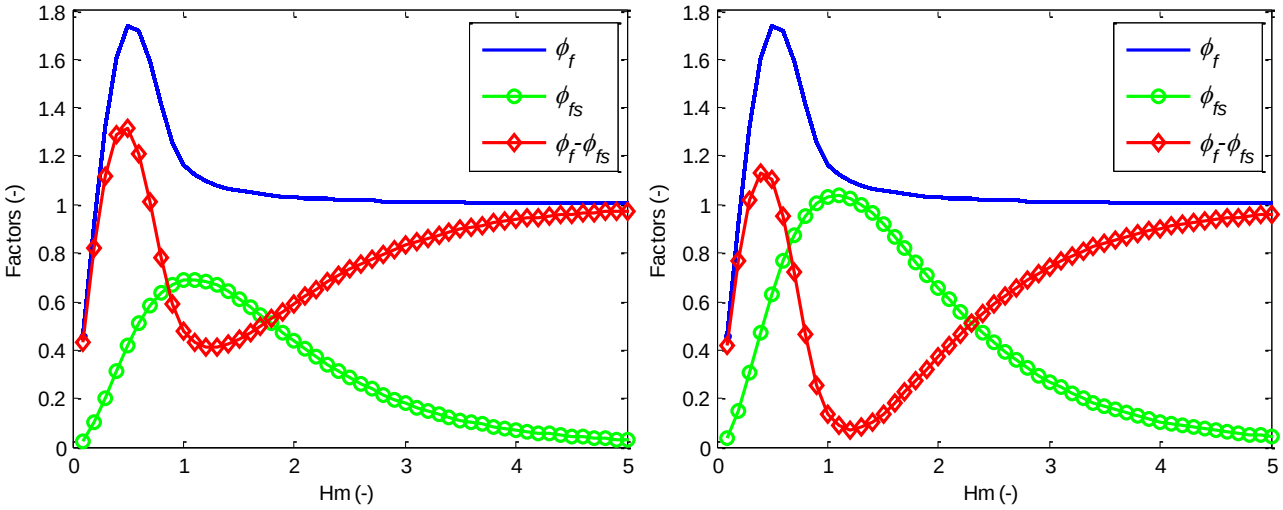

(a) Original values; (b) The improved factors with considering surface deformations

Figure 7- 10 The flow shear factors ϕ_f, ϕ_{fs} and their difference [ϕ_f- ϕ_{fs}].

As shown in Figure 7.10, with the introduction of surface deformations, the shear stress factor ϕ_{fs} has been significantly elevated, as seen in Fig7-10(b). With the increase of ϕ_{fs}, the difference between the sliding velocity correction factor ϕ_f and shear stress factor ϕ_{fs} subsequently exhibited obvious decrease. Therefore, the local shear stress τ can be reduced accordingly, with the increasing of shear stress factor ϕ_{fs}, as seen in equation 7.11. It suggests that the inclusion of surface deformations can cause changes in the flow shear factors and lead to the observable reduction in viscous friction forces.

Around the combustion TDC at 360 °, the value of total friction considering liner deformation is lower than the original model value. Due to the introduction of dynamic deformation, the lubricating condition between the matched surfaces is improved, with a larger geometric gap and higher sliding speed, thereby resulting in the reduction of asperity friction. This might indicate that the dynamic deformation of the liner can help to reduce the friction near the combustion TDC, normally regarded as the most serious position of wear, and to enhance the operation efficiency and service life.

From about 380 ° to 385 °, both the asperity friction and viscosity friction curves show a drastic fluctuation, indicating high instantaneous friction or wear. That is due to the application of the high combustion pressure and its associated intense impact force to the liner surface at this crank angle range, consequently resulting in the high deformations of the liner surface. In addition, due to the relatively lower sliding speed and harshest inlet pressure boundary conditions, the film thickness at this crank angle is very low and close to the amplitude of liner deformations. Localised contact, or partial contact, can easily occur between the matched surfaces, thereby leading to such sharp rises.

In fact, this phenomenon of instantaneous drastic asperity friction after combustion TDC can be observed in almost all operating conditions. Based on the numerical prediction, it can be deduced that severe wear is likely to occur on a narrow band of liner surface which corresponds to the crank angle of 385 °-380 °. To confirm this finding, a cylinder liner used for approximately 500 hours was detached from the test engine QCH1110 and photographed from the inside the cylinder. By splicing and reorganising multiple photographs, a panoramagram of the inner surface of this used liner can be obtained as shown in Figure 7.12.

Figure 7- 11 Configuration of piston rings

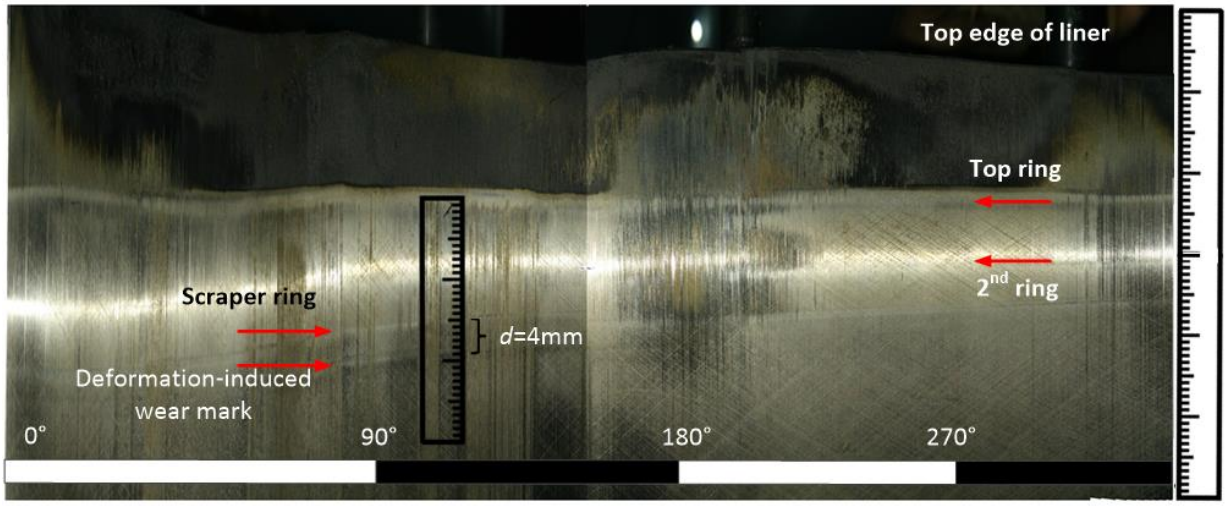

Figure 7- 12 Panoramagram of the inner surface of a used liner

As seen in the panoramagram, there exist four wear marks that can be clearly observed on the inner surface of the used liner. The first three wear marks can well correspond to the top compression ring, the second compression ring and the oil scraper ring respectively, as illustrated in Figure 7-11. When the piston reaches the top dead centre, due to the low sliding speed and harsh pressure boundary conditions, the lubricant film between the ring and the liner is extremely thin and insufficient to separate the matched surfaces, resulting in the severe wear, i.e., these observable marks.

In addition, there is another wear mark below the scraper ring's mark, with a distance of 4 mm, marked as *d* in Figure 7-12. Further calculations suggest that, the position of the mark corresponds well to the crank angle of 380 °. This indicates that the predicted instantaneous harsh friction does appear in this position, around crank angle 380 °, as predicted in the mathematical model.

The experimental study conducted by Michael Gore et al. [59] strongly confirmed the existence of fluctuations in the piston axial friction force through a direct measurement, as seen in Figure 7-13(a). Their study shows that the dynamic behaviour between the pistons and liners results in an unbalanced response at a multitude of engine order harmonics, thus introducing many fluctuations into the piston friction force.

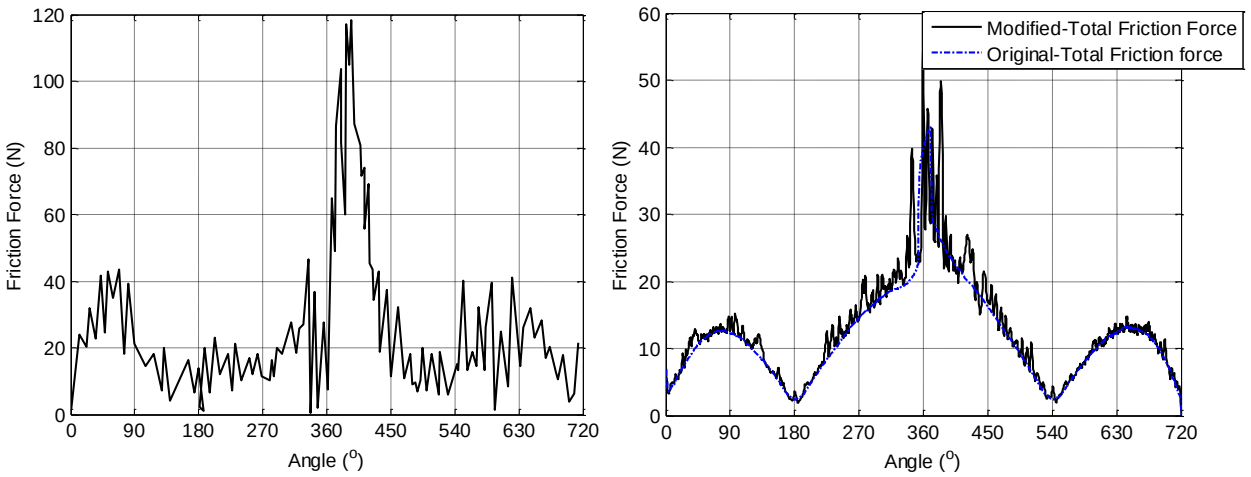

Figure 7- 13(a) Measured friction in a diesel engine [59], (b) Predicted friction based on improved lubrication model

As shown in Figure 7-13 (a), a peak with obvious fluctuations can be observed at a crank angle of about 380 ° in the measured friction, which is agreeable with the predicted total friction force presented in Figure 7-13(b). In addition to the known peak at 360 ° predicted by the original film calculation model, another peak around 380 ° predicted in the modified model, considering liner deformations, can well correspond to the measured result, indicating that the modified model can better represent and characterise the actual friction status. The proposed explanation for the phenomenon of instantaneous harsh friction has been strongly supported by practical conclusions.

Regarding the cause of fluctuations in the friction force, Michael Gore et al. [59] suggested that these fluctuations might be related to the order harmonics of the engine, without offering more vigorous evidence. To fill this gap, it is essential to analyse the relationship between the dynamic friction and input deformations of the liner surface. As shown in Figure 7-14, a short-time Fourier transform (STFT) result of friction force predicted by the improved model under the operating condition of 1800rpm engine speed and 40Nm torque is presented.

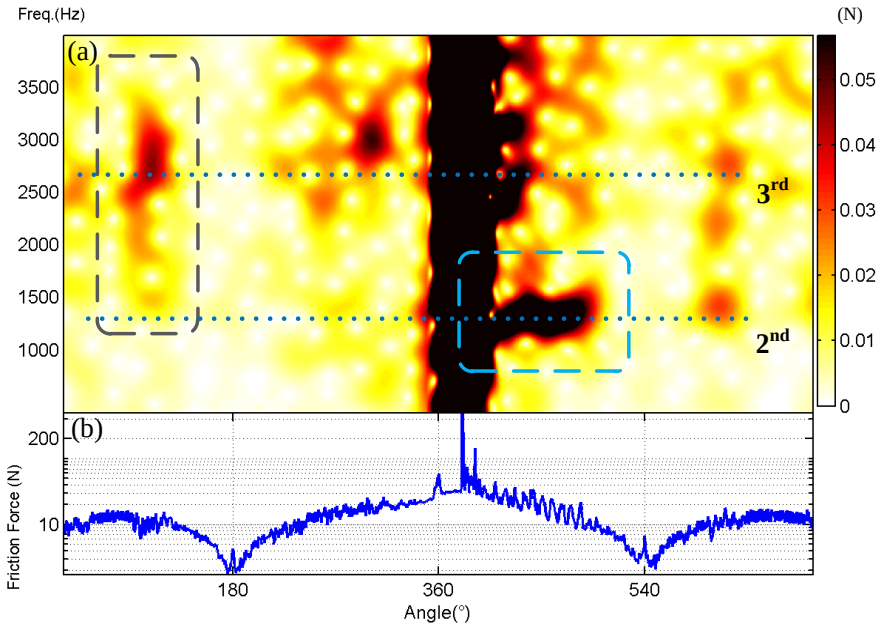

Figure 7- 14 The STFT of friction force predicted by the improved model

As can be seen in Figure 7-14(a), in the power stroke, sustained oscillations can be clearly observed in the frequency range of 1000-1600Hz at the mid-stroke, as marked with a blue rectangle. Its frequency band is close to the 1229Hz of the 2nd mode of cylinder liner identified by the modal experiment as shown in Section 3.2 and Table 3.1. This suggests that the dynamic deformations of the cylinder liner, especially the local deformations in the upper portion of the liner associated with the 2nd mode shape, produced a profound influence on the friction behaviours between rings and liners.

In addition, the other local features of friction force can also be associated with the dynamic responses of the cylinder liner. As seen in Figure 7-14, the significant dynamic response around the crank angle of 100 °and located in the frequency range from 1500 to 3500Hz, marked with a grey rectangle, can well correspond to the local dynamic event Ⓕ caused by piston slap as drawn in Figure 3-6. Likewise, the local response at the crank angle of 630 °in the frequency band of 2nd mode response can also perfectly correspond to the dynamic event Ⓓ in the STFT result of the liner vibration in Figure 3-6.

All of these results indicate that the dynamic deformation of the cylinder liner is one of the most important factors causing and affecting the fluctuations in friction. In other words, the fluctuating characteristics of friction and lubrication behaviours between the piston and liners are greatly determined by the dynamic responses of cylinder liners.

For comparing and analysing the influences of the operating condition and fuel properties on the friction changes, the RMS result of the calculated friction force during the power stroke from 400 ° to 500 °, considering the effect of liner deformations, has been drawn as shown in Figure 7-15(a). Meanwhile, in order to facilitate the analysis of the amplitude of variation in friction force caused by the inclusion of liner deformations, the differences between the original and improved total friction force with different operating conditions and fuel types, $F_{reduction} = F_{total\_original} - F_{total\_improved}$, were calculated as seen in Figure 7-15(b).

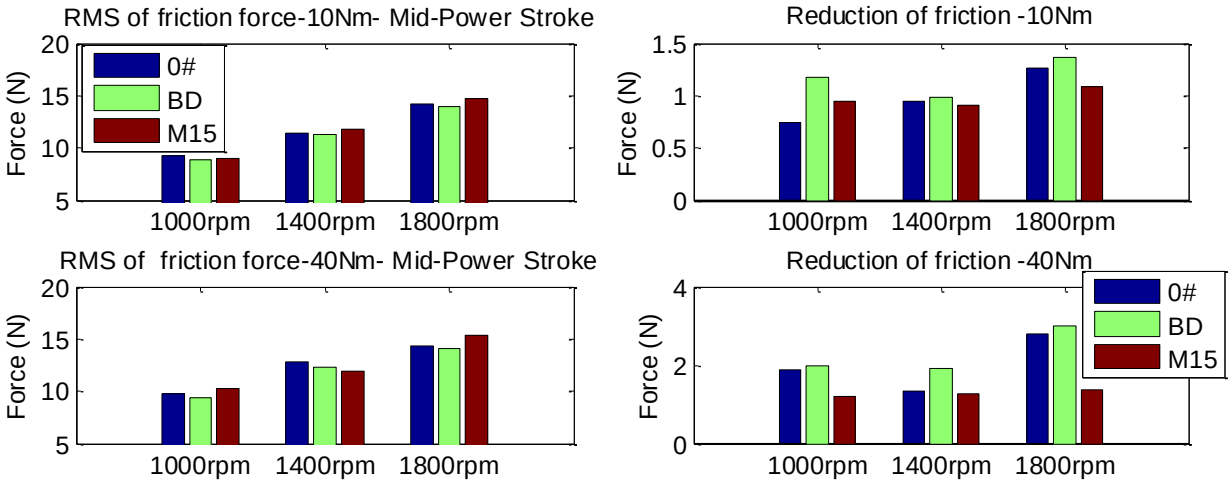

(a) RMS of improved friction force from 400 ° to 500 °; (b) Difference of forces between original and improved

Figure 7- 15 Comparison of friction forces fuelled with alternative fuels

As shown in Figure 7-15(a), with the increase of operating speed and load, the friction force in the middle of the power stroke from 400 ° to 500 °, mainly the viscous friction force, show a steady rising trend. It should be noted that the friction difference of fuel

types shows an almost opposite trend to their corresponding vibration result, as shown in Figure 6.9(a), indicating that the intense vibration of the liner is prone to causing a reduction in friction losses. More specifically, the RMS value of biodiesel is always slightly lower than the diesel, while the RMS of M15, the methanol-diesel blended fuel, is slightly higher than the other two fuels in most conditions. These trends are just the opposite of their corresponding vibration trends. As shown in Figure 7-15(b), with the increase of operating speed and load, the amplitude of friction reduction also shows a basic upward trend. The reduction value of biodiesel is always greater than the other two fuels, while the M15 exhibits a relatively small value.

The results of the two figures in Figure 7-15 show that more intense vibration of cylinder liners can cause more significant friction reduction. The biodiesel with more intense vibration emissions is able to effectively reduce the friction loss between the pistons and liners, while the methanol-diesel blend with weakened liner dynamic response may exacerbate the friction loss of IC engines. This may indicate that, from the perspective of friction reduction, a fuel with intense vibrational response may be more conducive to the lubrication improvement of IC engines.

It can be briefly concluded as follows:

- Due to the inclusion of dynamic deformation, the lubricating condition between the matched surfaces can be improved, with a larger geometric gap and higher sliding speed in local areas. The dynamic deformations of the liner surface can be beneficial to reduce the friction losses around the combustion TDC, and to enhance the operational efficiency.
- In the middle of the piston strokes, the reduction of friction can also been observed in the simulated friction forces based on the models with and without considering deformations. This suggests that the viscous friction between the pistons and liners can also be reduced by the inclusion of liner vibrations.
- Due to thinner film thickness, the substantial deformations of the liner surface as a result of the most intense piston-slap event near the combustion TDC, can always

cause the occurrence of localised or partial asperity contact, resulting in a phenomenon of instantaneous harsh friction after combustion TDC at crank angle of 380 ° to 385 °. This finding has been confirmed by feature analysis based on a panoramagram of wear patterns on liner surface.

- According to diagnostic and comparative analysis, the intense vibrational responses of cylinder liners can cause more significant friction reduction. From the perspective of friction reduction, a fuel with intense vibrational response may be more conducive to the lubrication improvement of IC engines.

In summary, it has been shown that the dynamic responses of cylinder liners can indeed affect the tribological characteristics of piston and cylinder assemblies. Particularly, the simulation studies from improved lubrication model indicate that the biodiesel with more intense vibration emissions is able to effectively reduce the friction loss between pistons and liners, while the methanol-diesel blend with weakened liner dynamic response may exacerbate the friction loss of IC engines. This may indicate that, from the perspective of friction reduction, a fuel with an intense vibrational response may be more conducive to the lubrication improvement of IC engines.

However, in terms of whether or not it is possible to achieve the most significant reduction in friction and wear of engines, by optimising the parameters of additional vibrations, or superimposed excitations, no in-depth investigation has so far been performed or published.

Chapter 8

Influence of Additional Vibration on the Engine Friction

This chapter investigates the influence of additional vibrations on friction reduction between pistons and liners in IC engines based on a motoring test bench.

Added vibrations were examined at different powers and frequencies that are determined based on the model predictions in Chapter3 and 4 and existing mechanisms available in friction reduction.

A torque-temperature characteristic was established for minimising the temperature effect on the measured motoring torques.

8.1 Introduction

As noted in Chapter 7, tribological behaviours between pistons and liners can be drastically affected by the vibration of cylinder liners. The lubricating condition between the matched surfaces around the crank angle of 360°, i.e. combustion TDC, can be distinctly improved by the introduced geometric deformations. However, an instantaneous (short-period) drastic asperity friction around 380°to 385° can also be observed after introducing the dynamic distortions of the liner surface. These seemingly contradictory results point to a more realistic question: If the influence of structural vibration on tribological behaviour can be positive, is it possible to improve the lubrication status and to reduce the friction and wear of engines by optimising the parameters of vibration?

To answer this question, a preliminary experimental study (on the influence of superimposed vibration on engine friction) was carried out based on a motoring test system.

8.2 Friction Reduction based on Vibrations

The reduction of friction achieved by additional vibrations has been observed in many experiments. This effect can be applied to actively control frictional forces by modulating vibrations.[89] Unlike in other areas, where an identical dominant principle governs system general characteristics, there is no single theory that can be used to explain most vibration-induced friction reductions.

The friction reduction has been explored by changes in the magnitude and frequency of the normal load, or by changes of the additional vibration acting parallel or perpendicular to the sliding direction.

8.2.1 Friction Reduction based on the Vibration of Normal Load

Douglas Godfrey and D. M. Tolstoi [90]–[92] examined the mechanism leading to friction reduction induced by normal vibrations. It was found that the normal vibrations influence the mean surface separation, and therefore the real area of contact[92].

If the dynamic normal force is $F_n(t)$ and friction force is $F_f(t)$, then the instantaneous friction coefficient can be expressed as

$$\mu(t)=F_f(t)/F_n(t) \tag{4.24}$$

In Eq.(4.24), μ can be treated as a kind of variable of the dynamic system. The expression Eq. (4.24) is convenient for experimental observation. In most engineering applications, of particular interest is the interpretation of average friction for simplification purposes[93]. Assuming the average of friction is to take the time average of $\mu(t)$, denoted by $<\mu(t)>$:

$$<\mu(t)>=\int \mu(t)dt \tag{4.25}$$

Alternatively, we can also denote an average friction coefficient μ_{av}, then

$$\mu_{av}=<\hat{F}_f(t)>/<\hat{F}_n(t)> \tag{4.26}$$

in which,

$$<\hat{F}_f(t)>=\int F_f(t)dt, \quad <\hat{F}_n(t)>=\int F_n(t)dt \tag{4.27}$$

Consider an interface with Hertzian contact. Let us assume an oscillating normal load is applied, $F_{n0}(1+\cos\Omega t)$, and also that it is just enough to give impending contact loss at one extreme of the motion[94]. Let us now suppose that the friction coefficient is μ_0 when the normal load is at its mean value F_{n0}. For a Hertzian contact, the instantaneous friction force is proportional to the instantaneous real area of contact. It is shown in the

comparative study of D. P. Hess and A. Soom [65] that μ_{av}/μ_0= 0.92, whereas $\langle\mu(t)/\mu_0\rangle$ =1.84. Thus, for the proper definition of average friction, μ_{av} is usually preferred.

Next we consider the normal motion of a single-degree-of-freedom (SDOF) system with a contact interface under normal excitation by following [65]. Assuming Hertzian contact, the equation of motion is given by

$$m\ddot{y} + c\dot{y} - f(\delta) = -F_{n0}(1+\alpha\cos\Omega t) - mg, \quad \text{for} \quad \delta > 0 \tag{4.28}$$

where y is the normal displacement, $\delta=(y_0-y)$ is the contact compression, and $f(\delta)$ is the restoring force given by

$$f(\delta) = \frac{4}{3}ER^{1/2}\delta^{3/2} = k_1(y_0 - y)^{3/2}, y_0 = [(F_{n0} + mg)/k_1]^{2/3} \tag{4.29}$$

According to the adhesion theory of friction, the instantaneous friction force is proportional to the real area of contact. Since the contact area is proportional to compression, we have

$$F_f(t)/F_{n0} = A(t)/A_0 = 1 - y(t)/y_0 \tag{4.30}$$

The normal oscillation, $y(t)$, is asymmetrical due to non-linear contact stiffness. The above equation can be derived as

$$< F_f(t) > /F_{n0} =< A(t) > /A_0 = 1 - < y(t) > /y_0 \tag{4.31}$$

With the increase of oscillation $<y(t)>$, the average contact area $<A(t)>$ is reduced, causing a reduction in the average friction force.

8.2.2 Friction Reduction based on the In-plane Vibrations

In addition to vibrations of normal load, friction reduction can be attained by fast vibrations in the interface contact plane. A widely accepted mechanism for this kind of friction reduction is the time-averaged friction reduction through fast vibrations, normally

ultrasonic vibrations [68], [95], [96]. Fast vibrations can provide great oscillation velocity to the object through high frequency, even though the motion amplitude is very small. When a fast vibration is added to the contact surface, the relative sliding velocity of the object is altered by the superposition of the original relative velocity and the added vibration velocity, which can allow transient reversal to occur. This can lead to the transient reversal of friction and accordingly reduce the averaged friction.

To investigate the influence of ultrasonic vibration on sliding friction in a contact plane both parallel and perpendicular to the sliding direction, two simple analytical models for friction reduction are proposed[97], as seen in Figure 8-1 and Figure 8-3. In the case of longitudinal or parallel vibration, the directions of vibration and sliding are assumed to be collinear. Thus, in the part of each cycle of relative vibration, the contacting asperities on the interacting surfaces move in the same direction.

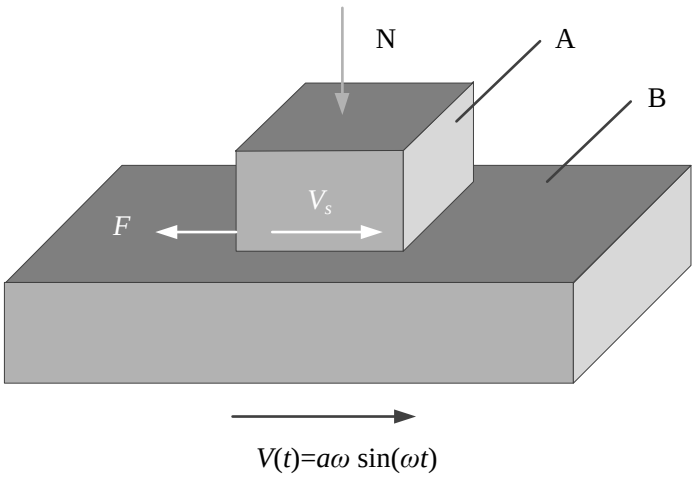

Figure 8- 1 Schematic influence on sliding friction of ultrasonic vibration parallel to the sliding direction

As shown in Figure 8-1, body A is supposed to slide with a constant speed V_s above body B, which has an oscillatory motion $V(t)=a\omega \sin \omega t$ along the same line of motion as that of V_s. When the instantaneous velocity $V(t)$ is greater than V_s, and their directions are opposite, the friction force F will reverse its direction and act in the same direction as the constant sliding velocity V_s.

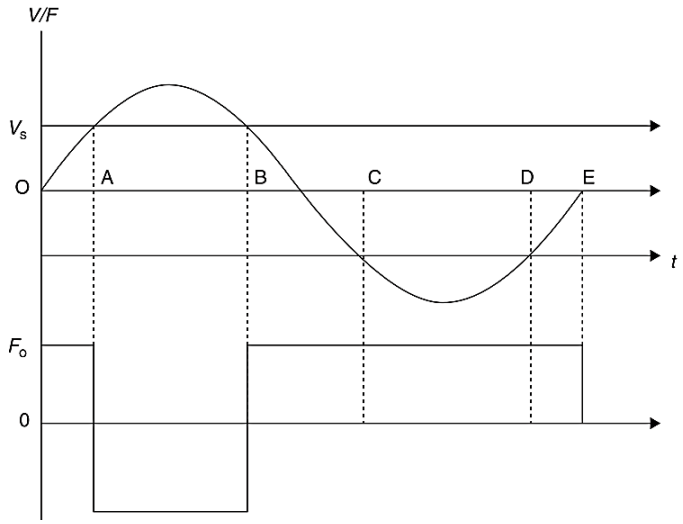

Figure 8- 2 Variation of vibration velocity with time and corresponding change in direction of frictional force [97]

Figure 8-2 shows the instantaneous velocity V_s of body B and the friction force over one cycle of vibration F_o. It is assumed that the friction law follows Coulomb friction. The time t_s taken for the vibration velocity to reach the sliding velocity V_s is given by

$$t_s = (1/\omega)\sin^{-1}(V_s / a\omega) \qquad (4.32)$$

During the interval OA, $V_s > V$ and hence the friction force on body A is positive. While, during the interval AB, $V > V_s$; thus the friction force is negative.

Over the rest cycle BE, the friction is positive. Symmetrically, the interval AB with negative friction force is exactly equal to the time CD with positive friction force. In the time average, the two opposite forces will cancel each other out. The resultant average friction force over a whole cycle, F_a can be expressed as

$$F_a = F_0(4t_s / T) = F_0[(2/\pi)\sin^{-1}(V_s / a\omega)] \qquad (4.33)$$

in which F_0 is the friction force in the absence of vibration and T is the period of the oscillation cycle. This equation is valid only for the condition $V_s<a\omega=V_v$. In other words, the reduction of friction can be achieved only if the amplitude of oscillating velocity is greater than the constant sliding velocity. It can be concluded that the reduction in friction increases with an increase in the ratio of vibration velocity to sliding velocity V_v/V_s.

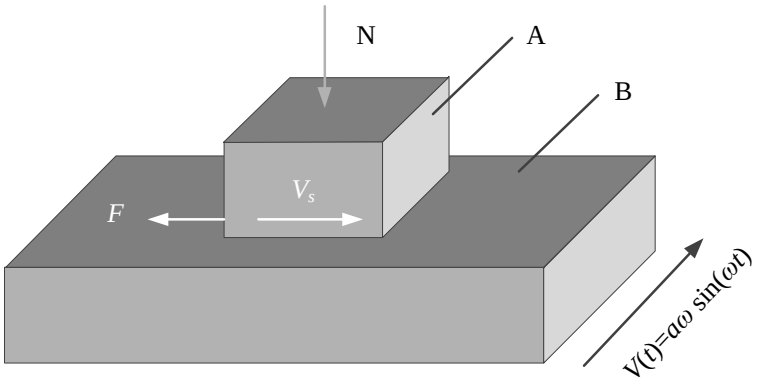

Figure 8- 3 Schematic influence on sliding friction of ultrasonic vibration perpendicular to the sliding direction

As demonstrated in Figure 8-3, in the case of transverse vibration, the direction of additional vibration is supposed to be at right-angles to the sliding direction. As mentioned above, V_v is the additional vibration velocity and V_s is the relative sliding velocity. When the transverse oscillating velocity V_v reaches its maximum value, it will be at an angle α to the sliding direction. At any moment the direction of the friction force will be in the opposite direction to the resultant sliding velocity. Hence, during one cycle of the additional vibration, the direction of the friction force will fluctuate between angles α and $-\alpha$ to the bulk sliding direction V_s. The time-averaged resultant friction force will be the time average of the component of the frictional force vector projecting on the direction of the relative sliding velocity [97]. Let θ be the instantaneous angle between these two vectors, the time-averaged friction force can be given as

$$F_a = \frac{1}{T}\int_0^T F_0 \cos\theta dt = \frac{1}{T}\int_0^T F_0 \cos(\tan^{-1}\frac{V_v}{V_s}\sin\omega t)dt$$
$$= \frac{1}{T}\int_0^{2\pi} F_0 \cos(\tan^{-1}\frac{V_v}{V_s}\sin\phi)d\phi \qquad (4.34)$$

in which $\phi=\omega t$ is the phase angle. It can be inferred that with the increase of velocity ratio V_v/V_s, the time-averaged resultant friction force will show a gradual reduction [97].

V.C. Kumar and I.M. Hutchings [97] conducted an experimental study of the friction between two metallic surfaces in the presence of ultrasonic vibration. Their study has shown that both the additional vibrations in longitudinal and transverse directions can effectively reduce the sliding friction between matching surfaces. The reduction of friction induced by longitudinal vibration is much larger than by transverse vibration.

8.2.3 Friction Reduction Mechanisms between Rings and Liners by Added Vibrations

As stated above, both the out-of-plane (normal) and in-plane (within contact plane) vibrations with appropriate parameters can reduce friction effect between sliding surfaces. However, the two friction reduction mechanisms are confined to the explanation for reduction in asperity friction. In fact, the tribological behaviours between the piston rings and liners are complex in that it includes all three kind lubrication regimes over an operating cycle. In addition to the asperity friction appeared near the dead centres, the friction force in the middle of piston stroke is mainly present in the form of viscous friction. The simulation result proposed in Chapter 7 indicates that, in the middle of piston stroke, the viscous friction force can be evidently reduced by the introduction of dynamic deformation of liner surface. This indicates that the structural vibration can also cause a reduction in the viscous friction. However, this cannot be sufficiently explained by the two previously proposed mechanisms: the in-plane and out-plane one. Therefore, further reduction mechanisms are needed to be investigated for interpreting the reduction in viscous friction between the rings and liners.

As determined in Chapter 3 and 4, the magnitude of liner dynamic deformation is close to the order of surface roughness amplitude, indicating that the inclusion of dynamic deformations can cause changes in the flow shear factors and lead to the noticeable reduction in viscous friction forces. Specifically, when the matched rough surface is moving, the fluid in the valleys is carried along with the surface, resulting in a more or less uniform velocity near the surface. The mediums continuity will be weakened by the different laminar velocities between parallel flow layers. The reduction of the shear stress in the valleys overcomes the increase in the shear stress below the asperities, resulting in a net decrease in the mean shear stress acting on the rough surface. This friction-reducing mechanism is derived from the Navier-Stokes and continuity equations for incompressible flow under an ideal assumption that the lubricant between the rings and liners follow the laminar flow. It may be used to explain the reduction in viscous friction caused by the changes of flow shear factors, but also lead to a lack of the consideration to another influence factor: changes in the oil properties affected by the liner vibration.

In addition, the vibration-induced changes in oil properties and their effects on lubrication behaviours also could play an effective role reducing in viscous friction forces. As surveyed in Section 2.2, the dynamic responses of a cylinder liner can cause liquid cavitation when the pressure of lubricating oil below its saturated vapour pressure. W.W.F. Chong and M. Teodorescu[21] et al. found that the cavitation occurring in lubricant film can usually survive as a confined bubble at the leading edge after the reversal of the piston movement direction near the combustion top dead centre (TDC). Furthermore, Hugo M. Checo et al.[98] found that the cavitation bubbles in lubricant film could effectively reduce the fluid shear force and may result in lower friction losses between the frictional surfaces. Therefore, cavitation-induced friction reduction mechanism can be a considerable and acceptable interpretation for the reduction in viscous friction force of the cylinder liners.

Based on above discussion, vibration induced viscous friction reduction can be understood by two preliminary mechanisms:

1 The inclusion of dynamic deformation can increase the shear stress factor ϕ_{fs} and weaken the mediums continuity of lubricant film, leading to the reduction in the local shear stress τ, and

2 The occurrence of cavitation can cause disruptions between the parallel flow layers, and weaken the mediums continuity of lubricant film, resulting in reduced viscous friction.

8.3 Test Design and Facilities

To verify the mechanisms proposed or investigate the influence of additional vibrations on friction reduction between the pistons and liners in IC engines, a motoring test bench was designed and constructed based on the single-cylinder engine test bench described in Section 5.2. This motored engine allows different types of vibration actuators and sensors to be mounted. In addition, it is easy for the test to control the characteristics of added vibrations.

The primary task for the reconstruction of a motoring test bench based on an engine test rig is to change the form of the driving unit. Firstly, the fuel supply system of the single-cylinder engine was cut off, and the intake and exhaust valves were set to the normal open state, thereby blocking the power output of the IC engine. Then, to motor the engine running at specified speeds at which mechanical losses are measured, an external motoring system should be connected to the engine, as shown in Figure 8-4. The motoring system is composed of an alternating current (AC) motor and a frequency inverter, allowing the motor to operate at different test speeds up to 1500rpm.

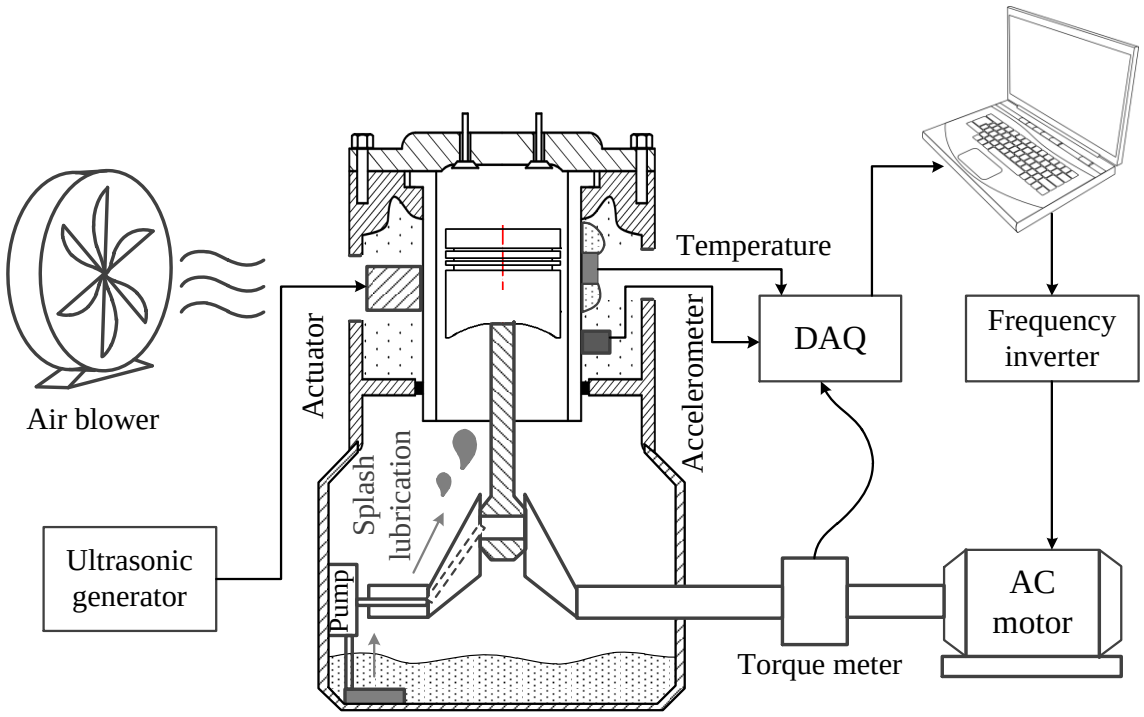

Figure 8- 4 Schematic of motoring test bench

The friction force between piston and liner can hardly be directly measured without a series of complex transformations and restructurings of engines [59]. As stated previously, the in-cylinder friction is assumed to be 43.5% of the total friction and it accounts for the highest portion of friction.[3] This implies that the changes in the cylinder friction can directly affect the friction performance of the whole engine. In other words, the total friction force of the engine can be a good indicator of the variations in the cylinder friction force. Based on this analysis, a torque meter is mounted between the AC motor and single-cylinder engine to measure the motoring torque for monitoring the friction condition of cylinder assembly, as shown in Figure 8-4.

The installations of excitation actuators caused a loss in the function of the cooling system, also making it difficult to maintain the surface temperature of the liner to a relatively constant state. The temperature changes have a dramatic influence on the oil properties such as the lubricating oil viscosity, modulus and viscosity coefficient, thereby introducing complex errors into the study. Two mutually complementary techniques are applied to solve this problem. To reach a heat balance at the outer surface of the liner, a controllable

high-powered air blower was set beside the engine to blow away the heat generated by tribological behaviours, as illustrated in Figure 8-4.

Another technique for solving the heat balance problem is a technical solution. By slowly raising the temperature of the cylinder liner, the friction condition can be correspondingly changed, resulting in variations in the motoring torque for maintaining engine at certain speed. Based on the acquired temperature and motoring torque data, a correlation curve of torque-temperature characteristic can be obtained, for excluding the interference of temperature changes to the friction measurement. Specific implementation and effectiveness analysis will be described in detail in Section 8.3.5.

The test facilities and instruments are presented in this section, particularly the motoring system specification, the torque measurement and the data acquisition system

8.3.1 Test Rig Construction

The engine used for this research is modified based on the single-cylinder engine described in Section 5.2.1. Figure 8-5 shows an overview of the test rig. The major specifications of the A.C. motor and its associated frequency inventor drive are detailed in Table 8-1. The power of the AC motor is determined mainly based on the peak friction and pumping torques.

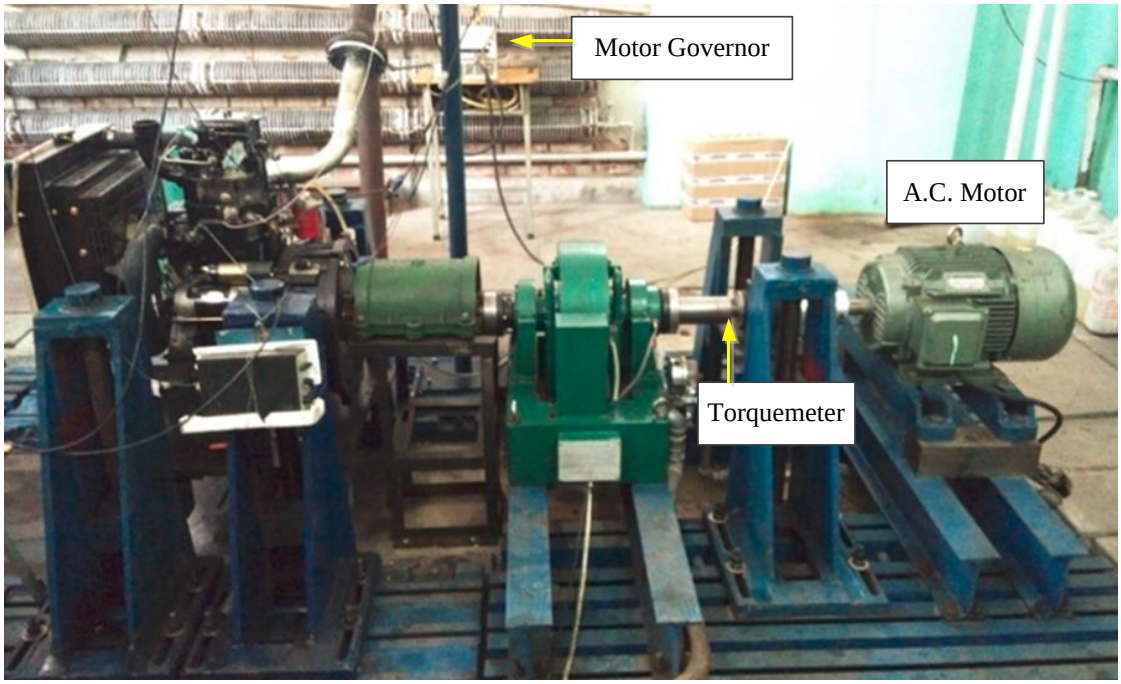

Figure 8- 5 A photograph of the motoring test rig

Table 8- 1 Specification of the motoring system

	Motor		**Frequency inverter**
Manufacturer	Shanxi Electric Motor Co., Ltd	**Manufacturer**	Sinovo Electrical Tech. Co., Ltd
Type	Y2-160M-4	**Type**	EH623A11
Output (kW)	11	**Input Voltage (V)**	Three-phase 220
Electric Current (A)	22.6	**Power Capacity (kVA)**	17
Rated Speed (r/min)	1460	**Input Current (A)**	50.0
Efficiency (%)	88	**Output Current (A)**	49.0
Power Factor	0.84	**Adaptable Motor (kW)**	11
Rated Torque (Nm)	71	**Maximum output frequency (Hz)**	650
Max. Torque (Nm)	78	**Gross Weight (kg)**	2.6
Weight (kg)	120		

Compared to the engine test bench in Section 5.2, both the controllable variables and measured variables in the motoring test rig are relatively simple, which leads to substantial simplification in the control system of the motoring test rig. The outputs from the torque meter and temperature transducer are sent to the control room where the data acquisition equipment and the operating computer are located.

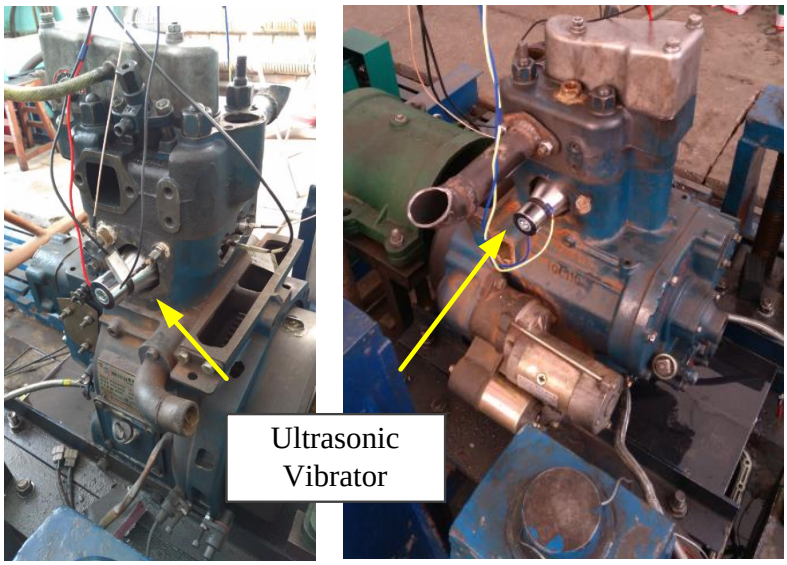

Figure 8- 6 The installation photographs of ultrasonic vibrators

8.3.2 Vibration Actuators

Ultrasonic vibrator is a controllable vibration actuator that can produce cavitation in the liquid. Furthermore, Sa'ardin Abdul Aziz's work [99]suggested that the amplitude of surface deformation excited by ultrasonic vibrations is at the order of 0.1 to 1 microns, being close to the surface roughness amplitude. This indicates that the structural surface may exhibit substantial dynamic deformations close to the surface roughness amplitude by controlling the vibration parameters adequately. Because of these characteristics close to the actual lubrication state of cylinder liner, the ultrasonic vibration can be selected as an appropriate means of applying controllable external vibration on the liner surface, to study the influence of additional vibrations on friction reduction between pistons and liners in IC engines based on a motoring test bench.

To impose external vibrations on the cylinder liner, two vibration actuators are directly mounted on the external surface of the cylinder liner. As shown in Figure 8-7, these actuators are fixed on the external surface of the cylinder liner (one at the intake-side and the other at the exhaust-side) through a special bronze adaptor, which helps to achieve a better transmission of vibrations from the head of actuator to the cylindrical surface.

Since there is no combustion behaviour occurred in the motored engine, a severe heat accumulation will no longer occurs in the liner structure. Therefore, it is feasible to penetrate the cylinder block (shell of water jacket), i.e. to remove the function of cooling system, to facilitate the installation of the vibration actuators, as illustrated in Figure 8-6.

To facilitate applying vibration excitations with different frequencies and energy levels, three different types of adjustable ultrasonic actuators are selected in this study. Specifications of the vibration actuators are presented in Table 8-2.

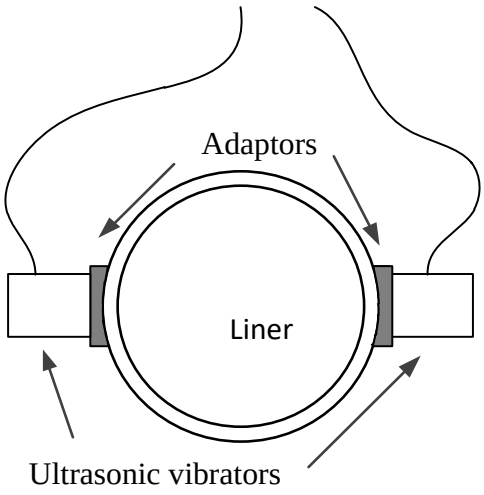

Figure 8- 7 Schematic of ultrasonic vibrator installation

Table 8- 2 Specification of the vibration actuators

	Ultrasonic vibrator
Manufacturer	Clangsonic Co., Ltd., PR. China

Type	CN4025-25HA/28HA/40HA
Frequency (kHz)	25±1 / 28±1/ 40±1
Load Capacitance (%pF)	3000±10
Max. Input Power (W)	50
Resonant Resistance (Ω)	≤25

Based on the mechanisms proposed in Section 8.2.3, it is essential to adjust appropriate vibration magnitudes which can cause dynamic deformations close to the order of surface roughness amplitude and induce sufficient cavitation in the lubricant liquid, for investigating the effect of additional vibrations on friction reduction of cylinder assemblies.

8.3.3 Measurement Instrumentation

To obtain accurate motoring torque for engine friction condition monitoring, the engine motoring test system was carefully set up allowing the motoring torque variation, the changes in cylinder vibration and liner temperature under different excitation conditions to be monitored.

Various transducers have been installed on the test rig in order to collect the operating parameters of the engine, namely: motoring torque, cylinder vibration, liner temperature and engine speed. These signals were collected by the following main transducers:

- Torque transducer
- Revolution speed transducer
- Temperature transducer
- Accelerometer

The liner temperature signal is used to monitor the thermal condition of the cylinder structure under different engine conditions, to further eliminate the interference caused by the oil temperature changes in motoring torque. It is different from the separate Hall encoder in Section 5.2; the revolution speed transducer used in the motoring test rig is integrated into the selected torque meter.

- **Torque and rotational speed transducer**

Torque transducers are a widely used device for measuring the torque of rotating machinery, and have been used extensively in machinery monitoring applications. The torque transducer is typically mounted between two transmission shafts of a power train for measuring the rotational torque. In this research, a strain gauge torque transducer (model YB-1) is used to measure the motoring torque for the test engine. In Figure 8-8, it shows the installation of the torque transducer in the test rig. Its technical specifications are shown in Table 8-3

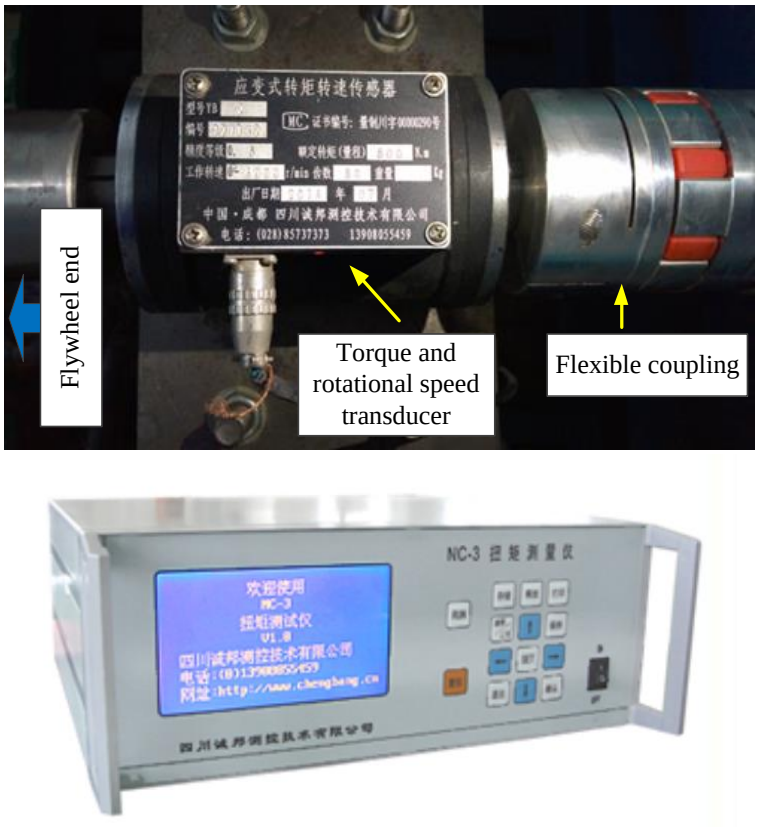

Figure 8- 8 (a) Torque and rotational speed transducer; (b) microcomputer torque meter.

To reduce the interference of the shaft coupling weight in the torque measurement, and to prevent the transducer from bending torque, a flexible column pin shaft connector with a lighter weight is selected in this study to link the transducer and other components in this study, as seen in Figure 8.8(a).

Table 8- 3 Specification of the torque transducer and torque meter

	Torque and rotational speed transducer		**Microcomputer torque meter**
Manufacturer	Chengang Co., Ltd., PR. China	**Manufacturer**	Chengang Co., Ltd., PR. China
Type	YB-1	**Type**	NC-4
Rated Torque (Nm)	200	**Input Frequency Range (Hz)**	0 to 10kHz
Max. Speed (r/min)	4000	**Output Signal (V)**	0 to 5
Weight (kg)	9.4	**Input Impedance (kΩ)**	10
Accuracy (%F.S.)	≤ 0.5	**Accuracy (%F.S.)**	≤ 0.1
Operating Temperature (℃)	-20 to 60	**Operating Temperature (℃)**	-20 to 60

- **Temperature Transducer**

The temperature sensor is typically immersed in liquid or exposed to gas for measuring the temperature variation. For a solid surface of the measured object, a surface mount device (SMD) temperature transducer is often chosen to measure the structural temperature. In this research, a SMD temperature transducer (model GL91) is attached to the external surface of cylinder liner, coupled with heat-resistant structural adhesive, for measuring the liner temperature. Figure 8-9 shows the installation of the temperature transducer in the test rig. Its technical specifications are shown in Table 8-4.

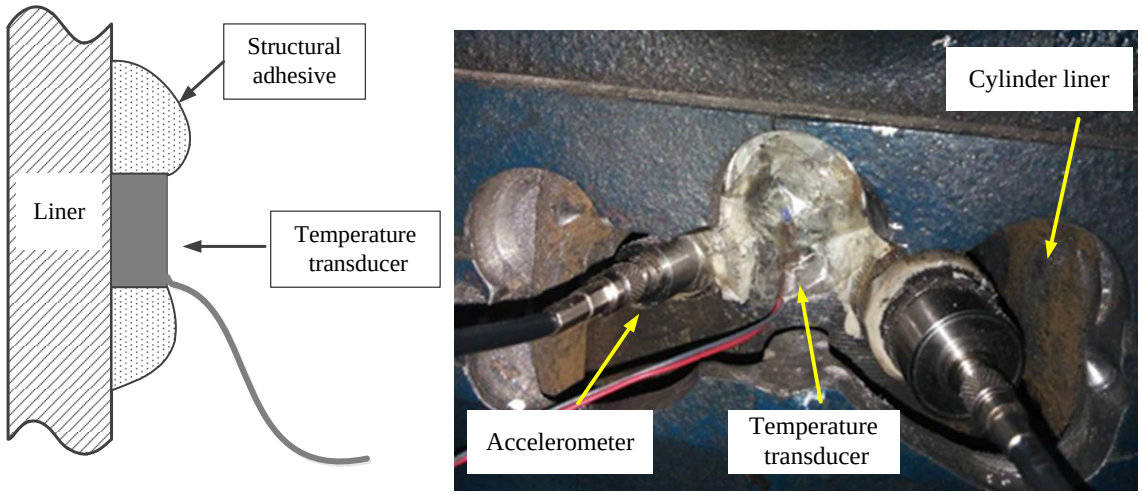

Figure 8- 9 Installation schemes of temperature transducer and accelerometer.

Table 8- 4 Specification of the SMD temperature transducer

	Temperature transducer
Manufacturer	Heraeus
Type	PT100
Measurement Range (℃)	-50 to 150
Output Signal (V)	0 to 5
Accuracy (%F.S.)	≤ 0.5

- **Accelerometer**

The accelerometer used in this test is just the same as the one used in the experiments introduced in Section 5.2.2. The installation of the accelerometer attached to the external surface of cylinder liner, as shown in Figure 8-9(b).

8.3.4 Test Operation

Testing was carried out on the modified QCH1110 test engine. The data was collected using related transducers for future analysis. For comparison purposes raw signals were collected from the sensors under various speeds excited by the vibration actuator and ultrasonic vibrator, respectively. The sampling time is 30 seconds for every operating condition. In the experiment, the test engine was tested with excitations of three kinds of

ultrasonic vibrators and operated at different speeds as shown in Table 8-5. Wherein, the 0W represents that the output power of ultrasonic vibrator is zero i.e. no vibration is added to the cylinder liner, which is the baseline for making compassion with different vibration added tests.

Table 8- 5 Test operating setup (Unit of exciting power: W)

Frequency / **Speed**	23**(kHz)**	28**(kHz)**	40**(kHz)**
800 rpm	0W, 25W, 50W	0W, 25W, 50W	0W, 25W, 50W
1000 rpm	0W, 25W, 50W	0W, 25W, 50W	0W, 25W, 50W
1200 rpm	0W, 25W, 50W	0W, 25W, 50W	0W, 25W, 50W
1400 rpm	0W, 25W, 50W	0W, 25W, 50W	0W, 25W, 50W

8.3.5 Torque-Temperature Characteristics

In the process of motoring test, the friction-induced heat will lead to an increase in temperature of lubricating oil. The thermal balance, i.e. oil temperature of lubrication system continues to rise with the increasing of operating speed. When the oil temperature is lower, lubricating oil in lubrication system has a higher viscosity, which means that more input torque is needed to offset the viscous friction loss.

Preliminary tests show that the torques of motoring the test engine exhibit a high correlation with the temperature of the cylinder liner, which may be attributed to the distinctive trade off phenomenon in the viscosity-temperature characteristics of lubricating oil. Even a small change in liner temperature can cause a significant variation in motoring torque, which would inevitably introduce errors into the study of vibration-induced friction reduction. The difficulty is that the temperature of the cylinder liner can hardly be maintained to a stable value or state by only controlling the external air blower.

To overcome this problem, a hypothesis has been put forward: the effect of the temperature on motoring torque may be a deterministic interference, which can be

quantified and excluded. Taking the effect of temperature changes on the torque as a quantifiable and removable interference, after removing this predictable torque variation, the remaining torque variation mainly reflect the friction response to the external excitations.

Based on this concept, a calibration test for determining the torque-temperature characteristics of the motoring test rig was designed and implemented. The fundamental principle of this calibration test can be expressed using the following Eq. (8.12),

$$T_{torque\_new} = T_{torque\_old} + K(T_{temperature\_new} - T_{temperature\_baseline}) \quad (4.35)$$

wherein, K is a proportional coefficient obtained from the calibration test. T_{torque} is the motoring torque and $T_{temperature}$ is the temperature measured from the outer surface of the cylinder liner.

The scheme and steps of the calibration test are described as follows.

1. After booting the test bench, increase the running speed rapidly to 1400rpm and keep it there, to raise the liner temperature from an ambient temperature (20 ℃) to approximately 75 ℃. During this warming process, both the temperature and torque data were collected and recorded at a temperature increment of 5 ℃.
2. Then, decrease the running speed from 1400rpm to 800rpm rapidly, to lower the liner temperature to a stable temperature. Sample the temperature and torque data at the same interval of 5 ℃ for subsequent analysis.
3. Based on the acquired temperature and motoring torque, a correlation curve of torque-temperature characteristic can be obtained, for excluding the interference of temperature changes to friction measurement.

As shown in Figure 8-10 (a) to Figure 8-10 (d), with the increase of liner temperature, the motoring torque shows a steady downward trend. When the liner temperature is higher than 65 ℃, the motoring torque shows obviously fluctuations. Nevertheless, a higher-order linear relationship can still be clearly observed between the torque and temperature data from 60 ℃ to 75 ℃.

In order to obtain the polynomial expression of torque-temperature characteristic, the raw data were fitted by the linear, 2nd and 3rd order polynomial functions respectively, as shown in Figure 8-10(a) to Figure 8-10(c), to facilitate the follow-up processing of disturbance removing.

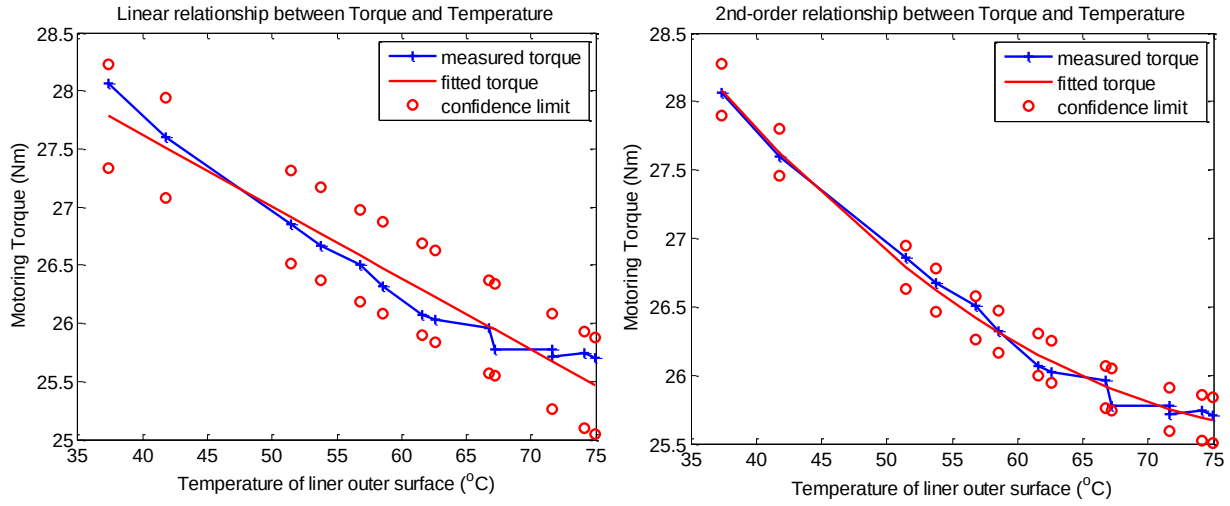

(a) Comparison of linear fitting with raw data; (b) 2nd fitting result with 95% confidence intervals

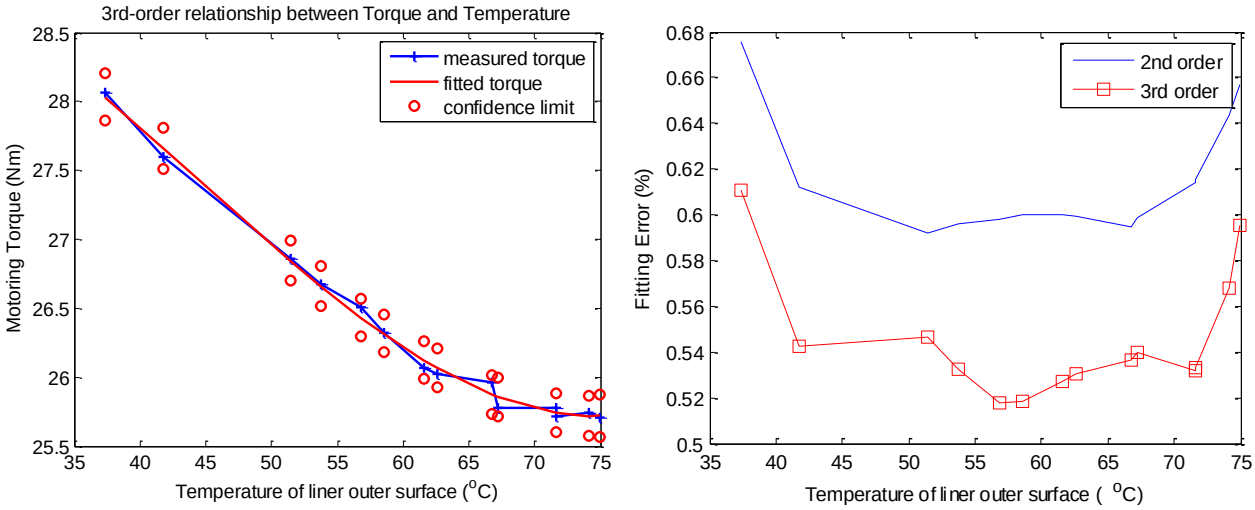

(c) 3rd fitting result with 95% confidence intervals; (d) Errors of different fitting results

Figure 8- 10 The comparison of fitting results

Confidence limits for the fitted result are an interval estimated based fitting residuals. Instead of a single estimate for the mean, a confidence interval generates a lower and upper limit for the mean. In particular, the computation of confidence limit in this work

was achieved by calling the *polyconf* function in MATLAB. The fitting error was obtained through the division operation of confidence interval and measured data. With respect to the large errors that appeared in the linear fitting curve, the results of the second-order polynomial fitting show better integration with the changing trend of data. Moreover, as seen in Figure 8-10 (d), the errors of second-order fitting are much closer to that of third-order fitting in magnitude than the linear fitting. Therefore, it is reasonable to choose the second-order fitting polynomial expression to characterise the torque-temperature characteristic of the test rig.

Though repeated experiments, the determinacy and inherency of the torque-temperature characteristic in the test rig have been verified, based on the high degree of repeatability and reliability presented in the test results. Thus, based on the measured torque-temperature curve, after removing the influence of temperature changes, the correlation between the motoring torque and friction state can be strongly enhanced.

8.4 Analysis of Friction Responses to Ultrasonic Vibrations

In order to study the variation trends of engine friction responses to additional ultrasonic vibrations, the time average of motoring torque under different excitation conditions and different operating conditions are calculated and presented in Figure 8-11.

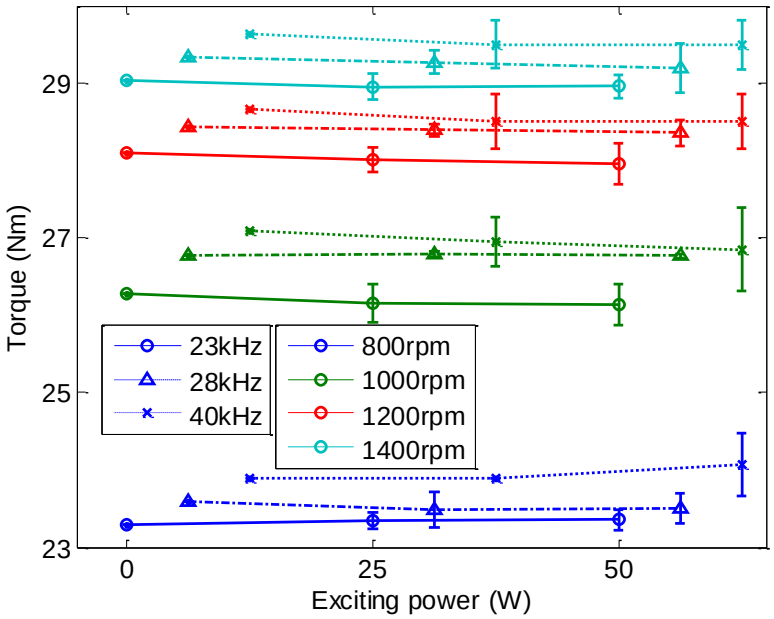

Figure 8- 11 Motoring torques excited by three different vibrators and their corresponding reduction amplitude

Under the same operating speeds, the average of motoring torque excited by three different ultrasonic frequencies (23kHz, 28kHz, 40kHz) and different exciting powers (0W, 25W and 50W) present various changing trends. Under high speed operating conditions above 800rpm, with the increase of exciting power, the motoring torque obviously shows downward trends. These downward trends indicate that the superimposition of ultrasonic vibrations can indeed cause friction reduction, which is agreeable with the results based on limited prototypes and mechanical test benches [100], [101].

To facilitate a comparative analysis of vibration-induced torque reductions, both the motoring torque and its absolute variations under different conditions are drawn in Figure 8-11. It should be noted that, the torque results of 28 kHz and 40 kHz have been slightly shifted by 0.3Nm and 0.6Nm respectively, for better observation. It can be clearly seen that the motoring torque excited by ultrasonic vibrator with a resonant frequency of 40 kHz shows the most obvious reductions when the input exciting power equals 50W. Compared to the operating conditions without external excitation, the motoring torque excited by ultrasonic vibration of 40kHz and 50W shows the obvious drops by -0.357Nm,

0.471Nm, 0.309Nm and 0.285Nm, or -1.52%, 1.79%, 1.10% and 0.98%, corresponding to running speeds of 800rpm, 1000rpm, 1200rpm and 1400rpm. This shows that the external vibration with higher excitation energy and appropriate exciting frequency can more significantly reduce the frictional losses of the engine.

However, it should be noted that, under the operating speed of 800rpm, the motoring torques under excitations of all three vibrators have slightly increased along with the increase of exciting power, which can hardly be explained by the vibration-induced friction reduction proposed in Section 8.2.

As mentioned in Section 6.4, in low-speed conditions, the dynamic responses of the liner lubricated by high-viscosity lubricating oils are more intensive than the low-viscosity oils. The lubrication condition of cylinder assembly can be worsened by the severe situation of oil supply for the splash lubrication of cylinder assembly at low-speed conditions. The low mobility of high-viscosity oil can further aggravate the already severe lubrication conditions of cylinder assembly. It can be concluded that the cylinder assembly is prone to suffer lubricant starvation as a result of insufficient lubricant supply. When the oil in valleys of the rough surface is insufficient, the cavitation caused by ultrasonic excitations will exacerbate the state of lubricant starvation, resulting in the increased friction losses at low speed operating conditions.

To examine the effects of additional excitation on the dynamic responses of cylinder assembly, and to evaluate the lubricant film state based on the validated local feature associated with film dynamic parameters, the frequency spectrum analysis was employed to process the measured liner vibrations. To obtain a general understanding on the amplitude of liner deformations, the displacement responses of liner surface were calculated from measured vibrations through twice integration in the frequency domain. As shown in Figure 8-12, frequency spectra of dynamic responses in the operating condition of 1400rpm and under different excitation conditions have been calculated and drawn.

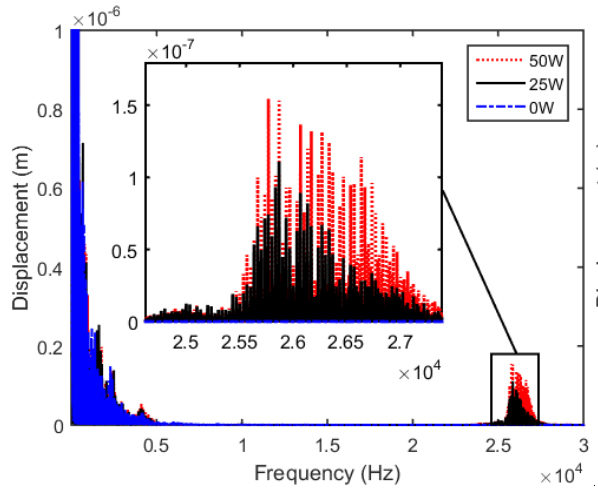

(a) Excitation frequency=25 kHz;

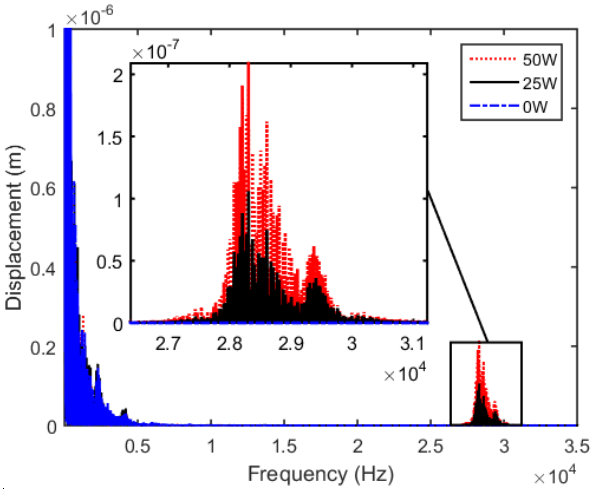

(b) Excitation frequency=28 kHz.

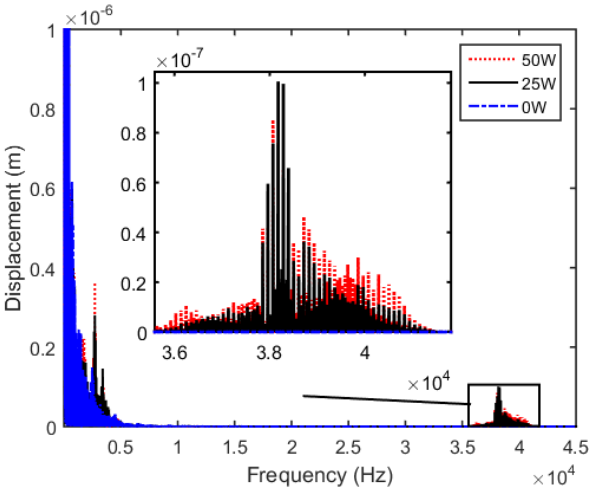

(c) Excitation frequency=40 kHz.

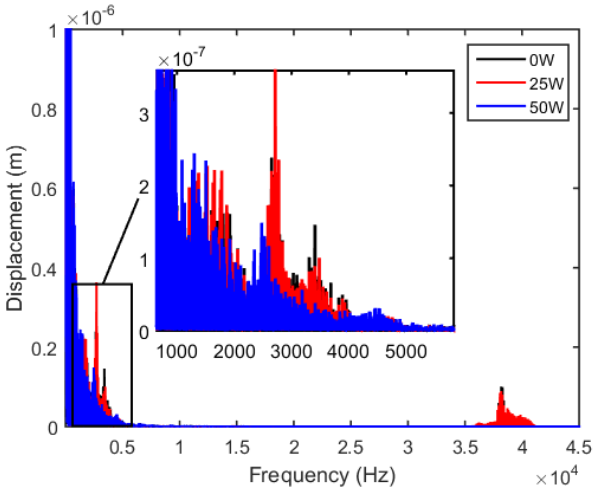

(d) Magnified plot of spectra in 1kHz - 5kHz, excited by 40 kHz.

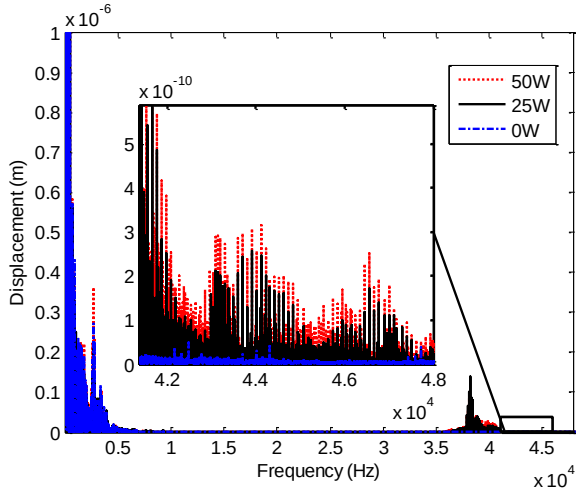

(e) Magnified plot of spectra in 40kHz - 48kHz, by 40 kHz.

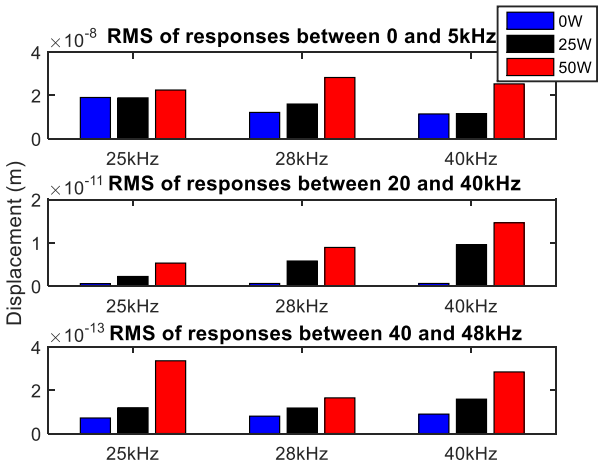

(f) RMSs of displacement responses.

Figure 8- 12 Frequency spectra of vibrations excited by vibration actuators with different frequencies

As seen in Figure 8-12, due to the addition of ultrasonic vibrations, frequency spectra of measured vibrations show obvious peaks corresponding to the exciting frequencies, near the 25 kHz, 28 kHz and 40 kHz. It can be seen in Figure 8-12(a), (b) and (c) that the amplitude of additional vibration-induced deformation is at the order of 0.1 microns, being close to the predicted amplitude of dynamic deformation based on the FE model in Chapter 3. This suggests that the additional vibrations applied by ultrasonic vibrators are appropriate for the simulating the dynamic deformations of liner surface caused by the piston slaps. With the increase of exciting power, the amplitude of all these frequency peaks showed obvious increasing trends.

As shown in Figure 8-12(d), the difference in dynamic responses at the frequency range of 1 kHz to 5 kHz is not obvious, indicating that the applying of external vibrations did not introduce too much influence into the structural characteristic-related responses. When the cavitation bubble burst, the vibrational energy released is more evenly distributed in the frequency range of 20 kHz to 100kHz[102]. As seen in Figure 8-12(e), the amplitude of responses above the frequency of 40 kHz gradually increased with the increase of exciting power, it may be attributed to the exacerbated cavitation bubble crashes. The RMS result of these responses have been calculated and shows as shown in Figure 8-12(f), which gives much clearer presentation of variation trends observed in the previous figures.

As illustrated and proved in Section 6.4, changes in the film performance can directly affect the kinetic parameters of impact behaviours between the piston and cylinder liner, thus causing changes in the responses characteristics of the liner surface. This means that it is feasible to characterise and evaluate the formation state of lubricant film based on the localised response features of measured vibration signals.

As indicated in Figure 8-11(d), the external ultrasonic vibrations with frequency of 40 kHz are prone to cause more reduction in the friction of piston and cylinder assembly. To determine whether the ultrasonic vibration caused a change in the tribological behaviours, especially in the film performance between the piston and liner, the continuous wavelet

transform (CWT) was applied to the liner vibration to highlight the dynamic responses localised in both the time and frequency domains and to facilitate comparative analysis.

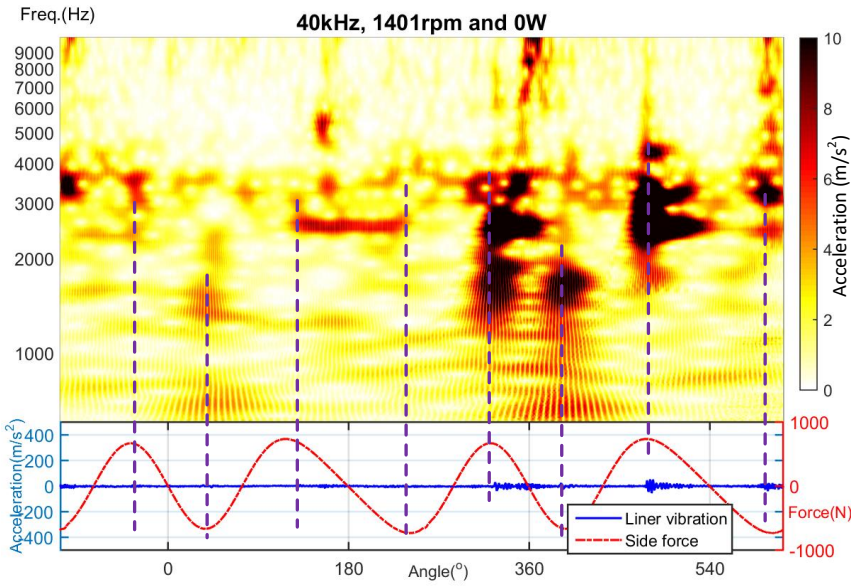

Figure 8- 13 CWT of liner vibration at 1400rpm without ultrasonic excitation

Figure 8-13 shows the STFT of vibration signal measured from cylinder surface in the test engine motored by an AC motor rather than driven by the in-cylinder combustion. As a result, Figure 8-13 does not show the combustion shock-induced response event above 10000Hz corresponding to combustion shocks.

As seen in Figure 8-13(a), 8 slap-induced events could be observed on the CWT of liner vibration and these correspond well to the peaks and troughs of side-thrust force during one operating cycle. In the absence of gas pressure-driven and external vibration excitation, the dynamic response of cylinder liner mainly reflects the unceasing piston slap impacts driven by only the inertia force of piston assembly. That is why the number and timing of observable slap events under motored condition are different with those under combustion condition in chapter 6. As for the difference in response characteristics between the odd and even cycles, it may be mainly attributed to the changes in running speed caused by the remaining intake and exhaust system and other unremoved components.

Compared to the case of liner vibration without additional excitation, the CWT result shows more regular secondary features of the ultrasonic excitations, as shown in Figure 8-14. Nevertheless, the slap-induced events can still be identified from the CWT diagram. These events are highly consistent with the previous case without external excitations, as shown in Figure 8-13, indicating that the external excitation did not affect the dynamic process of the piston-cylinder pair. Therefore, with the premise that the overall dynamic behaviour of cylinder assembly is the same, a local feature which has proven to correlate with film dynamic parameters, was selected to study the film performance of the cylinder liner, and to investigate the influence of external excitation on lubrication status.

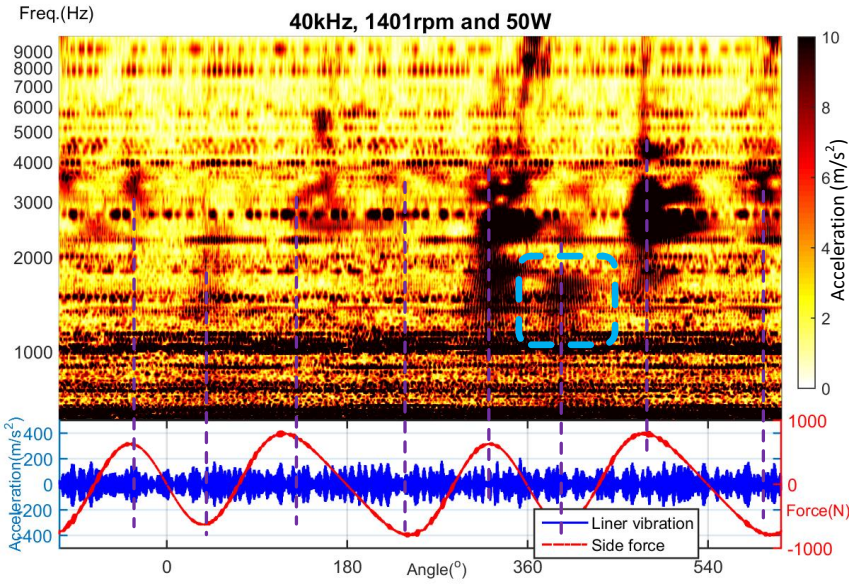

Figure 8- 14 CWT of liner vibration at 1400rpm under excitation of 40 kHz and 50W

As indicated in Chapter 4 and proved in Section 6.4, the local features associated with mode responses can well reflect the impact intensity between the piston and liner surfaces. In particular, the local feature of liner vibration after TDC and in the frequency range of 1000 Hz to 2000 Hz is highly correlated with the damping effect of lubricant film between the pistons and liners. Therefore, a local feature, whose generating position is close to the mounting position of the accelerometer on liner surface, was selected for diagnostic analysis, as marked by the blue dashed rectangle in Figure 8-14.

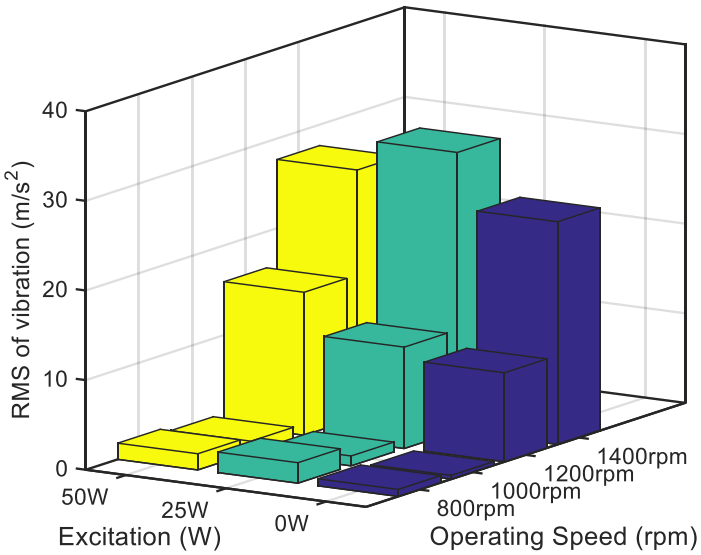

Figure 8- 15 RMS result of local feature under different operating conditions

As shown in Figure 8-15, the RMS of slap-induced local response shows obviously increasing trends with the rising of exciting power. In high speed conditions, the increasing trend is more obvious. It indicates that, with the increase of exciting power, the lubrication condition of cylinder assembly was changed, and the damping effect of lubricant film was greatly reduced, thereby leading to the increased responsive intensity of the liner vibration.

Thus, the reason for friction reduction may lie in the fact that, with the weakening of the damping effect of the lubricant film, the shear flow factors ϕ_{fs} of lubricating oil that determine the viscous friction (as seen in Section 7.2 and in Eq. 7.11) have also been drastically reduced, ultimately leading to a reduction in the total friction force. This explanation agrees well with the downward trends appeared on viscous friction force in Section 7.4. It provides strong evidence that external vibrations, especially the ultrasonic excitation, can indeed affect the tribological behaviours between the pistons and liners, which include both asperity friction and viscous friction, and cause the friction reduction of IC engines.

It can be summarized that the reduction amplitudes of friction losses varies with different excitation conditions. The most significant reduction is 1.79% under 50W at 40 kHz. Nevertheless, the results verify that additional vibrations can affect the tribological behaviours between the pistons and liners, including both asperity friction and viscous friction, and resulting in the friction reduction of IC engines when the vibration parameters are tuned adequately.

Chapter 9
Conclusions and Future Work

This chapter summarizes the achievements of this research and draws conclusions based on the results obtained from the entire research work. It is followed by a summary of the author's novel contributions to knowledge. Finally, suggestions are made for further improvements of the schemes developed in this thesis.

9.1 Objectives and Achievements

The primary aim of this research was to: '*investigate the potential impacts of alternative fuels' burning on the dynamic responses and tribological characteristics of cylinder liners in an IC engine. It further seeks to disentangle the effects of dynamic responses on the friction and lubrication processes between piston rings and liners, by introducing dynamic deformations of liners into a two-dimensional mathematical model of film formation and distribution.'*

This central aim was achieved through a numerical simulation study based on a validated finite element model for predicting dynamic responses of cylinder liners in an IC engine, with consideration of the characteristics of structural modes and nonlinearities of assembly constraints. The findings about relationship between combustion of alternative fuels and the liner vibrations raised in FE model have been confirmed through a series of experimental researches based on a single-cylinder engine test bench. Moreover, the FE model also presented the dynamic deformations of liner surface, which offers the possibility to study the influence of liner deformations to friction behaviours. Based on these dynamic deformations, a dynamic deformation based model of film formation and distribution between the piston rings and liners was developed to take into consideration of potential influences from liner dynamic distortions. Both the minimum oil film thickness and friction forces were found to be sensitive to the dynamic characteristics of liners determined by operating conditions and fuel types. To further investigate the possibility of friction reduction induced by external vibration excitations, a preliminary experimental study has been conducted based on a motoring test bench.

In the following a summary of the objectives and the key achievements achieved by this research is clarified by following that setup in Chapter 1 respectively:

Objective 1. To perform a literature review and identify any gaps in the theory, evidence and knowledge in relation to the influences of alternative fuels on dynamic responses and frictional behaviours of IC engines (see Chapter 2)

Achievement 1. The review of excitation sources of liner vibrations (see Section 2.2), vibration and noise performances of engines (see Section 2.3) and tribological characteristics of cylinder assemblies (see Section 2.4) affected by the usage of alternative fuels were presented. Development of theoretical research, especially the mathematical modelling studying, on the tribo-dynamic behaviours between piston rings and liners was reviewed and introduced in Section 2.4. Finally, the basic mechanism of vibration-induced friction reduction and its development in mechanical engineering was reviewed in Section 2.5.

Objective 2. To develop a finite element dynamic model of cylinder assembly for prediction and interpretation of liner responses to excitation sources: in-cylinder combustion shocks and piston side-thrust slaps.

Achievement 2. A finite element model is established to predict the dynamic responses of cylinder liners under respective excitation sources. The model takes into account both the characteristics of structural modes and nonlinearities of assembly constraints when selecting adequate elements for efficient computation of the responses under both the highly nonlinear combustion pressure excitations and subsequent piston slap impacts (see Chapter 3). Then, based on the established model, the causal relationship and correspondences between the localised response features with the excitation sources were analysed.

Objective 3. To theoretically study the influences of alternative fuels on the excitation sources and their consequent dynamic responses of liners based on the established FE model. This includes a diagnostic analysis to explore the localised features of dynamic responses for better understanding of the correspondence between response characteristics and specific combustion properties of alternative fuels.

Achievement 3. According to the physical and chemical characteristics of alternative fuels, the changes in in-cylinder combustion force and piston side-thrust force induced by combusting of alternative fuels have been compared and analysed. Then the dynamic responses of cylinder liners under two main excitation sources were calculated and

compared. For a better understanding of the nonlinear variations appeared in liner vibration fuelled with alternative fuels, a decomposition analysis of piston side-thrust force was performed for studying the localised response characteristics corresponding to the coupling interaction of combustion force with piston inertia force (see Chapter 4).

Objective 4. To verify and diagnostically analyse the impacts of alternative fuels on the dynamic responses of liners (see Chapter 6) based on a single-cylinder diesel engine test rig (see Chapter 5).

Achievement 4. To verify the simulation investigation, a single-cylinder engine test bench has been developed (see Chapter 5). The predictions presented previously are evaluated against experimental results under different engine operating conditions fuelled with alternative fuels. In addition, continuous wavelet analysis was employed to process the non-stationary complicated responses for charactering key response events and their frequency ranges (see Chapter 6). The analysis result of measured vibration signals shows agreeable correspondences with the numerical predictions (proposed in Chapter 3 and 4), showing that the established model is sufficient to represent and characterise the dynamic features of cylinder liner in the frequency range below 10kHz, which paves the way for following studies on the vibration-induced dynamic friction.

Objective 5. To theoretically study the differences in minimum oil film thickness and friction forces of piston-cylinder assembly between the conditions with and without consideration of dynamic deformations (see Chapter 7).

Achievement 5. To investigate the dynamic friction process between the piston rings and liners, a dynamic deformation based lubrication model were developed in Section 7.2 and 7.3. After processing of geometric extraction and coordinate transformation, dynamic deformations of liner acquired from FE model were loaded into the lubrication model and a series of runs were performed under different speed and load conditions. To explore the cause of fluctuations appeared in friction forces, spectrum analysis was employed to process the simulated friction forces for key oscillation events and their frequency ranges. For the phenomenon of instantaneous harsh friction after combustion TDC predicted in

lubrication model, a panoramagram of wear patterns on liner surface was made and used for confirmation and interpretation of this finding.

Objective 6. To explore the influence of additional vibrations to friction behaviours between pistons and liners, especially the possibility of friction reduction achieved by adjusting frequency and input power of excitation.

Achievement 6. A motoring test bench was designed and constructed based on the single-cylinder engine test bench established in Chapter 5 (see Section 8.3). To eliminate the interference of temperature changes to motoring torque, a calibration test for determining the torque-temperature characteristics of the motoring test rig was designed and implemented. Torques for motoring test engine, which representing the mechanical losses especially the friction loss of cylinder assembly, were measured and analysed under different operating speeds and excitation conditions. Finally, the reduction amplitudes of friction losses corresponding to different excitation conditions (frequency and input power) were compared and analysed.

9.2 Conclusions

This research investigated the influences of alternative fuels' usage on dynamic responses and friction characteristics of cylinder liners in CI engines. The key conclusions from this study can be summarised as follows:

1. Both the influences of excitation characteristics and structural modal characteristics on the dynamic responses of cylinder liner were investigated and discussed based on the validated finite element dynamic model established in this research. Based on the comparison between FE model-based prediction and experimental evaluation in the form of CWT representation, it can be concluded that the developed FE model is acceptable as it provides dynamic responses agreeable with measurements. Particularly, the dynamic responses of cylinder liner to combustion shocks appear in a higher frequency modes from 4 kHz to 12 kHz; whereas that of piston impacts are in a lower frequency modes from 1 kHz to 4 kHz. Furthermore,

the predicted amplitude of local responses is at the order of 0.01 microns due to the combustion shocks, which may be negligible to affect lubrications. However, piston slaps can lead to deformation as high as 0.1 micros, being about 20% of roughness amplitude. Consequently, its impact on lubrication performance and friction losses of cylinder liners has been investigated subsequently.

2. Due to the different physicochemical properties, combustions of alternative fuels caused the evident differences in dynamic responses of cylinder liners. **(1)** The variation trends of combustion shock-induced responses can well correspond to the combustion characteristics of alternative fuels regarding the peak value of pressure rise rate. Because of its high cetane number value, ignition delay period of biodiesel is significantly shortened, which leads to a smaller peak value in the rise rate of combustion pressure (in premixed combustion period). It means that the frequency contents of in-cylinder combustion pressure fuelled with biodiesel are relatively less than the fossil diesel, and insufficient to motivate much clear mode responses of cylinder liners. Oppositely, as a result of the combustion-supporting characteristic of methanol, the rise rate of combustion pressure fuelled with methanol-diesel blended fuel M15 is greater than the other fuels, resulting in the more intensive dynamic responses. **(2)** Comparative analysis of piston slap-induced responses indicated that the combustion duration, especially the sum of mixed-controlled combustion period and late combustion period, can dramatically affect the overall intensity of liner vibrations. The extended combustion duration of biodiesel can cause a relative increase in the kinetic energy of piston lateral movement, thereby resulting in a rise of vibration intensity near the exhaust TDC. **(3)** The localised responses near the combustion TDC showed more complex variation tendencies which are not linear with the combustion properties of alternative fuels. Cetane number, i.e. the flammable property of alternative fuels determines the duration of ignition delay period, leading to the significant differences in the phase delay of pressure peak. Due to the cancellation, or coupling effect between the combustion force and inertia force, the rise rate of

piston side-thrust force near the combustion TDC shows a nonlinear decrease as the rise of running speed. The advanced ignition caused by the high cetane number of biodiesel, makes a significant contribution to the cancellation effect on the piston side-thrust force, thereby resulting in a nonlinear trend of decrease after an increase in the RMS of local responses near the combustion TDC. However, due to the opposite effect of methanol on ignition delay, the cancellation effect of methanol-diesel blended fuel M15 on the piston side-thrust force is weakened. The slap-induced local responses of M15 shows more intensive responses than the other fuels around the combustion TDC.

3. Based on the dynamic deformation based lubrication model considering the impacts of dynamic deformations of liners, several conclusions about the vibration-induced fluctuations in friction forces can be drawn as: **(1)** Due to the introduction of dynamic deformation, the lubricating condition between the matched surfaces can be improved, with larger geometric gap and higher sliding speed in localised contact regions, thereby resulting in the reduction of asperity friction. The dynamic deformations of liner can be beneficial to reduce the friction losses around combustion TDC, where is normally regarded as the position of most serious wear occurred, and to enhance the operation efficiency. **(2)** Due to thinner film thickness, the substantial deformations of liner surface as a result of the most significant piston slap event, caused the occurrence of localised contact, or partial contact, between the matched surfaces after combustion TDC, which results in a phenomenon of instantaneous harsh friction after combustion TDC being observed in the friction forces at crank angle of $380°$ to $385°$. This finding has been confirmed by feature analysis based on a panoramagram of wear patterns on liner surface. **(3)** Diagnostic analysis of friction oscillation event related to the second-order mode response of liner in power stroke shows that the combustion of methanol blended fuel M15 can cause more severe friction losses and wears on the liner surface whereas the biodiesel shows the opposite effects.

4. The observable changes in motoring torque verify that proper external vibrations can affect the tribological behaviours between the pistons and liners, including both asperity friction and viscous friction, and resulting in the friction reduction of IC engines. Particularly the 40 kHz vibration at the maximal driving power of the test device can achieve a maximum reduction of 1.79% in the motoring torque.

9.3 Research Contributions to Knowledge

This research has led to a number of novel developments in the subject that have not considered by previous researchers. For clarification, key novel aspects are summarised as follows:

Contribution 1: The dynamic response of the cylinder liners and thereby the engine body is well correlated with the combustion of alternative fuels and tribological behaviours. The tight correspondence among local features on time-frequency spectra of vibration, combustion characteristics of fuels and modal characteristics of liner structure was first proposed and verified.

Contribution 2: The establishment of validated finite element model of cylinder assembly for investigating dynamic responses to combustion shocks and piston slaps in a diesel engine is novel (see Chapter 3). No work has been found in the literature that describes the development of a dynamic model considering both the characteristics of structural modes and nonlinearities of assembly constraints.

Contribution 3: Decomposition analysis of piston side-thrust force for interpreting the nonlinear variations of liner vibrations fuelled with alternative fuels is novel (see Chapter 4). Combustion characteristics of fuel is one of the important factors that affect the dynamic behaviour, but its effect is implemented by coupling with inertia force of piston assembly, thereby resulting in the nonlinear tendency of liner responses. Based on the decomposition analysis of piston side-thrust force and improved FE model-based dynamic simulation, a novel approach to determine and investigate the relationship between the

combustion characteristics of alternative fuels with engine vibrations is proposed for the combustion diagnosis, fuel performance evaluation and friction monitoring.

Contribution 4: A novel measurement scheme of liner vibrations is proposed and implemented on a single-cylinder engine test rig (see Chapter 5). Compared to the traditional vibration measurement of engine block, direct measurement of liner vibrations is able to effectively isolate the potential disturbances from other mechanical components of engines. While compared to the other direct measurements, such as Geng's measuring method [25] with help of a steel transmitting rod, the direct bonding of accelerometer to liner surface proposed in this research work can substantially prevent the vibration signal attenuation in the transmission process, thereby greatly enhancing the signal to noise ratio.

Contribution 5: The dynamic deformation of the liner surface was first introduced into the modelling of lubricant film formation and distribution, which leads to a novel dynamic deformation based lubrication model for predicting the dynamical and tribological behaviours between the piston rings and liners (see Chapter 7).

Contribution 6: The motoring test bench established for investigating vibration-induced friction reduction is novel (see Chapter 8). The vast majority of studies on vibration-induced friction reduction are conducted based on limited prototype or mechanical test benches, rather than machines in actual operations. The experimental study on the influence of additional vibrations on friction reduction was first performed on an IC engine in actual operation in this research.

9.4 Recommendations for Future Work

A great deal of preliminary research work has been undertaken as part of this study to investigate the influences of alternative fuels to engine dynamic responses and friction characteristics. If a wider and more extensive study was to be undertaken, some key recommendations should be considered for future work in this research area.

- **Recommendation 1:**

The integration of dynamic model with lubrication model of cylinder assembly requires further improved. At low-speed operating conditions, when the oil supply for piston and

cylinder pair is deficient, the estimation of oil film thickness should not be performed based on a conventional manner. A more effective multidisciplinary model of cylinder assembly needs to be developed to take into consideration the oil supply and filling process for more accurate description and analysis of the dynamic behaviours.

- **Recommendation 2:**

To further identify the specific location and timing of piston slaps on the cylinder wall, it is recommended to upgrade to the established test bench. More transducers, such as high-frequency accelerometers, acoustic emission (AE) sensors and micro electro mechanical system (MEMS) devices, are needed to measure and locate the dynamic responses of cylinder block and liners.

- **Recommendation 3:**

Several signal processing algorithms have been employed within the current study for the processing of non-stationary vibration signals. Other new methods may be developed for accurate feature extraction from the non-stationary signals for sources recognition and fault diagnosis and these should be considered.

- **Recommendation 4:**

The effects of dynamic deformations of liner surface on tribological behaviours between the piston rings and liners have been investigated based on an improved dynamic deformation based lubrication model with considering the dynamic deformations of liner surface. However, to further understand the potential influences of dynamic deformations on some more detailed and localised behaviours such as the micro fluid dynamics and micro-morphology of matched surfaces, more theoretical and experimental works are required to explore the microcosmic mechanism of vibration-induced friction reduction.

- **Recommendation 5:**

In the motored test, the friction status of cylinder assembly was obtained by measuring the motoring torque, rather than by a direct measurement of friction force. To improve the accuracy and real-time performance of friction measurement, a direct measuring equipment of piston friction force using floating-liner principle should be designed and developed in the future work.

- **Recommendation 6:**

Based on the proposed findings on the relationship among the fuel properties, dynamic responses and tribological characteristics of engines, further works about the design and optimization of multi-component alternative fuels should be carried out with the goal of improving NVH performance and mechanical efficiency of the IC engines.

- **Recommendation 7:**

By optimizing the structure of cylinder assembly, the combustion shock or piston slaps may enable the contact surface to produce appropriate vibration responses so as to achieve the reduction of friction losses. Alternatively, a specialized vibration actuator may be designed and added on the outer surface of cylinder liner. By adjusting the parameters of additional vibration, the optimization of friction reduction under different operating conditions can be realised.

.

References

[1] D. Jung, J. Yong, H. Choi, H. Song, and K. Min, ‘Analysis of engine temperature and energy flow in diesel engine using engine thermal management’, *J. Mech. Sci. Technol.*, vol. 27, no. 2, pp. 583–592, Mar. 2013.

[2] D.-C. Han and J.-S. Lee, ‘Analysis of the piston ring lubrication with a new boundary condition’, *Tribol. Int.*, vol. 31, no. 12, pp. 753–760, 1998.

[3] A. Comfort, ‘An Introduction to Heavy-Duty Diesel Engine Frictional Losses and Lubricant Properties Affecting Fuel Economy - Part 1’, Dec. 2004.

[4] B. C. Majumdar and B. J. Hamrock, ‘Effect of surface roughness on hydrodynamic bearings’, *NASA TM-81711 Oct*, vol. 9, 1981.

[5] Y. Hu, H. S. Cheng, T. Arai, Y. Kobayashi, and S. Aoyama, ‘Numerical Simulation of Piston Ring in Mixed Lubrication—A Nonaxisymmetrical Analysis’, *J. Tribol.*, vol. 116, no. 3, pp. 470–478, Jul. 1994.

[6] O. Akalin and G. M. Newaz, ‘Piston Ring-Cylinder Bore Friction Modeling in Mixed Lubrication Regime: Part I—Analytical Results’, *J. Tribol.*, vol. 123, no. 1, pp. 211–218, 1999.

[7] J. A. Greenwood and J. H. Tripp, ‘The Contact of Two Nominally Flat Rough Surfaces’, *Proc. Inst. Mech. Eng.*, vol. 185, no. 1, pp. 625–633, Jun. 1970.

[8] R. Prasad and N. K. Samria, ‘Transient heat transfer analysis in an internal combustion engine piston’, *Comput. Struct.*, vol. 34, no. 5, pp. 787–793, 1990.

[9] S. Edberg and E. Landqvist, ‘The impact of honing process parameters on the surface quality of cylinder liners’, Master, KTH Royal Institute of Technology, 2015.

[10] J. J. A. Jocsak, ‘The effect of surface finish on piston ring-pack performance in advanced reciprocating engine systems’, Massachusetts Institute of Technology, 2005.

[11] M.-T. Ma, E. H. Smith, and I. Sherrington, ‘Analysis of lubrication and friction for a complete piston-ring pack with an improved oil availability model: Part 2: Circumferentially variable film’, *Proc. Inst. Mech. Eng. Part J J. Eng. Tribol.*, vol. 211, no. 1, pp. 17–27, Jan. 1997.

[12] M.-T. Ma, I. Sherrington, and E. H. Smith, ‘Analysis of lubrication and friction for a complete piston-ring pack with an improved oil availability model: Part 1: Circumferentially uniform film’, *Proc. Inst. Mech. Eng. Part J J. Eng. Tribol.*, vol. 211, no. 1, pp. 1–15, Jan. 1997.

[13] T. Yamada, H. Kobayashi, K. Kusama, J. Sagawa, M. Takiguchi, and T. Ishikawa, ‘Development of a Technique to Predict Oil Consumption with Consideration for Cylinder Deformation - Prediction of Ring Oil Film Thickness and Amount of Oil Passing Across Running Surface under Cylinder Deformation -’, 2003.

[14] Hiroshi Kanda, M. Okubo, and T. Yonezawa, ‘Analysis of Noise Sources and Their Transfer Paths in Diesel Engines’, SAE Technical Paper, Warrendale, PA, SAE Technical Paper 900014, Feb. 1990.

[15] J. Heywood, *Internal Combustion Engine Fundamentals*, 1 edition. Tata Mcgraw Hill Education, 2011.

[16] M. F. Brunt, H. Rai, and A. L. Emtage, 'The calculation of heat release energy from engine cylinder pressure data', SAE Technical Paper, 1998.

[17] D. Zhen, 'A Study of Non-stationary Signal Processing for Machinery Condition Monitoring', doctoral, University of Huddersfield, 2012.

[18] S. Periyasamy and T. Alwarsamy, 'Combined effects of inertia and pressure on engine vibration', *J. Vib. Control*, vol. 19, no. 16, pp. 2469–2480, Dec. 2013.

[19] R. A. Huls, A. X. Sengissen, P. J. M. van der Hoogt, J. B. W. Kok, T. Poinsot, and A. de Boer, 'Vibration prediction in combustion chambers by coupling finite elements and large eddy simulations', *J. Sound Vib.*, vol. 304, no. 1–2, pp. 224–229, 2007.

[20] X. Wang and K. Ohta, 'Study on Piston Slap Induced Liner Cavitation', *J. Vib. Acoust.*, vol. 137, no. 5, pp. 051010–051010, 2015.

[21] W. W. F. Chong, M. Teodorescu, and N. D. Vaughan, 'Cavitation induced starvation for piston-ring/liner tribological conjunction', *Tribol. Int.*, vol. 44, no. 4, pp. 483–497, 2011.

[22] N. Dolatabadi, S. Theodossiades, and S. J. Rothberg, 'On the identification of piston slap events in internal combustion engines using tribodynamic analysis', *Mech. Syst. Signal Process.*, vol. 58–59, pp. 308–324, 2015.

[23] S. D. Haddad, 'Theoretical treatment of piston motion in I.C. piston engine for the prediction of piston slap excitation', *Mech. Mach. Theory*, vol. 30, no. 2, pp. 253–269, 1995.

[24] E. E. Ungar and D. Ross, 'Vibrations and noise due to piston-slap in reciprocating machinery', *J. Sound Vib.*, vol. 2, no. 2, pp. 132–146, 1965.

[25] Z. Geng and J. Chen, 'Investigation into piston-slap-induced vibration for engine condition simulation and monitoring', *J. Sound Vib.*, vol. 282, no. 3–5, pp. 735–751, 2005.

[26] J. P. D. Hartog, *Mechanical Vibrations*. Courier Corporation, 1985.

[27] Z. Geng and J. Chen, 'Investigation into piston-slap-induced vibration for engine condition simulation and monitoring', *J. Sound Vib.*, vol. 282, no. 3–5, pp. 735–751, 2005.

[28] S.-H. Cho, S.-T. Ahn, and Y.-H. Kim, 'A simple model to estimate the impact force induced by piston slap', *J. Sound Vib.*, vol. 255, no. 2, pp. 229–242, 2002.

[29] J. R. Cho and S. J. Moon, 'A numerical analysis of the interaction between the piston oil film and the component deformation in a reciprocating compressor', *Tribol. Int.*, vol. 38, no. 5, pp. 459–468, 2005.

[30] H. Murakami, N. Nakanishi, N. Ono, and T. Kawano, 'New Three-dimensional Piston Secondary Motion Analysis Method Coupling Structure Analysis and Multi Body Dynamics Analysis', *SAE Int. J. Engines*, vol. 5, no. 1, pp. 42–50, Nov. 2011.

[31] A. A. Jafari, S. M. R. Khalili, and R. Azarafza, ‘Transient dynamic response of composite circular cylindrical shells under radial impulse load and axial compressive loads’, *Thin-Walled Struct.*, vol. 43, no. 11, pp. 1763–1786, 2005.

[32] I. Gravalos *et al.*, ‘Detection of fuel type on a spark ignition engine from engine vibration behaviour’, *Appl. Therm. Eng.*, vol. 54, no. 1, pp. 171–175, 2013.

[33] A. S. for Testing and Materials, *Standard specification for biodiesel fuel blend stock (B100) for middle distillate fuels*. ASTM International, 2012.

[34] E. Uludamar, E. Tosun, and K. Aydın, ‘Experimental and regression analysis of noise and vibration of a compression ignition engine fuelled with various biodiesels’, *Fuel*, vol. 177, pp. 326–333, 2016.

[35] A. Taghizadeh-Alisaraei, B. Ghobadian, T. Tavakoli-Hashjin, S. S. Mohtasebi, A. Rezaei-asl, and M. Azadbakht, ‘Characterization of engine’s combustion-vibration using diesel and biodiesel fuel blends by time-frequency methods: A case study’, *Renew. Energy*, vol. 95, pp. 422–432, 2016.

[36] Z. Huang *et al.*, ‘Combustion behaviors of a compression-ignition engine fuelled with diesel/methanol blends under various fuel delivery advance angles’, *Bioresour. Technol.*, vol. 95, no. 3, pp. 331–341, 2004.

[37] C. Sayin, ‘Engine performance and exhaust gas emissions of methanol and ethanol–diesel blends’, *Fuel*, vol. 89, no. 11, pp. 3410–3415, 2010.

[38] G. Najafi and T. Yusaf, ‘Experimental investigation of using methanol-diesel blended fuels in diesel engine’, in *Proceedings of the 4th International Conference on Thermal Engineering Theory and Applications*, Abu Dhabi, UAE, 2009.

[39] Z. Huang *et al.*, ‘Combustion behaviors of a compression-ignition engine fuelled with diesel/methanol blends under various fuel delivery advance angles’, *Bioresour. Technol.*, vol. 95, no. 3, pp. 331–341, 2004.

[40] Y. Li, M. Jia, Y. Liu, and M. Xie, ‘Numerical study on the combustion and emission characteristics of a methanol/diesel reactivity controlled compression ignition (RCCI) engine’, *Appl. Energy*, vol. 106, pp. 184–197, 2013.

[41] Z. H. Zhang, C. S. Cheung, and C. D. Yao, ‘Influence of fumigation methanol on the combustion and particulate emissions of a diesel engine’, *Fuel*, vol. 111, pp. 442–448, 2013.

[42] L.-J. Wang, R.-Z. Song, H.-B. Zou, S.-H. Liu, and L.-B. Zhou, ‘Study on combustion characteristics of a methanol—diesel dual-fuel compression ignition engine’, *Proc. Inst. Mech. Eng. Part J. Automob. Eng.*, vol. 222, no. 4, pp. 619–627, Apr. 2008.

[43] Y. Li, C. Zhang, W. Yu, and H. Wu, ‘Effects of rapid burning characteristics on the vibration of a common-rail diesel engine fueled with diesel–methanol dual-fuel’, *Fuel*, vol. 170, pp. 176–184, 2016.

[44] I. Gravalos *et al.*, ‘Detection of fuel type on a spark ignition engine from engine vibration behaviour’, *Appl. Therm. Eng.*, vol. 54, no. 1, pp. 171–175, 2013.

[45] X. Zhen and Y. Wang, ‘An overview of methanol as an internal combustion engine fuel’, *Renew. Sustain. Energy Rev.*, vol. 52, pp. 477–493, 2015.

[46] K. N. Mistry, ‘Simulation and Modeling of Friction Force and Oil Film Thickness in Piston Ring–Cylinder Liner Assembly of an IC Engine’, in *Proceedings of the World Congress on Engineering*, 2009, vol. 2.

[47] S. Eilon and O. A. Saunders, ‘A Study of Piston-Ring Lubrication’, *Proc. Inst. Mech. Eng.*, vol. 171, no. 1, pp. 427–462, Jun. 1957.

[48] L. L. Ting and J. Mayer J. E., ‘Piston Ring Lubrication and Cylinder Bore Wear Analyses, Part II—Theory Verification’, *J. Lubr. Technol.*, vol. 96, no. 2, pp. 258–266, 1974.

[49] L. L. Ting and J. Mayer J. E., ‘Piston Ring Lubrication and Cylinder Bore Wear Analysis, Part I—Theory’, *J. Lubr. Technol.*, vol. 96, no. 3, pp. 305–313, 1974.

[50] N. Patir and H. S. Cheng, ‘An Average Flow Model for Determining Effects of Three-Dimensional Roughness on Partial Hydrodynamic Lubrication’, *J. Lubr. Technol.*, vol. 100, no. 1, pp. 12–17, 1978.

[51] N. Patir and H. S. Cheng, ‘Application of Average Flow Model to Lubrication Between Rough Sliding Surfaces’, *J. Lubr. Technol.*, vol. 101, no. 2, pp. 220–229, 1979.

[52] M. Priest and C. M. Taylor, ‘Automobile engine tribology — approaching the surface’, *Wear*, vol. 241, no. 2, pp. 193–203, 2000.

[53] P. Andersson, J. Tamminen, and C.-E. Sandström, ‘Piston ring tribology’, *Lit. Surv. VTT Tied.-Res. Notes*, vol. 2178, no. 1, 2002.

[54] R. J. Chittenden and M. Priest, ‘Analysis of the Piston Assembly, Bore Distortion and Future Developments’, in *Tribology Series*, vol. 26, C. M. Taylor, Ed. Elsevier, 1993, pp. 241–270.

[55] P. Reipert and M. Voigt, ‘Simulation of the Piston / Cylinder Behavior for Diesel Engines’, 2001.

[56] A. Usman, T. A. Cheema, and C. W. Park, ‘Tribological performance evaluation and sensitivity analysis of piston ring lubricating film with deformed cylinder liner’, *Proc. Inst. Mech. Eng. Part J J. Eng. Tribol.*, vol. 229, no. 12, pp. 1455–1468, Dec. 2015.

[57] L. Ning, X. Meng, and Y. Xie, ‘Incorporation of deformation in a lubrication analysis for automotive piston skirt–liner system’, *Proc. Inst. Mech. Eng. Part J J. Eng. Tribol.*, vol. 227, no. 6, pp. 654–670, Jun. 2013.

[58] F. M. Meng, X. F. Wang, T. T. Li, and Y. P. Chen, ‘Influence of cylinder liner vibration on lateral motion and tribological behaviors for piston in internal combustion engine’, *Proc. Inst. Mech. Eng. Part J J. Eng. Tribol.*, vol. 229, no. 2, pp. 151–167, Feb. 2015.

[59] M. Gore, M. Theaker, S. Howell-Smith, H. Rahnejat, and P. D. King, ‘Direct measurement of piston friction of internal-combustion engines using the floating-liner principle’, *Proc. Inst. Mech. Eng. Part J. Automob. Eng.*, vol. 228, no. 3, pp. 344–354, Feb. 2014.

[60] K. Siegert and J. Ulmer, ‘Superimposing Ultrasonic Waves on the Dies in Tube and Wire Drawing’, *J. Eng. Mater. Technol.*, vol. 123, no. 4, pp. 517–523, 2001.

[61] T. Jimma *et al.*, ‘An application of ultrasonic vibration to the deep drawing process’, *J. Mater. Process. Technol.*, vol. 80–81, pp. 406–412, 1998.

[62] K. Siegert and J. Ulmer, ‘Influencing the Friction in Metal Forming Processes by Superimposing Ultrasonic Waves’, *CIRP Ann. - Manuf. Technol.*, vol. 50, no. 1, pp. 195–200, 2001.

[63] K. Egashira, K. Mizutani, and T. Nagao, ‘Ultrasonic Vibration Drilling of Microholes in Glass’, *CIRP Ann. - Manuf. Technol.*, vol. 51, no. 1, pp. 339–342, 2002.

[64] M. Wiercigroch, J. Wojewoda, and A. M. Krivtsov, ‘Dynamics of ultrasonic percussive drilling of hard rocks’, *J. Sound Vib.*, vol. 280, no. 3–5, pp. 739–757, 2005.

[65] D. P. Hess and A. Soom, ‘Normal Vibrations and Friction Under Harmonic Loads: Part I—Hertzian Contacts’, *J. Tribol.*, vol. 113, no. 1, pp. 80–86, 1991.

[66] D. M. Tolstoi, ‘Significance of the normal degree of freedom and natural normal vibrations in contact friction’, *Wear*, vol. 10, no. 3, pp. 199–213, 1967.

[67] Douglas Godfrey, ‘Vibration Reduces Metal to Metal Contact and Causes an Apparent Reduction in Friction’, *E Trans.*, vol. 10, no. 2, pp. 183–192, 1967.

[68] V. C. Kumar and I. M. Hutchings, ‘Reduction of the sliding friction of metals by the application of longitudinal or transverse ultrasonic vibration’, *Tribol. Int.*, vol. 37, no. 10, pp. 833–840, 2004.

[69] D. Lee, Y. H. Jang, and E. Kannatey-Asibu Jr., ‘Numerical analysis of quasistatic frictional contact of an elastic block under combined normal and tangential cyclic loading’, *Int. J. Mech. Sci.*, vol. 64, no. 1, pp. 174–183, 2012.

[70] C. Tinghai, G. Han, B. Gang, and G. Xiangdong, ‘Influence of ultrasonic oscillations on static friction characteristics of pneumatic cylinder’, in *Fluid Power and Mechatronics (FPM), 2011 International Conference on*, 2011, pp. 160–163.

[71] G. Han, C. Tinghai, B. Gang, and X. Chengfeng, ‘Research on pneumatic cylinder static friction and ultimate displacement upon ultrasonic vibrations’, in *Proceedings of the 2012 third international conference on mechanic automation and control engineering, IEEE Computer Society*, 2012, pp. 2600–2604.

[72] A. J. Sadowski and J. M. Rotter, ‘Solid or shell finite elements to model thick cylindrical tubes and shells under global bending’, *Int. J. Mech. Sci.*, vol. 74, pp. 143–153, 2013.

[73] E. Wang and T. Nelson, ‘structural dynamic capabilities of ANSYS’, in *ANSYS 2002 Conference, Pittsburg, Pennsylvania, USA*, 2002.

[74] R. K. SINGHAL, W. GUAN, and K. WILLIAMS, ‘Modal analysis of a thick-walled circular cylinder’, *Mech. Syst. Signal Process.*, vol. 16, no. 1, pp. 141–153, 2002.

[75] Boštjan Brank, Said Mamouri, and Adnan Ibrahimbegović, ‘Constrained finite rotations in dynamics of shells and Newmark implicit time-stepping schemes’, *Eng. Comput.*, vol. 22, no. 5/6, pp. 505–535, 2005.

[76] A. Farshidianfar, M. H. Farshidianfar, M. J. Crocker, and W. O. Smith, ‘Vibration analysis of long cylindrical shells using acoustical excitation’, *J. Sound Vib.*, vol. 330, no. 14, pp. 3381–3399, 2011.

[77] ‘ISO 1083:2004 - Spheroidal graphite cast irons - Classification’. [Online]. Available: http://www.iso.org/iso/catalogue_detail.htm?csnumber=33243. [Accessed: 22-Mar-2016].

[78] H. Wei, J. Wei, and G. Shu, ‘Calculation on cylinder pressure fluctuation by using the wave equation in KIVA program’, *Chin. J. Mech. Eng.*, vol. 25, no. 2, pp. 362–369, Feb. 2012.

[79] N. Dolatabadi, B. Littlefair, M. De la Cruz, S. Theodossiades, S. J. Rothberg, and H. Rahnejat, ‘A transient tribodynamic approach for the calculation of internal combustion engine piston slap noise’, *J. Sound Vib.*, vol. 352, pp. 192–209, Sep. 2015.

[80] C. Sayin, M. Ilhan, M. Canakci, and M. Gumus, ‘Effect of injection timing on the exhaust emissions of a diesel engine using diesel–methanol blends’, *Renew. Energy*, vol. 34, no. 5, pp. 1261–1269, 2009.

[81] *ASTM D6751-09, Standard Specification for Biodiesel Fuel Blend Stock (B100) for Middle Distillate Fuels, ASTM International, West Conshohocken, PA, 2009, www.astm.org*. .

[82] J. J. Truhan, J. Qu, and P. J. Blau, ‘A rig test to measure friction and wear of heavy duty diesel engine piston rings and cylinder liners using realistic lubricants’, *Tribol. Int.*, vol. 38, no. 3, pp. 211–218, 2005.

[83] P. S. Dellis, ‘Effect of friction force between piston rings and liner: A parametric study of speed, load, temperature, piston-ring curvature, and high-temperature, high-shear viscosity’, *Proc. Inst. Mech. Eng. Part J J. Eng. Tribol.*, vol. 224, no. 5, pp. 411–426, May 2010.

[84] M.-T. Ma, E. H. Smith, and I. Sherrington, ‘A Three-Dimensional Analysis of Piston Ring Lubrication Part 1: Modelling’, *Proc. Inst. Mech. Eng. Part J J. Eng. Tribol.*, vol. 209, no. 1, pp. 1–14, Mar. 1995.

[85] H. Xu, ‘Predictive modeling of piston assembly lubrication in reciprocating internal combustion engines’, The University of Texas at Austin, 2005.

[86] C. Wu and L. Zheng, ‘An Average Reynolds Equation for Partial Film Lubrication With a Contact Factor’, *J. Tribol.*, vol. 111, no. 1, pp. 188–191, 1989.

[87] P. C. Mishra, H. Rahnejat, and P. D. King, ‘Tribology of the ring—bore conjunction subject to a mixed regime of lubrication’, *Proc. Inst. Mech. Eng. Part C J. Mech. Eng. Sci.*, vol. 223, no. 4, pp. 987–998, Apr. 2009.

[88] N. Patir and H. S. Cheng, ‘Application of Average Flow Model to Lubrication Between Rough Sliding Surfaces’, *J. Tribol.*, vol. 101, no. 2, pp. 220–229, Apr. 1979.

[89] C. C. Tsai and C. H. Tseng, ‘The effect of friction reduction in the presence of in-plane vibrations’, *Arch. Appl. Mech.*, vol. 75, no. 2–3, pp. 164–176, Dec. 2005.

[90] D. Godfrey, ‘Vibration Reduces Metal to Metal Contact and Causes an Apparent Reduction in Friction’, *E Trans.*, vol. 10, no. 2, pp. 183–192, 1967.

[91] D. M. Tolstoi, ‘Significance of the normal degree of freedom and natural normal vibrations in contact friction’, *Wear*, vol. 10, no. 3, pp. 199–213, 1967.

[92] L. Afferrante and M. Ciavarella, ‘Thermo-Elastic Dynamic Instability (TEDI)—a review of recent results’, *J. Eng. Math.*, vol. 61, no. 2–4, pp. 285–300, Sep. 2007.

[93] I. L. Singer and H. Pollock, *Fundamentals of Friction: Macroscopic and Microscopic Processes*. Springer Science & Business Media, 2012.

[94] D. P. HESS, ‘Interaction of vibration and friction at dry sliding contacts’, *Dyn. Frict. Model. Anal. Exp. Ser. Stab. Vib. Control Syst. World Sci. Singap. River Edge NJ*, pp. 1–27, 2002.

[95] H. Storck, W. Littmann, J. Wallaschek, and M. Mracek, ‘The effect of friction reduction in presence of ultrasonic vibrations and its relevance to travelling wave ultrasonic motors’, *Ultrasonics*, vol. 40, no. 1–8, pp. 379–383, 2002.

[96] W. Littmann, H. Storck, and J. Wallaschek, ‘Sliding friction in the presence of ultrasonic oscillations: superposition of longitudinal oscillations’, *Arch. Appl. Mech.*, vol. 71, no. 8, pp. 549–554.

[97] V. C. Kumar and I. M. Hutchings, ‘Reduction of the sliding friction of metals by the application of longitudinal or transverse ultrasonic vibration’, *Tribol. Int.*, vol. 37, no. 10, pp. 833–840, 2004.

[98] H. M. Checo, A. Jaramillo, M. Jai, and G. C. Buscaglia, ‘Texture-induced cavitation bubbles and friction reduction in the Elrod–Adams model’, *Proc. Inst. Mech. Eng. Part J J. Eng. Tribol.*, vol. 229, no. 4, pp. 478–492, Apr. 2015.

[99] S. A. Aziz, ‘Characterising the effective material softening in ultrasonic forming of metals’, PhD, University of Glasgow, 2012.

[100] G. Han, C. Tinghai, B. Gang, and X. Chengfeng, ‘Research on pneumatic cylinder static friction and ultimate displacement upon ultrasonic vibrations’, in *Proceedings of the 2012 third international conference on mechanic automation and control engineering, IEEE Computer Society*, 2012, pp. 2600–2604.

[101] C. Tinghai, G. Han, B. Gang, and G. Xiangdong, ‘Influence of ultrasonic oscillations on static friction characteristics of pneumatic cylinder’, in *Fluid Power and Mechatronics (FPM), 2011 International Conference on*, 2011, pp. 160–163.

[102] N. A. Chang and S. L. Ceccio, ‘The acoustic emissions of cavitation bubbles in stretched vortices’, *J. Acoust. Soc. Am.*, vol. 130, no. 5, pp. 3209–3219, Nov. 2011.